Rep. Prog. Phys. **62** (1999) 61–122. Printed in the UK PII: S0034-4885(99)83774-9

The pseudogap in high-temperature superconductors: an experimental survey

Tom Timusk† and Bryan Statt‡

† Department of Physics and Astronomy McMaster University, Hamilton ON, Canada L8S 4M1
‡ Department of Physics, University of Toronto, Toronto ON, Canada M5S 1A7

Received 6 July 1998

Abstract

We present an experimental review of the nature of the pseudogap in the cuprate superconductors. Evidence from various experimental techniques points to a common phenomenology. The pseudogap is seen in all high-temperature superconductors and there is general agreement on the temperature and doping range where it exists. It is also becoming clear that the superconducting gap emerges from the normal state pseudogap. The d-wave nature of the order parameter holds for both the superconducting gap and the pseudogap. Although an extensive body of evidence is reviewed, a consensus on the origin of the pseudogap is as lacking as it is for the mechanism underlying high-temperature superconductivity.

0034-4885/99/010061+62$59.50

Contents

1. Introduction

High-temperature superconductivity was discovered by Bednorz and Müller (1986) in a complex oxide containing quasi-two-dimensional copper–oxygen planes. Copper is a multivalent ion and by chemical doping, either by heating in an oxygen atmosphere or by adjusting the composition in the layers away from the CuO_2 plane, these oxides can be made conducting. For example, by replacing some of the trivalent La in La_2CuO_4 (La 214) with the divalent Sr, this material, which is an antiferromagnetic insulator at zero Sr doping, becomes a superconductor. From the point of view of the band theory of solids this is a surprise since by simply counting charges one expects the undoped materials to be metals with half-filled bands. We will see in this review that the approach to the insulating state is closely related to the growth of a *pseudogap* at the Fermi surface. By a pseudogap we mean a partial gap. An example of such a partial gap would be a situation where, within the band-theory approximation, some regions of the Fermi surface become gapped while other parts retain their conducting properties and with increased doping the gapped portion diminishes and the materials become more metallic. We view the pseudogap as a fundamental property of underdoped copper oxides. Our story of the pseudogap starts with the search for the superconducting gap in the newly discovered high-temperature superconductors.

The energy gap is one of the defining properties of a superconductor, but despite considerable effort, early experiments failed to find one in high-T_c cuprates. Well understood physical properties such as the frequency-dependent conductivity, the Raman efficiency or the tunnelling conductance did not show the familiar signatures of the energy gap, namely a zero density of excitations below an energy 2Δ appearing abruptly at the superconducting transition temperature T_c. Instead, in the cuprates, the depression of excitations was incomplete and often started well above T_c in the normal state. We now know that this behaviour was not the result of poor sample quality or faulty experimental technique, but a consequence of two basic properties of high-temperature superconductors—the d-wave nature of the superconducting gap function varying as the cosine function around the Fermi surface with nodes at $k_x = \pm k_y$, and the persistance of this gap into the normal state. It is the aim of this review to provide an introduction to the experiments that have established the pseudogap state as the normal state from which superconductivity emerges as the temperature is lowered through T_c. An earlier review focusing on transport properties was presented by Batlogg *et al* (1994).

A number of families of high-temperature superconductors have been discovered, all of which have shown evidence of a pseudogap. Within each family the properties vary with the doping level through the control of carrier density. Properties can also be changed through substitution of impurities into the copper–oxygen planes. The system that has received the largest amount of attention is $YBa_2Cu_3O_{6+x}$ (YBCO 123) with less work done on the closely related systems $YBa_2Cu_4O_8$ (YBCO 124) and $Pb_2Sr_2(Y/Ca)Cu_3O_8$ (PSYCCO). These systems are characterized by a CuO_2 bilayer as well as a third layer containing copper: chains in the case of YBCO 123, double chains for YBCO 124 and isolated twofold coordinated coppers for PSYCCO. In transport, the effect of the one-dimensional chains can be separated by doing polarized measurements with electric fields normal to the chains. A second important bilayer system is $Bi_2Sr_2CaCu_2O_8$ (Bi 2212) and the more recently discovered thallium and mercury versions (Tl 2212 and Hg 2212). Single-layer materials include the much studied $La_{2-x}Sr_xCuO_4$ (LaSr 214) with a low $T_c < 40$ K as well as the 90 K materials $Tl_2Sr_2CuO_{6+\delta}$ (Tl 2201).

There are technical reasons why all the experimental probes have not been used with success on all the families of high-temperature superconductors. For example, magnetic neutron scattering requires very large single crystals and has almost exclusively been done

on YBCO 123 and LaSr 214. On the other hand, tunnelling spectroscopy and angle-resolved photoemission (ARPES) are surface-sensitive probes where the focus has been on $Bi_2Sr_2CaCu_2O_8$ which cleaves easily in a vacuum along the BiO planes normal to the c-direction yielding a high-quality virgin surface. Techniques like the dc conductivity, ab-plane transport and nuclear magnetic resonance (NMR) place less onerous demands on the crystal growers and have consequently been been applied with success to a larger number of high-temperature superconducting (HTSC) systems.

We have organized our review in terms of different experimental techniques starting with ARPES and tunnelling. Ideally these techniques measure the density of single electronic states as a function of energy and momentum, occupied states in the case of ARPES and both occupied and unoccupied in the case of tunnelling. For various practical reasons both techniques yield an average over large regions of momentum space, particularly tunnelling.

Other experimental techniques do not yield information about single electronic states but involve an excitation of the electronic system where a transition takes place from an initial state to a different final state. These techniques include transport properties where, in the optical conductivity and Raman scattering, the initial and final states have the same momentum and in the case of the dc conductivity, the same energy. Magnetic neutron scattering is a spectroscopic technique where there is a spin flip and the experimenter can also choose the momentum transfer between the initial and final states.

NMR is a low-energy technique which is sensitive to various momentum averages of the spin excitations. By probing various nuclei in the unit cell one can probe different parts of momentum space. The electronic specific heat also measures the density of all excitations within a broad window of width k_BT centred at the Fermi surface.

While NMR experiments were the first to show evidence of a normal-state gap, recent ARPES data have provided us with the most detailed picture of the evolution of the electronic structure in the pseudogap state and form a good starting point. We then turn to transport measurements including the optical conductivity where the pseudogap manifests itself through reduced scattering below a certain temperature T^*. The electronic specific heat also shows evidence of a pseudogap through a depression of the specific heat coefficient, γ, at low temperature. Finally we review the results of two other spectroscopies, electronic Raman scattering and magnetic neutron scattering.

2. Angle-resolved photoemission

Angle-resolved photoemission spectroscopy is a technique that yields the energy and momentum of the filled electronic energy states below the Fermi surface. It is a refinement of the classical photoelectric effect. In the modern version, a high-energy photon from a synchrotron, typically $\approx$20 eV in energy, is selected by a monochromator and illuminates the surface of a single crystal cleaved in an ultra-high vacuum. A photoelectron is ejected from the sample at an angle θ to the surface normal, defined by an aperture or a position on a fluorescent screen. The kinetic energy of the electron is measured with an electron spectrometer to an energy resolution of 20 meV or better. To establish a zero of energy, the sample is connected electrically to a reference metal, for example platinum, and the photoelectron energies from the reference metal are compared with those of the sample under study. When the two systems are in equilibrium their Fermi levels coincide. Figure 1 shows how one can measure a gap Δ below the Fermi level of a metal this way. ARPES experiments in high-temperature superconductors have been reviewed by Shen and Dessau (1995) and more recently by Randeria and Campuzano (1997).

Since the photoelectron emerges from a plane surface with translational symmetry, its

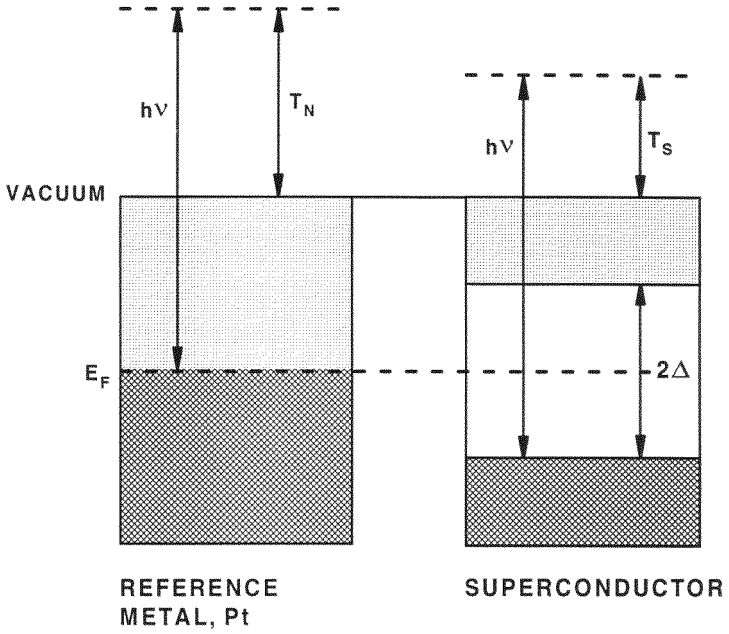

Figure 1. Measurement of the superconducting gap by photoemission. The kinetic energies of photoelectrons emerging from a normal metal T_N and a superconductor T_S will differ by Δ, the superconducting gap. The two systems are electrically connected and charge will flow until their Fermi levels are equal.

momentum component parallel to the surface has to be balanced by the momentum of excitations created inside the sample. By varying the angle θ between the sample normal and the direction of the detected photolectrons, it is possible to map out the $\boldsymbol{k}$ dependence of the filled states below the Fermi level. In this oversimplified model an electron of momentum $\boldsymbol{k}_\parallel$, in occupied state of energy $\epsilon_{\boldsymbol{k}_\parallel}$ below the Fermi energy, gives rise to a photoelectron distribution with a sharp peak at momentum $\boldsymbol{k}_\parallel$ and energy $\epsilon_{\boldsymbol{k}}$ measured from the Fermi level of the reference sample. The measured energy distribution curve of the photoelectrons is given by (Randeria and Campuzano 1997):

$$I(\boldsymbol{k}, \omega) = I_0(\boldsymbol{k}) f(\omega) A(\boldsymbol{k}, \omega) \tag{1}$$

where $\boldsymbol{k}$ is the momentum component parallel to the surface and ω its energy relative to the Fermi level. $A(\boldsymbol{k}, \omega)$ is the spectral function of the hole:

$$A(\boldsymbol{k}, \omega) = \frac{\Sigma''(\boldsymbol{k}, \omega)/\pi}{(\omega - \epsilon_{\boldsymbol{k}} - \Sigma'(\boldsymbol{k}, \omega))^2 + \Sigma''(\boldsymbol{k}, \omega)}. \tag{2}$$

In a non-interacting Fermi liquid $A(\boldsymbol{k}, \omega)$ is simply a δ-function in both $\boldsymbol{k}$ and ω centred on $\epsilon_{\boldsymbol{k}}$ but in a real material $A(\boldsymbol{k}, \omega)$ acquires a width in ω. $I_0(\boldsymbol{k})$ is an intensity factor and $f(\omega)$ the Fermi function.

ARPES spectra in the transition metal oxides have been reviewed by Shen and Dessau (1995). They are dominated by a broad background that extends to lower kinetic energies from the peak at $\epsilon_{\boldsymbol{k}}$. This background is in part caused by energy loss of the photoelectron within the surface layer before escaping. However, in strongly correlated materials, such as the high-T_c oxides, a large part of the background is due to electron–electron interactions. The electron states acquire an incoherent tail at higher energy and the sharp coherent peak at $\epsilon_{\boldsymbol{k}}$ rapidly

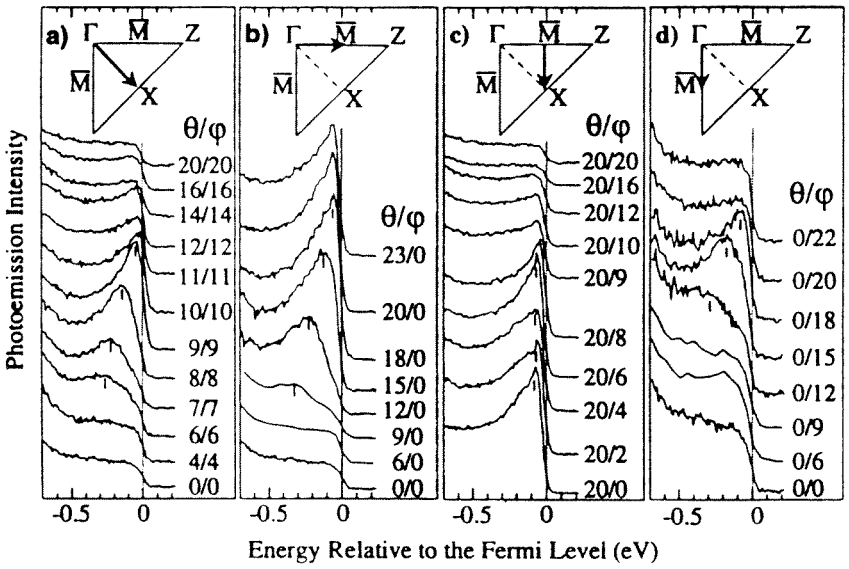

Figure 2. Photoelectron spectra at different angles θ and ϕ to the crystal normal. In (*a*) $\theta = \phi$ and the vertical line shows the state dispersing as it approaches the Fermi energy at $\theta = \phi \approx 12^\circ$. The peak disappears for empty states above the Fermi level at $\theta = \phi \approx> 11^\circ$. The other panels show other combinations of θ and ϕ.

broadens for states below the Fermi level. This loss of coherence is also seen in the optical conductivity where the transport scattering rate is found to equal the quasiparticle energy, a sign of very strong electron–electron interaction and a breakdown of the Fermi liquid picture. This is described in detail in the section on the transport properties below. Quantum Monte Carlo calculations, based on the Hubbard model, also typically show a tail extending to as far as 0.5 eV from the coherence peak (Rozenberg *et al* 1995, Georges *et al* 1996).

Nevertheless, a well-defined quasiparticle peak can be seen in the spectra of many HTSC oxides with carefully prepared surfaces under ultra-high vacuum conditions. An example is shown in figure 2 from the work of Dessau *et al* (1993) where a broad peak, denoted by a short vertical line, can be seen to narrow as its energy approaches the Fermi level. The various curves are photoelectron spectra taken at different angles relative to the sample normal with varying in-plane momentum component of the outgoing photoelectron. The left panel scan is from the zone centre, the Γ point, at 45° to the CuO bond direction towards the X point (π, π). One can clearly see that at $\theta = 11^\circ$ the peak becomes very sharp and disappears altogether at steeper angles. This point is taken to be the position of the Fermi momentum $\boldsymbol{k}_F$. The second and third panels of figure 2 are scans in the bond direction and reveal a region of flat dispersion where quasiparticle energies are just below the Fermi surface for a large region of the Brillouin zone.

The whole Fermi surface can be mapped out this way by locating the transverse momentum where the quasiparticle peak disappears as it moves towards zero energy. This is shown in figure 3 where we see a hole-like Fermi surface centred on the X point with filled states at the Γ point (0, 0) and empty states at the X point. Figure 4 shows the band structure obtained from the ARPES spectra (full circles) and a simple band model compatible with the data. One can see the steep Fermi surface crossing on the Γ–X line whereas in the vicinity of the M $(\pi, 0)$ points the bands are flat. Detailed local density approximation (LDA) calculations predict such

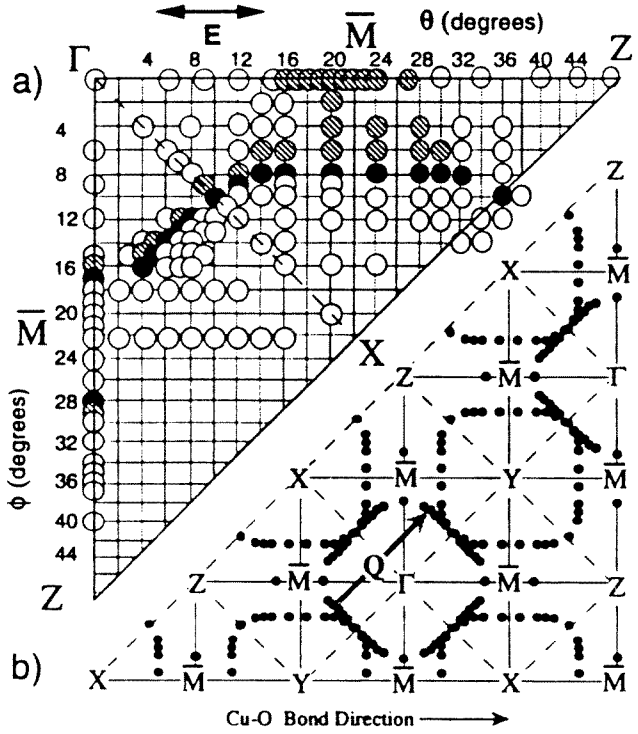

Figure 3. The Fermi surface in Bi 2212 mapped out with photoemission. Each measurement is denoted by a circle. The full circles denote points where the dispersion curves cross the Fermi surface and the shaded circles filled states that lie close to the Fermi energy. After Dessau *et al* (1993).

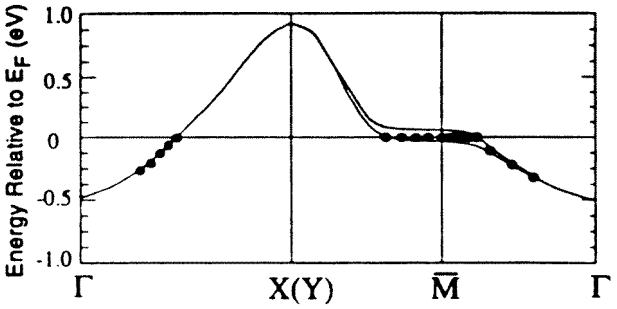

Figure 4. E versus $\boldsymbol{k}$ along symmetry directions in Bi 2212 obtained by photoemission. The full curve is an interpretation of the dispersion relationship. There is clear Fermi surface crossing on the zone diagonal and a flat region, an extended van Hove singularity, near the zone boundary M $(\pi, 0)$. After Dessau *et al* (1993).

a band structure but there are serious discrepancies that are outside the scope of this review, as discussed in Dessau *et al* (1993). In particular there is an absence of BiO bands predicted by band theory.

The large Fermi surface has also been seen in YBCO by Campuzano *et al* (1990) and Liu *et al* (1992), in optimally doped Bi2212 by Olsen *et al* (1989) and in the electron-doped $Nd_{1-x}Ce_xCuO_4$ by King *et al* (1993) and by Anderson *et al* (1993). Such a large surface is

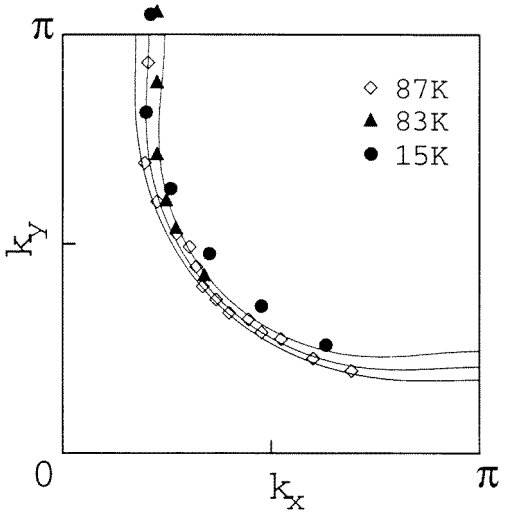

Figure 5. Fermi surface of Bi 2212 of samples with different T_c obtained by varying the doping level. Tight binding theory, shown as the full curves, predicts that the hole Fermi surface (centred on (π, π)) expands as $1 + x$ with doping. Photoemission data, shown as symbols, show a large Luttinger-type Fermi surface at all doping levels but lack the resolution to discern the change in area with x.

consistent with Luttinger's theorem which states that the area enclosed by the Fermi surface is independent of interaction and should therefore equal the free electron value. As a function of doping x, the Luttinger–Fermi surface is expected to vary in area as $1 - x$. As the doping level x approaches zero the Fermi surface should remain large. Photoemission lacks the resolution to detect the $1 - x$ variation with doping. This is shown in figure 5 where Ding *et al* (1997) plot the Fermi surface from samples of Bi 2212 with different doping levels. The full curves are tight binding rigid-band calculations. The authors note that the error bars are larger than the separation between the calculated Fermi surfaces at the different doping levels. Furthermore, as discussed below, the underdoped sample shown in figure 5 is in the pseudogap state with a gapped Fermi surface and the curve shown is not an actual Fermi surface but a locus of points of minimum gap.

The idea of a large $1 - x$ Fermi surface is not in accord with transport measurements where the Drude spectral weight has been shown to be proportional to x (Orenstein *et al* 1990, Uchida *et al* 1991) and not $1 - x$ as expected from Luttinger's theorem. This observation has led to the suggestion that there are small pockets of carriers in the vicinity of the d-wave nodes at $(\pi/2, \pi/2)$ at low doping. Another possibility within the conventional Fermi liquid picture is that a dramatic increase in effective mass is responsible for the reduced spectral weight with underdoping. This, however, is in disagreement with specific heat data that do not show any large changes in the specific heat coefficient γ with underdoping (Loram *et al* 1994a). As we will see in the next section the presence of the pseudogap in the normal state offers a way out of the x versus $1 - x$ dilemma.

2.1. The superconducting gap and the pseudogap

The earliest observations of the superconducting gap by photoemission were in the angle-integrated mode or with low momentum resolution. It was found that in optimally doped, vacuum-cleaved samples of Bi 2212 there was a shift in the leading edge of the electron

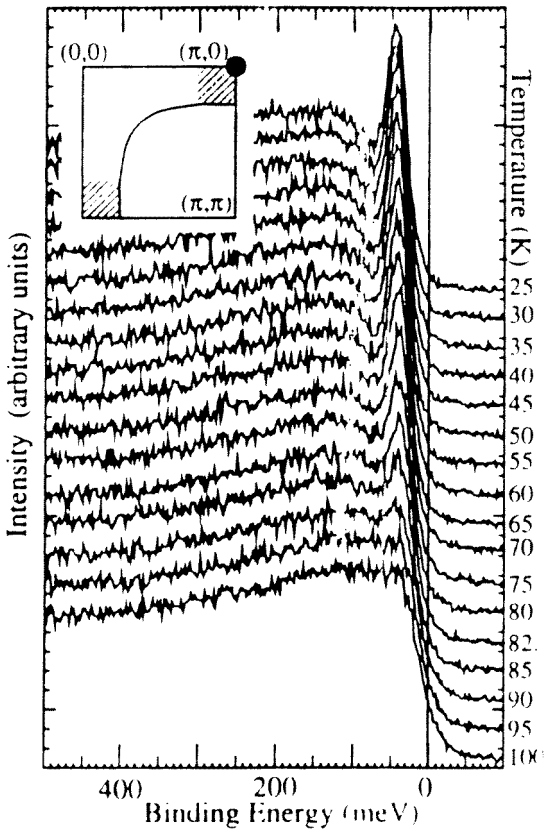

Figure 6. Temperature dependence of the photoemission spectra at the $(\pi, 0)$ point. A sharp peak followed by a dip grows below T_c. The energy of the peak does not change with temperature, suggesting that the superconducting gap Δ does not close at T_c.

loss spectrum below T_c (Imer *et al* 1989, Manzke *et al* 1989, Olsen *et al* 1989). Since the photoelectron spectral peak is quite broad, particularly in underdoped samples, it has become customary to use the difference between the midpoint of the leading edge and the Fermi energy as the 'leading-edge gap'. The true gap is larger than the leading-edge gap since the linewidth and the experimental resolution have to be added. Leading-edge gap values of Δ are typically in the 25 meV range in Bi 2212 whereas true gaps, determined by fits, are 10 meV larger (Randeria and Campuzano 1997).

A second striking feature seen in the superconducting state is the appearance of a strong, resolution limited peak followed by a dip structure (Dessau *et al* 1991, Hwu *et al* 1991) as shown in figure 6 from Loeser *et al* (1997). The spectra are taken in the momentum region near the $(\pi, 0)$ point as a function of temperature on an underdoped sample of Bi 2212 ($T_c = 79$ K). A sharp peak appears 42 meV below the Fermi level at approximately 95 K, about 15 K above the superconducting transition temperature. It is followed by a dip in the photoelectron intensity at approximately 75 meV. Below the dip is a broad peak centred at approximately 100 meV. Comparisons with recent vacuum tunnelling spectra show that the peak and the dip are symmetric about the Fermi energy whereas the broad peak only occurs on the negative energy side, suggesting it may be a band structure effect.

Olsen *et al* found that the gap in the superconducting state was isotropic but later work

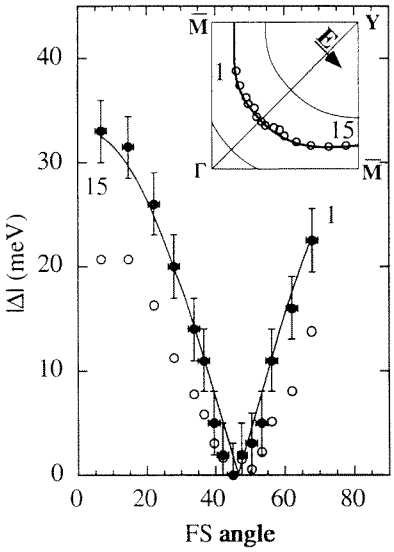

Figure 7. The superconducting gap as function of angle around the Fermi surface. The gap has d-wave-like nodes on the zone diagonals and rises to a maximum value of ≈35 meV at the M point $(\pi, 0)$. The open circles are the measured leading-edge shifts of the raw photoemission spectra and the full circles the estimated gap.

with better sample quality and improved resolution showed a clear anisotropy. Wells *et al* (1992) and Shen *et al* (1993) found that the gap has d-wave symmetry with a minimum in the (π, π) direction. This was confirmed with better resolution by Ding *et al* (1996). A recent plot of the gap as a function of angle around the Fermi surface is shown in figure 7 from Randeria and Campuzano (1997). The open circles are the leading-edge shifts while the full circles are the results of fits based on a BCS model. It is clear that the gap has the form predicted for a d-wave superconductor with a minimum gap along the diagonal at 45° to the CuO bond direction (i.e. in the Γ–Y direction) and a maximum gap in the M direction.

Loeser *et al* (1996) and Ding *et al* (1996) reported that the leading-edge gap seen in the superconducting state was also present in the normal state in underdoped Bi 2212. Both groups found that the momentum dependence and the magnitude of this normal-state gap resembled the gap seen in the superconducting state. It had the characteristic d-wave symmetry with a node in the Γ–Y direction and a maximum gap in the Γ–M direction. The gap was only seen in the underdoped samples and its onset temperature T^* was found to approach the superconducting transition temperature at optimal doping. Figure 8 from Harris *et al* (1996) shows the gap for two underdoped samples of Dy-doped Bi 2212 MBE grown films. The trivalent Dy substitution on the Ca site reduces the hole concentration resulting in underdoping. The leading-edge gap is shown as a function of $0.5|\cos k_x a - \cos k_y a|$. A d-wave gap would be a straight line on this plot. It can be seen that the d-wave model fits well in the superconducting state and that the normal-state gap also has clear d-wave symmetry but that there is considerable smearing out of the node as expected in the 'dirty d-wave' picture.

Harris *et al* (1996) plot the size of the gap as a function of doping and find that in the underdoped samples the gap magnitude *decreases* with doping. This is just the opposite of what is expected in BCS theory where the ratio of $2\Delta/k_B T_c$ is a constant, in other words the gap is proportional to T_c. In overdoped samples of Bi2212 the gap *does* decrease as T_c is reduced (White *et al* 1996) and there is no normal-state gap. These results are summarized in figure 9 which shows the leading-edge gap variation with hole doping. In the underdoped samples the normal-state gap and the superconducting gap are both approximately 25 meV whereas in the overdoped sample the superconducting gap has dropped to 20 meV and the normal-state gap is almost zero.

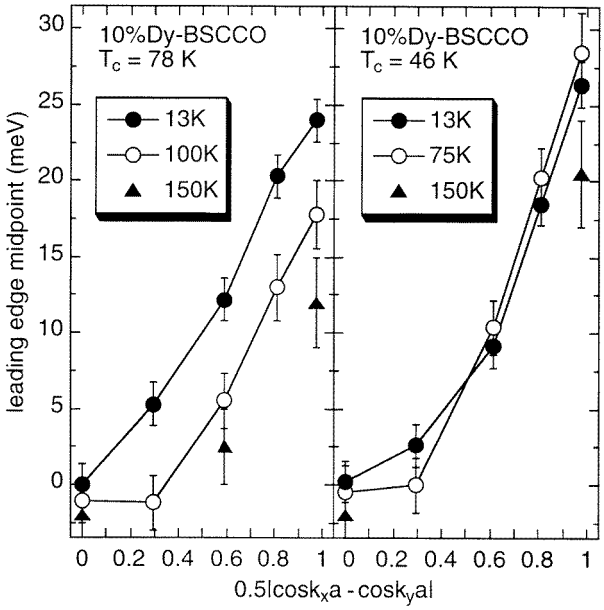

Figure 8. Pseudogap in photoemission. Leading-edge shifts plotted in such a way as to yield a straight line for a d-wave gap which is found in the superconducting state at high doping (left panel). The gap fills in near the node as the temperature is raised or as the doping level is reduced. The striking observation is that a pseudogap remains in the normal state in both samples with an overall symmetry and magnitude similar to the superconducting gap.

The presence of the pseudogap in the normal state also offers an explanation of the loss of spectral weight seen in transport measurements in the underdoped samples which, when interpreted in conventional terms, suggests the presence of small pockets at $(\pi/2, \pi/2)$. The pseudogap simply reduces the large Luttinger–Fermi surface by gapping the $(\pi, 0)$ region (Marshall *et al* 1996). Figure 10 shows the large Fermi surface of the overdoped sample as a full line and the partially gapped Fermi surface in the underdoped sample. The chain curve that would extend the short Fermi surface arc to form a closed pocket centred at $(\pi/2, \pi/2)$ corresponds to weak features of uncertain, possibly structural, origin. The authors suggest theoretical scenarios that would fold the zone along the broken line and give rise to a closed pocket.

The issue of the shape of the Fermi surface is addressed in a recent paper by Ding *et al* (1997). They follow the minimum gap locus in the pseudogap state and find it to coincide with the locus of gapless excitations in the ungapped state above T^* where a Fermi surface can be seen. These results suggest precursor pairing and not the presence of a spin density wave (SDW) gap: where the gap is tied to the SDW nesting vector and would coincide with the Fermi surface only in the case of perfect nesting. The implication of this work to transport measurements is that the reduced Drude weight in underdoped samples is due to the formation of the pseudogap, away from the $(\pi/2, \pi/2)$ points, thus restricting the volume of phase space of carriers that are available for conduction.

The nature of the Fermi surface in underdoped Bi 2212 has been addressed in a recent paper by Norman *et al* (1997a). They do not find evidence for a large Luttinger-type Fermi surface in the underdoped material but neither is there evidence for pockets in the Γ–Y direction. Instead, the Fermi surface consists of arcs that, in the optimally doped material, coincide

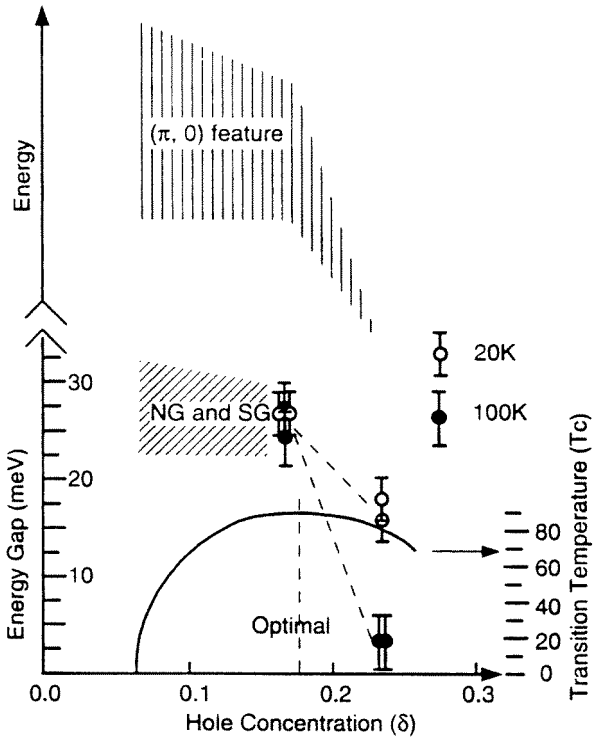

Figure 9. Leading-edge shifts as function of hole concentration. In the underdoped samples there is no difference in the magnitude of the superconducting (SG) and normal-state (NG) gaps whereas in the overdoped samples the superconducting gap is reduced and the normal-state gap goes to zero. The shaded area at high energy refers to the electronic structure near the $(\pi, 0)$ point discussed in Marshall *et al* (1976).

with the Luttinger–Fermi surface but shrink in size to approach point nodes of the $d_{x^2-y^2}$ superconducting gap as the temperature is decreased (figure 11). They find that in underdoped materials, as the temperature is lowered, the pseudogap first opens up at $(\pi, 0)$ and progressively gaps larger portions of the Fermi 'contour' (the arc in k space that would be the Luttinger–Fermi surface) leading to gapless arcs. In the overdoped case the behaviour is more conventional: the gap opens at the same temperature at all points of the Fermi surface. The authors find that in the underdoped case near the $(\pi, 0)$ point, the gap 'fills in' (its frequency does not change but spectral weight at E_F drops). In contrast, near the d-wave node, the gap 'closes' (its frequency decreases as it fills in) in a mean-field fashion. Figure 12 illustrates this where the ARPES data have been artificially symmetrized to remove the Fermi function.

Harris *et al* (1997) studied the single-layer Bi 2201 compound $Bi_{2+x}Sr_{2-(x+y)}La_yCuO_{6-\delta}$ which had been underdoped by the substitution of the trivalent La in place of the divalent Sr or Bi. With $y = 0.35$ an optimally doped sample with a $T_c = 29$ K was obtained, while by varying the Bi/Sr ratio an underdoped sample with $T_c < 4$ K and an overdoped one with $T_c = 8$ K were made. Figure 13 shows that the leading-edge shifts have a pseudogap of 10 ± 2 meV in the underdoped and optimally doped samples but no gap of any kind in the overdoped sample.

The one-plane material Bi 2201 differs from its two-plane counterpart Bi 2212 in the line shape in the superconducting state: it lacks the sharp peak followed by a dip. As figure 13

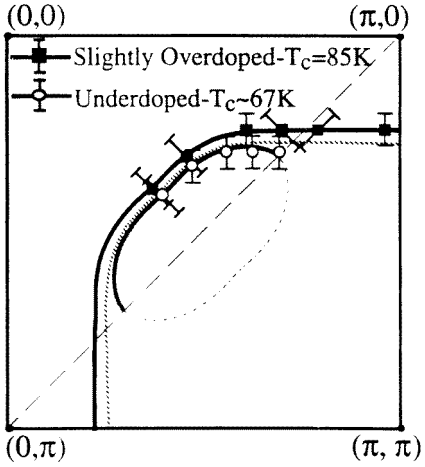

Figure 10. Fermi surface in underdoped Bi 2212 shown as open circles in contrast with an overdoped sample where a continuous arc can be seen. The disappearance of the Fermi surface is due to the formation of the pseudogap. The chain curve extends the short Fermi surface arc to form a pocket, an interpretation that would require a new zone boundary along the broken line.

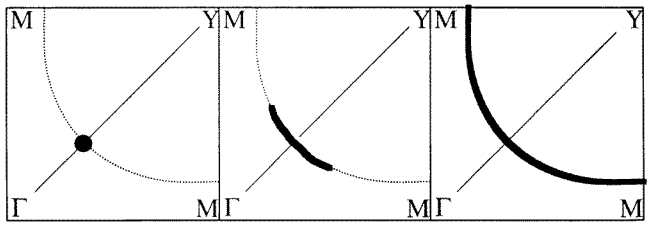

Figure 11. Destruction of the Fermi surface by the pseudogap at three doping levels. The dotted curve shows the large Fermi surface seen in the overdoped materials on the left. As the doping is reduced, the Fermi surface becomes gapped and only the full arcs remain. Data show that even at low doping (left panel) the minimum gap follows the original dotted Fermi surface.

shows, the spectra for the optimally doped sample ($T_c = 29$ K) look very similar in the normal and superconducting states. In contrast, the two-plane material has a striking peak that appears in the superconducting state followed by a dip. Harris *et al* argue that the lack of the coherent quasiparticle peak in the superconducting state could be the result of either an overall lower-energy scale, by a factor of three, or perhaps enhanced impurity scattering.

In conclusion, Harris *et al* (1997) note that the main effect in going from a two-layer to a single-layer material is the reduction of the maximum gap value by a factor of three which is quite different from the effect of underdoping, which has the effect of reducing T_c and *increasing* the gap.

We next discuss some of the models for the narrowing of the ARPES peak and the formation of the peak and dip structure. The most common interpretation has been in terms of strong coupling effects in analogy with BCS superconductors (Arnold *et al* 1991, Coffey and Coffey 1993, Shen and Schrieffer 1997, Norman *et al* 1997a). In BCS superconductors the phonons produce minima in the tunnelling conductance at $eV = \Delta + \Omega$ where Ω is a phonon frequency. The narrowing is explained in terms of the formation of a gap Δ at the Fermi surface (Coffey and Coffey 1993). If the scattering is electronic, there will be no scattering for photoelectron

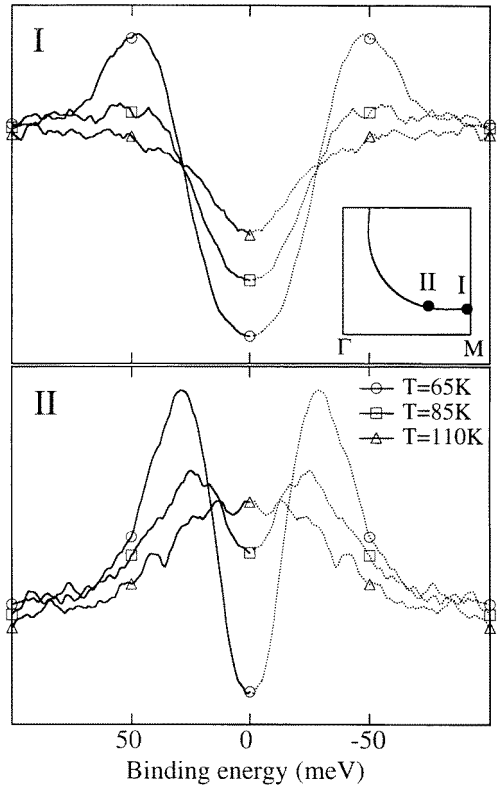

Figure 12. Temperature dependence of the gap in underdoped Bi 2212 at two locations in the zone. Symmetrized ARPES data show that the gap frequency is temperature independent in the region of the gap maximum but closes at points in the zone closer to the node. This can also be seen in figure 8.

energies less than 3Δ (in the s-wave case)—Δ to overcome the gap energy and 2Δ to create a pair of quasiparticles. Coffey and Coffey (1993) show that in a d-wave superconductor this dip occurs at 2Δ. (The corresponding energy for the conductivity is 4Δ since the photon creates an electron–hole pair, each particle of which can create a second electron–hole pair.) This reduction in scattering can be seen most dramatically in the reduction of microwave surface impedance at T_c (Bonn *et al* 1992). It is also responsible for the absence of a Hebel–Slichter coherence peak in the NMR spin-lattice relaxation rate just below T_c. This effect does give an explanation of the peak and dip structure in both ARPES and tunnelling spectra (see section 3).

Shen and Schrieffer (1997) suggest the coupling is to a strong collective excitation centred at (π, π) arguing that, because of Fermi surface geometry, a vector of length $\boldsymbol{Q} = (\pi, \pi)$ matches the two high density of states regions $(0, \pi)$ to $(\pi, 0)$ but not (π, π) to $(-\pi, -\pi)$. They point out that while the neutron peak is proportional to the susceptibility $\chi(\boldsymbol{q}, \omega)$ ARPES and tunnelling give the product of the coupling constant and the susceptibility $g^2_{\boldsymbol{kq}}\chi(\boldsymbol{q}, \omega)$.

Norman *et al* (1997b) also interpret the peak and hump structure of the ARPES spectra at $(\pi, 0)$ in the superconducting state in terms of a collective bosonic mode that appears in the superconducting state. They argue that the sharpness of the peak–dip structure is only consistent with a resonance peak and not just a step-like change in the lifetime of the carriers at 2Δ as suggested by Coffey and Coffey (1993). Norman *et al* find that by taking the

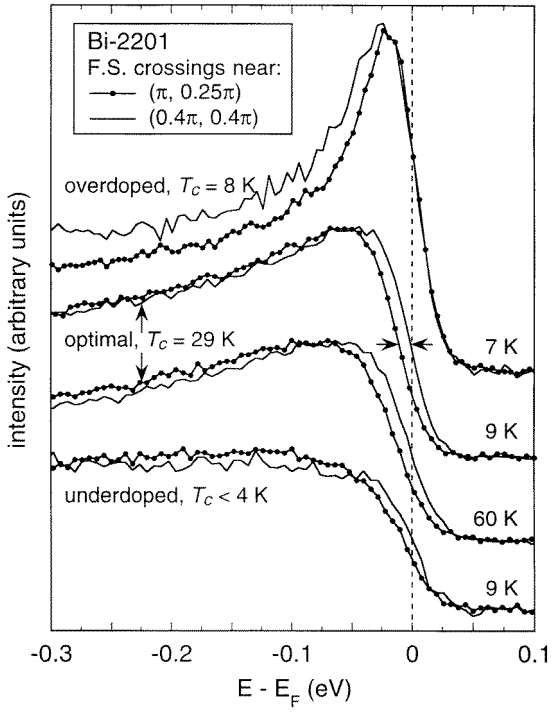

Figure 13. The pseudogap in single-layer Bi 2201. There is a clear leading-edge normal-state gap in the optimal and underdoped samples but no gap in the highly overdoped sample.

gap $\Delta = 32$ meV and $\Omega = 42$ meV they can account for the ARPES lineshape in the superconducting state. They argue that the collective mode is related to the 41 meV resonance seen in neutron scattering in the superconducting state of $YBa_2Cu_3O_{6+x}$ and suggest that a mode similar to the 41 meV resonance would also exist in Bi 2212. Related to these arguments is the discussion of the width of the 41 meV peak seen in neutron scattering by Morr and Pines (1998) who argue that heavy damping in the normal state is turned off when the gap in the excitations forms in the superconducting state.

Ino *et al* (1997) report on ARPES spectra in $La_{2-x}Sr_xCuO_4$ for both underdoped and overdoped samples. They find a remarkable change from an electron-like Fermi surface centred on Γ in the overdoped samples to a hole-like one in the underdoped materials. This occurs through a decrease in the energy of the states near $(\pi, 0)$ as the doping level is reduced. In the $x = 0.3$ samples the $(\pi, 0)$ states are *above* the Fermi surface whereas in the underdoped sample they form an extended saddle point about 100 meV *below* the Fermi surface. As figure 14 shows, this results in a transformation of the Fermi surface from electron-like, centred on $(0, 0)$, to hole-like, centred at (π, π). The authors contrast this 'high-energy pseudogap' of 100 meV with the low-energy pseudogap seen at the same $(\pi, 0)$ point in the Bi 2212 system. The authors also observe a superconducting gap at $(\pi, 0.2\pi)$ as a leading-edge shift of 10–15 meV and compare that with the Bi 2212 values of $\approx$25 meV. They suggest this gap may be consistent with d-wave symmetry. They observe no gap in the Fermi surface crossing along the $(0, 0)$–(π, π) line.

Fujimori *et al* (1998) discuss the change of chemical potential, μ, as determined by the shift of the La 3d and O 1s core levels in BIS spectroscopy. In a Fermi liquid the chemical

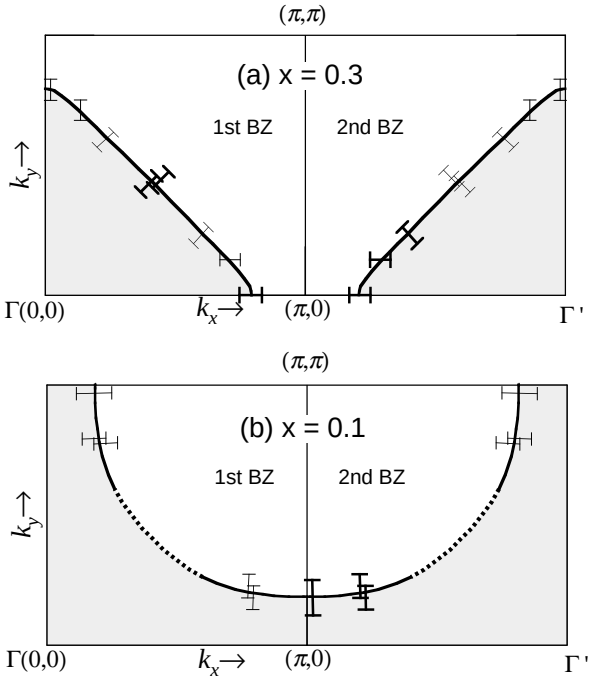

Figure 14. Fermi surface in LSCO. This material shows an electron-like Fermi surface in the underdoped state where the states at the $(\pi, 0)$ region lie above the Fermi surface. With reduced doping states at $(\pi, 0)$ drop 100 meV below the Fermi level, become filled, yielding a hole-like Fermi surface centred on (π, π).

potential shifts with doping in a characteristic way as the states near the Fermi level are filled. Fujimori *et al* find that this indeed happens in the overdoped case in $La_{2-x}Sr_xCuO_4$ but for $x < 0.15$ they find the chemical potential is pinned at the value for the insulating parent La_2CuO_4. The authors interpret this as evidence for the opening of a pseudogap that moves with μ as the doping proceeds.

3. Tunnelling spectroscopy

In the conventional BCS superconductors, tunnelling spectroscopy has been perhaps the most powerful tool used to investigate the electronic density of states near the Fermi level. Discovered by Giaver in 1960, it was used first to study the gap, and after further refinements, subtle changes in the density of states due to the electron–phonon interaction were found (Scalapino 1969) by inverting the tunnelling data to yield the spectrum of excitations responsible for superconducting pairing. For a recent review see Carbotte (1990).

The physics behind tunnelling spectroscopy is simple (Tinkham 1975). In SIN (superconductor–insulator–normal metal) tunnelling an oxide layer is grown on a superconductor which is then covered with a normal metal layer, figure 15. In thermodynamic equilibrium at zero degrees, the Fermi levels of the two systems are equal and no current flows through an external circuit connected between the metal and the superconductor. If an external positive voltage exceeding Δ/e is applied to the metal, electrons tunnel from the metal through the insulator to the unoccupied states of the superconductor. In a BCS superconductor there is

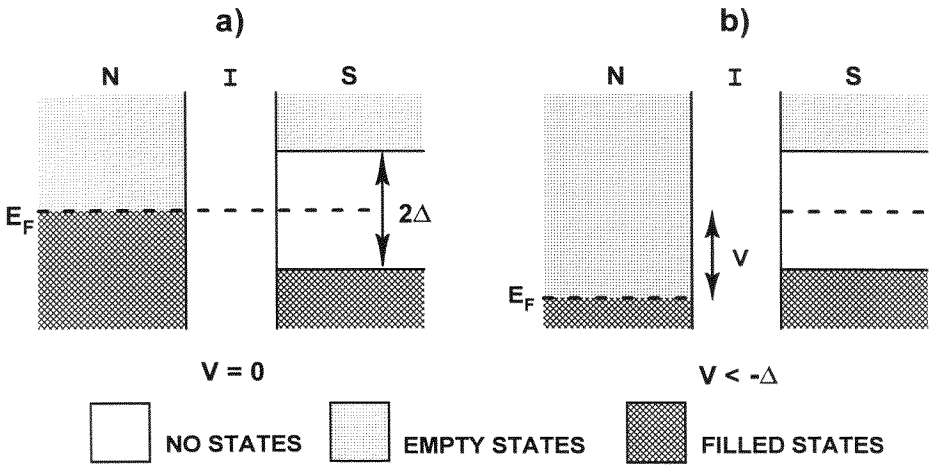

Figure 15. Tunnelling spectroscopy. In SNS tunnelling no current flows at zero-voltage difference between the normal metal and the superconductor (left panel). When the bias $V < -\Delta$ electrons from the filled states in the superconductor flow into the empty states of the metal above the Fermi level giving rise to a current proportional to the difference between V and Δ.

a peak in the density of states just above the gap edges. Therefore there will be a large peak in the tunnelling conductance as the bias voltage approaches the gap value, $eV = \Delta$. Conversely with negative bias, when $eV = -\Delta$, electrons will tunnel from the occupied states of the superconductor to the normal metal. Thus there will be a gap in the conductance of width 2Δ centred on the Fermi level at zero bias. In SIS tunnelling there is a superconductor on both sides of the barrier and the tunnelling current starts to flow when the bias $eV = \Delta_1 + \Delta_2$ where Δ_1 and Δ_2 are the gaps of the two superconductors.

In high-temperature superconductors, because of the short coherence length, the tunnelling electrons sample the density of states within a few atomic layers of the surface and the experiments are extremely sensitive to surface quality. The most reliable results have come from measurements where the tunnelling barrier has been prepared *in situ* by vacuum cleaving. The measurements are then carried out either by using a scanning tunnelling microscope tip at some distance above the surface (SIN vacuum tunnelling, Renner *et al* 1996, 1998) or by break-junction tunnelling where a crystal is broken in ultra-high vacuum to form a fresh surface and then the two pieces are allowed to come close enough for a tunnelling current to flow (SIS tunnelling, Mandrus *et al* 1991, 1993).

One of the earliest reports of a pseudogap in tunnelling spectroscopy is that of Tao *et al* (1997) who find a gap-like depression in the tunnelling conductance of Bi 2212 junctions in the normal state. The junctions were prepared by evaporating lead electrodes on cleaved faces on top of a natural insulating barrier. In the superconducting state they find results similar to those reported previously on this material: a depression of tunnelling conductance at low bias to 0.4–0.6 of the high bias value and a pile-up of conductance to peaks at $\approx \pm 35$ meV. The new result in this work is the observation that the depression in the tunnelling conductance remains in the normal state and, at least in one sample, can be traced all the way up to room temperature.

Renner *et al* (1998) report tunnelling into underdoped Bi2212 crystals cleaved in vacuum using a scanning tunnelling microscope (STM). They find reproducible voltage–current curves as the tip is scanned across the sample and suggest that many features previously observed

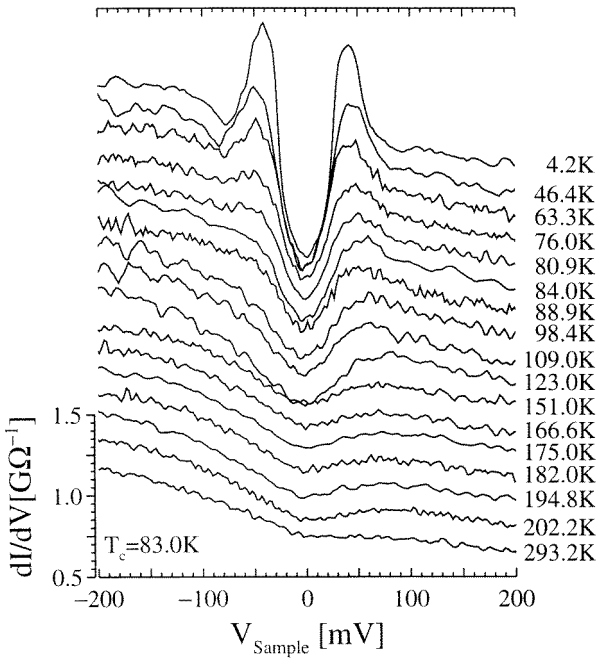

Figure 16. Tunnelling conductance for underdoped Bi2212. A gap-like feature at zero bias is seen to persist in the normal state which is direct evidence of a pseudogap in the tunnelling conductance. In the superconducting state a peak develops at ± 45 meV followed by a dip and a broad maximum. The gap frequency does not seem to be temperature dependent.

were due to spatial inhomogeneity. In regions that are uniform the tunnelling spectra are independent of bias voltage as the tip-to-sample distance is varied. As figure 16 shows, below the superconducting transition temperature they find a depression in the conductivity at zero bias and two symmetrically placed conductance peaks previously observed by several investigators in this material. The figure also shows that while the peaks disappear at T_c an inverted bell-like conductance depression remains in the normal state up to room temperature. The authors identify this conductance dip with the pseudogap. Finally there is an asymmetry with respect to the sign of the bias. When the bias is negative, corresponding to the removal of electrons from the sample (equivalent to ARPES where photoelectrons are removed, leaving a hole), a broad peak is seen in the spectrum at approximately 100 meV. This peak is not seen with positive bias. Also, there is some asymmetry in the disappearance of the sharp peaks: the positive bias peak persists into the normal state while the negative bias one vanishes at T_c.

As the temperature is raised, the magnitude of the gap in the superconducting state, as measured by the separation between the peaks, does not change. Renner *et al* confirm this by modelling the high-temperature spectrum by applying thermal broadening due to the Fermi function to the low-temperature spectrum (Renner *et al* 1996). Thus, unlike a BCS gap which closes as the temperature is raised, the gap magnitude is *temperature independent*. This is also true of the magnitude of the pseudogap which fills in with temperature but retains its frequency width up to room temperature.

While there is no change in peak separation with temperature, the magnitude of the gap does decrease as the *doping level* is increased, which is just the opposite to what one might expect for a superconductor where the ratio $2\Delta / kT_c$ would remain constant and the gap would

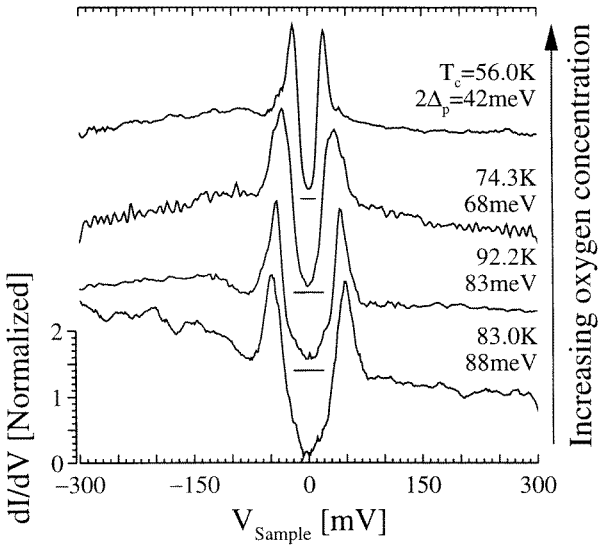

Figure 17. Doping dependence of tunnelling spectra measured at 4.2 K. The superconducting gap, as measured by the separation between the peaks, decreases in magnitude in the overdoped region (top two curves).

grow in proportion to T_c. As figure 17 shows, 2Δ falls from 88 meV (710 cm^{-1}) in the most underdoped sample with a T_c of 83.0 K to 42 meV (340 cm^{-1}) in the overdoped sample.

There is a close relationship between the superconducting gap, as represented by the conductance peaks, and the pseudogap as described by the depression of conductivity in the normal state. Both features are centred at zero bias, i.e. on the Fermi surface. The energy scales are similar and both scales are temperature independent. Furthermore, as the doping level is changed, both gaps scale in the same way in that their magnitude decreases with doping. It is important to note here that Ding *et al* (1997) report that in the ARPES spectra a similar parallel can be seen in the k dependence of the locus of minimum gap in the pseudogap and the superconducting gap—both seem to be tied to the Fermi surface.

Another parallel between the ARPES and the tunnelling results is the dip in the spectra seen in the superconducting state at a frequency of 2Δ above zero bias in SIN tunnelling. Figure 18 shows recent measurements in overdoped Bi 2212 by DeWilde *et al* (1998). The authors argue that since the peak is symmetrically placed and, as a function of doping, the dip scales with Δ, the superconducting gap determined from the conductance peaks and therefore the dip is not a band structure effect but is intimately associated with superconductivity. They note that Ω coincides with 2Δ, which is also seen in Pb where there is a feedback effect of a 2Δ electronic singularity on the phonon density of states, forming a singularity at $\Omega = 2\Delta$. This 4Δ feature was first observed in the optical conductivity of Pb by Farnworth and Timusk (1974) and has been discussed in detail in a high-T_c context recently by Coffey and Coffey (1993). It would occur at $eV = 2\Delta$ in SIN tunnelling. This view of the dip is related to the early interpretation of the dip in ARPES spectra discussed in section 2 and is in accord with the results of Renner *et al* (1998) who also note that, as a function of doping, the peak-to-dip distance tracks the gap, decreasing as the gap decreases with doping. The alternate explanation of the dip in terms of coupling to the (π, π) mode at 41 meV (whose frequency increases with doping) would predict an *increase* of the dip-to-peak distance with doping.

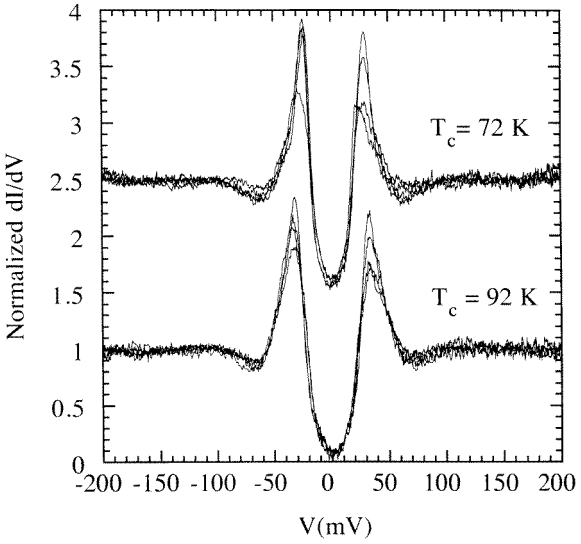

Figure 18. Tunnelling spectra in optimal and overdoped Bi 2212. The gap measured at 4.2 K increases as the doping level is reduced from overdoped (top curve) to underdoped (bottom curve). The dip is approximately symmetric, suggesting it is not a band structure effect but may instead be due to strong coupling effects.

4. Nuclear magnetic resonance

Magnetic resonance experiments were the first used to observe the pseudogap in underdoped YBCO. These experiments probe the spin channel as opposed to, say, optical conductivity which probes the charge channel. In a Fermi liquid one expects to observe the temperature-independent Pauli susceptibility. Instead, in the high-temperature superconductors a decrease in susceptibility with temperature is observed. This has been used to support the hypothesis of a spin gap (Warren *et al* 1989). Subsequent experiments have revealed that the pseudogap exists in both the spin and charge channels.

NMR is a versatile tool which allows one to probe the electronic state at different nuclear sites in the lattice as well as probe different parts of $\boldsymbol{q}$ space. As nuclear dipole moments are several orders of magnitude smaller than the Bohr magneton, nuclei are ideal probes of the electronic state. The Knight shift K_s is proportional to the real part of the susceptibility $\chi'(\boldsymbol{q} = 0, \omega)$, measuring the polarization of electrons by the applied magnetic field. The spin-lattice relaxation rate in the cuprates is dominated by antiferromagnetic (AF) spin fluctuations. For example, the spin-lattice relaxation rate for copper nuclei in the CuO_2 planes $1/^{63}T_1$ is enhanced by one to two orders of magnitude by these spin fluctuations. On the other hand, the relaxation rate $1/^{17}T_1$ seen by oxygen atoms in the plane, situated halfway between the copper sites, is barely enhanced. The spin-lattice relaxation rate is related to the susceptibility through

$$1/T_1 = \frac{k_B T}{4\mu_B^2 \hbar^2} \sum_{\boldsymbol{q}} |F(\boldsymbol{q})|^2 \chi''(\boldsymbol{q}, \omega)/\omega \tag{3}$$

where $F(\boldsymbol{q})$ is the form factor for the particular nuclear site. As $1/^{63}T_1$ is dominated by AF spin fluctuations it predominately probes $\boldsymbol{q} = \boldsymbol{Q} \equiv (\pi, \pi)$. Finally, the spin–spin relaxation rate $1/T_{2G}$ is related to $\chi'(\boldsymbol{q}, \omega)$.

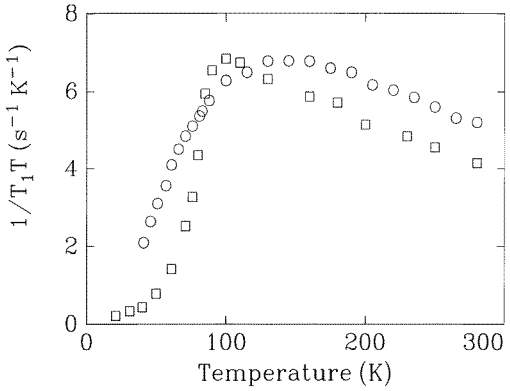

Figure 19. Planar ^{63}Cu spin-lattice relaxation rate in optimally doped $YBa_2Cu_3O_{6.95}$ (squares) and underdoped $YBa_2Cu_3O_{6.64}$ (circles). The pseudogap causes a suppression in the relaxation rate well above T_c.

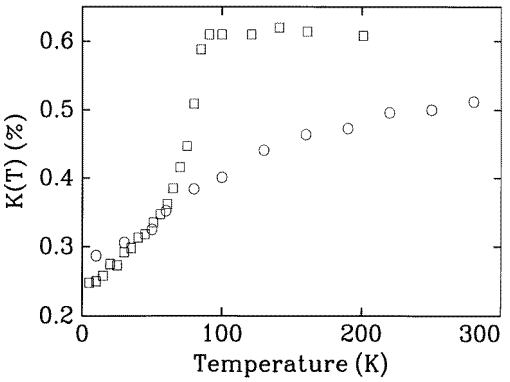

Figure 20. Planar ^{63}Cu Knight shift in $YBa_2Cu_3O_{6.95}$ (squares) and underdoped $YBa_2Cu_3O_{6.64}$ (circles). The normal-state susceptibility is temperature independent in the optimally doped compound but decreases with temperature in the underdoped compound.

In the context of a Fermi liquid the Knight shift is proportional to the density of states at the Fermi surface. The spin-lattice relaxation rate is dominated by electronic excitations. The pseudogap is observed in both the Knight shift and spin-lattice relaxation rate. Warren *et al* (1989) were the first to see the pseudogap in $1/^{63}T_1$ of underdoped YBCO. They suggested the possibility of spin pairing above T_c. Figure 19 displays the spin-relaxation rate in optimally doped YBCO and YBCO 6.7. As temperature decreases $1/T_1$ increases, as the AF spin coherence increases, until just above T_c in the optimally doped compound. On the other hand, for the underdoped compound, $1/T_1$ starts to decrease well above T_c. This is attributed to the presence of the pseudogap.

Walstedt *et al* (1990) have observed the pseudogap in $^{63}K_s$ of YBCO 6.7. As can be seen in figure 20 K_s drops to about 20% of its room temperature value at T_c, leaving a much smaller decrease in the superconducting state than for the optimally doped compound. Entry into the superconducting state is dramatic for YBCO 7.0 as the spins condense out into spin singlet pairs. YBCO 6.7, on the other hand, barely provides any hint of the superconducting transition in the Knight shift.

It is worth noting that if one views the pseudogap as a loss in density of states in the CuO_2 layers, then one would naturally expect it to be accompanied by a reduction in the AF spin fluctuations. This is particularly the case in a single-band model where the local moments on the copper sites are hybridized with the itinerant holes on the oxygen sites. From this perspective one should expect the temperature at which the pseudogap develops to be similar for the Knight shift and the relaxation rates.

Observation of the pseudogap is not constrained to copper nuclei. Alloul's group (Alloul

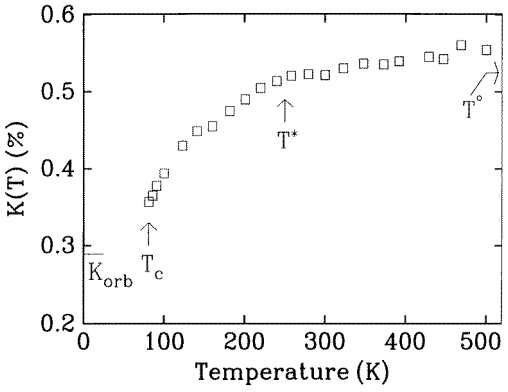

Figure 21. Crossover displayed in planar ^{63}Cu Knight shift in $YBa_2Cu_4O_8$. The upper crossover is taken from figure 23.

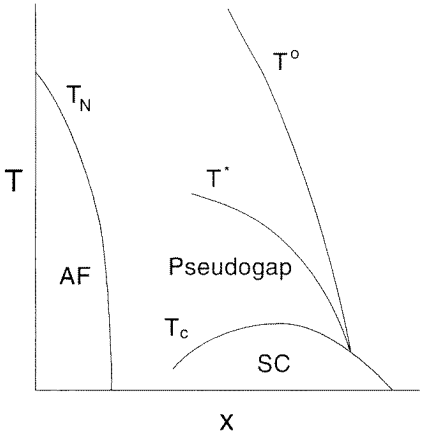

Figure 22. Pseudogap crossover temperatures (K) suggested from NMR data. Note that the crossover temperatures merge into T_c slightly into the overdoped region of the phase diagram.

et al 1989) have performed ^{89}Y NMR studies on underdoped YBCO which display the pseudogap. ^{17}O measurements on the planar oxygen sites by Takigawa *et al* (1991a) also show the pseudogap. These authors point out that the Knight shift for copper and oxygen have the same temperature dependence in the normal state. This suggests that a single-band model may apply where the Cu, O and Y nuclei all couple to the same $\chi(\boldsymbol{q}, \omega)$.

Many other underdoped compounds exhibit the pseudogap in their magnetic resonance properties. Some examples are the naturally underdoped and stoichiometric $YBa_2Cu_4O_8$ (Bankay *et al* 1994) and the related $Y_2Ba_4Cu_7O_{15}$ (Stern *et al* 1994), the two-layer bismuth compound (Walstedt *et al* 1991) and the mercury compounds (Julien *et al* 1996, Bobroff *et al* 1997). The pseudogap is observed in the Knight shift and relaxation rates of the planar copper and oxygen nuclei as well as in the nuclei situated between the CuO_2 planes in multilayer compounds.

Certain compounds exhibit crossovers in the pseudogap as a function of temperature. This is in contrast to others in which a smooth evolution with temperature is observed. The latter is typified by underdoped YBCO, illustrated in figure 20, whereas crossover temperatures can be discerned, for example, in YBCO 124 (Bankay *et al* 1994) displayed in figure 21. At the upper crossover temperature T° the Knight shift changes behaviour from being temperature independent to decreasing linearly with temperature below T°. Below the lower crossover temperature T^* the Knight shift decreases faster than linear with temperature. As we will discuss below, these two crossover temperatures may have their origin in different physical phenomena. Indeed, different scaling relations are observed in the relaxation rates delineated by T° and T^*.

The magnitude of the crossover temperatures increases with decreasing doping and is discussed below. Several slightly underdoped compounds have been observed with crossover temperatures much lower than those of YBCO 124. For example, the crossover temperatures of slightly underdoped $Pb_2Sr_2(Y,Ca)Cu_3O_{8+\delta}$ (Hsueh *et al* 1997) are about a factor of 2.5 lower than those of YBCO 124. Two other examples are slightly underdoped Bi 2212 (Walstedt *et al* 1991) and $Y_{0.95}Pr_{0.05}Ba_2Cu_3O_7$ (Reyes *et al* 1991). Optimally doped YBCO also exhibits crossover temperatures (Martindale *et al* 1996) not too far above T_c. This is consistent with the phase diagram in figure 22 where the crossover temperatures approach the superconductivity

Table 1. Pseudogap crossover temperatures (K) from NMR data.

		Knight shift		Relaxation rates	
	T_c	T^*	T°	T^*	T°
$YBa_2Cu_3O_{6.95}$[a]	92	110	150	—	—
$YBa_2Cu_4O_8$[b]	81	240	—	200	500
$Y_2Ba_4Cu_7O_{15}$[c]	93	190	250	130	250
$Pb_2Sr_2(Y,Ca)Cu_3O_{8+\delta}$[d]	80	100	180	140	—
$Bi_2Sr_2CaCu_2O_8$[e]	90	110	170	200	—
$HgBa_2Ca_2Cu_3O_{8+\delta}$[f]	115	250		250	—

[a] Martindale (1996).
[b] Corey (1996).
[c] Stern (1994, 1995).
[d] Hsueh (1997).
[e] Walstedt (1991).
[f] Julien (1996).

phase boundary on the overdoped side.

A common feature to the pseudogap observed in the slightly underdoped compounds is that the drop in the susceptibility in the normal state, as measured by the Knight shift, is less than that in the strongly underdoped compounds. This drop is smallest for the optimally doped YBCO. Thus as the doping is increased, the drop in the susceptibility in the normal state relative to that in the superconducting state decreases. In the overdoped region the pseudogap disappears; in this case the susceptibility drops only in the superconducting state.

Measurements of the pseudogap in the underdoped, three-layer mercury compound $HgBa_2Ca_2Cu_3O_{8+\delta}$ have been performed by Julien *et al* (1996). The lower crossover temperature T^* is detected in both the Knight shift and $1/^{63}T_1T$. As the authors point out, the value of $T^* = 250$ K is the largest reported to date and may indeed be related to the large value of $T_c = 115$ K.

Table 1 summarizes the crossover temperatures of various underdoped cuprates. Values of T^* and T° are presented from both Knight shift and relaxation data. Where available, the ratio $^{63}T_1T/^{63}T_{2G}^n$ is used, otherwise the point at which $^{63}T_1T$ breaks away from linearity is used to extract T^*. For comparison, T_c is also tabulated.

Comparing the Knight shift values of T^* with those obtained from the relaxation rates one sees that although they are comparable, they are nevertheless distinct. Thus the lower crossover temperature is not necessarily the same for the $\boldsymbol{q} = 0$ dynamic susceptibility as for the $\boldsymbol{q} = \boldsymbol{Q}$ dynamic susceptibility. This difference in values of T^* has been noted explicitly by Hsueh *et al* (1997). Many others have warned that one must be careful to distinguish between the $\boldsymbol{q} = 0$ and $\boldsymbol{q} = \boldsymbol{Q}$ regions of the susceptibility. Julien *et al* (1996) have noted that T° depends strongly on hole doping but is insensitive to Zn doping, whereas T^* is weakly dependent on hole doping but significantly suppressed by Zn doping. This suggests that the lower crossover temperature is related to magnetic phenomenon (e.g. spin gap) and that the upper crossover may be associated with a feature in the density of states. As we have noted in section 2, ARPES results also display a $\boldsymbol{q}$-dependent behaviour of the pseudogap.

There appears to be no strong connection between the presence of a pseudogap and the number of adjacent CuO_2 layers in the compound. Winzek *et al* (1993) have observed the pseudogap in the single-layer Hg-compound. More recently, Alloul's group (Bobroff *et al* 1997) has measured the ^{17}O Knight shift on the single-layer Hg-compound to find a pseudogap in the underdoped compound. The upper crossover temperature T° was observed with the

expected linear temperature dependence below T°. Itoh *et al* (1996) observed the pseudogap in the ^{63}Cu relaxation rates of $HgBa_2CuO_{4+\delta}$ as well. Another distinct case to consider is a three-layer compound where a pure bilayer coupling model (Millis *et al* 1993) would have a different dynamic susceptibility in the inner and sandwiching layers. Measurements of $1/^{63}T_1T$ in $HgBa_2Ca_2Cu_3O_{8+\delta}$ reveal that the two relaxation rates are identical. Thus it would seem that models of the pseudogap based exclusively on bilayer coupling are ruled out.

The peculiar behaviour of the lanthanum compound warrants special mention. The temperature dependence of the spin susceptibility suggests that a pseudogap may be present in the underdoped lanthanum compound. On the other hand the copper spin-lattice relaxation rate (Ohsugi *et al* 1991) shows no sign of a pseudogap for any strontium concentration between $0.075 \leqslant x \leqslant 0.15$. Further discussion on this compound appears below in sections 5 and 11.

Chakravarty *et al* (1989) have shown that the $S = \frac{1}{2}$ two-dimensional Heisenberg antiferromagnet crosses over from a mean-field state with a dynamical critical exponent of $z = 2$ to a quantum critical state with $z = 1$. Barzykin and Pines (1995) have extended this framework into the doped region of the phase diagram. Here one expects a crossover from mean-field behaviour with $z = 2$ to a pseudoscaling regime with $z = 1$ at T° followed by a crossover to a quantum-disordered state at T^*. These scaling relations have been observed in YBCO 124 by Corey *et al* (1996). Above T° the ratio $^{63}T_1T/^{63}T_{2G}^2$, which is dominated by $\boldsymbol{q} = \boldsymbol{Q}$, is found to be temperature independent (figure 23(*a*)), the same as for $z = 2$ scaling. Between T° and T^*, on the other hand, the ratio $^{63}T_1T/^{63}T_{2G}$ is temperature independent (figure 23(*b*)), consistent with $z = 1$ scaling. This temperature independence of $^{63}T_1T/^{63}T_{2G}$ above T^* has also been observed in $HgBa_2Ca_2Cu_3O_{8+\delta}$ (Julien *et al* 1996). A more thorough description of these scaling relations is found in the theory section, section 10.

Williams *et al* (1997) have fit planar oxygen Knight-shift data of several compounds to discern whether an s- or d-wave gap was applicable in the normal and superconducting states. The authors found that a d-wave model for both the superconducting gap and the pseudogap fit better than an s-wave model. Although not as direct a measurement, this is consistent with the ARPES results on the symmetry of the gaps.

Impurities not only affect superconductivity but also the pseudogap. Many studies have revealed Zn to be more effective at suppressing T_c than Ni. This may be related to the local moment associated with the Zn impurity in underdoped materials (Alloul *et al* 1991, Mahajan 1994). Zheng *et al* (1993, 1996) have investigated the Zn substituted YBCO 124 compound. They have monitored the pseudogap with both the Knight shift and spin-lattice relaxation rate of the planar ^{63}Cu nuclei. The crossover temperature T^* in $1/^{63}T_1T$ decreases as the Zn concentration is increased. With 1% Zn the effect of the pseudogap is completely suppressed, i.e. $T^* < T_c$. Further increasing Zn impurities to 2% increases $1/^{63}T_1T$ above the rate observed in pure YBCO 124 just above T_c. Most striking is the observation that the Knight shift is *unaffected* by Zn doping. Thus, the pseudogap in the $\boldsymbol{q} = \boldsymbol{Q}$ region of the susceptibility is strongly affected in sharp contrast to the $\boldsymbol{q} = 0$ region which is not discernibly affected by Zn impurities.

Suppression of the pseudogap in YBCO 124 by Zn impurities has been observed with other techniques. The deviation from T-linear dependence of the resistivity is also a signature of the pseudogap. This deviation is suppressed upon Zn doping of YBCO 124 (Miyatake *et al* 1991). Optical conductivity measurements also show a suppression of the pseudogap with Zn doping (Puchkov *et al* 1996a). As antiparamagnon scattering is largely responsible for the conductivity (Statt and Griffin 1992, 1993), one would expect the behaviour near $\boldsymbol{q} = \boldsymbol{Q}$ to dominate these measurements. Thus the suppression of the pseudogap observed with these various measurements is consistent.

Zheng *et al* (1996) have studied the effects of doping YBCO 124 and YBCO 6.7 with Zn

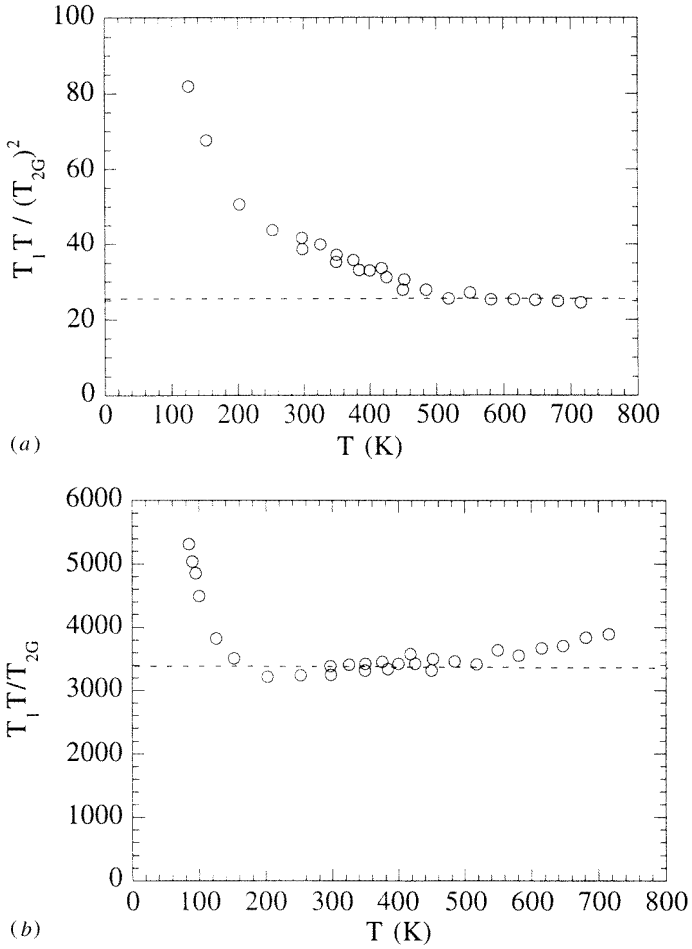

Figure 23. Relaxation rate ratios in $YBa_2Cu_4O_8$. (*a*) ${}^{63}T_1T/{}^{63}T_{2G}^2$, (*b*) ${}^{63}T_1T/{}^{63}T_{2G}$. These two ratios clearly indicate the presence of two distinct crossover temperatures.

and Ni impurities. They find that Zn is much more effective at suppressing the pseudogap than Ni. A plot of T_c versus impurity concentration x in YBCO 124 shows that Zn is about three times more effective in depressing T_c than Ni. A similar plot of T^* versus x illustrates the suppression of the pseudogap with doping. In this case Zn is found to be four times as effective in suppressing T^* as Ni. Thus it appears that Zn induces local moments in the CuO_2 plane which strongly affects the local antiferromagnetic correlations. This in turn suppresses T_c and the pseudogap at $\boldsymbol{q} = \boldsymbol{Q}$. On the other hand, doping has little or no effect on the $\boldsymbol{q} = 0$ susceptibility.

In summary, magnetic resonance experiments have been used to probe the nature of the pseudogap in the spin channel. Two crossover temperatures have been observed. The upper crossover temperature T° may very well be associated with a phenomenon affecting the density of states whereas the lower crossover temperature T^* seems to be a result of a gap in the antiferromagnetic excitations. These conclusions are based, in part, on differences noted in the behaviour of the dynamic susceptibility at $\boldsymbol{q} = 0$ and $\boldsymbol{q} = \boldsymbol{Q}$. They are also consistent with the ARPES results showing that the pseudogap opens up in the $(\pi, 0)$ region of the Fermi surface leaving an ungapped arc centred about $(\pi/2, \pi/2)$.

5. Transport properties

Within the Fermi liquid picture a gap or a partial gap in the density of states near the Fermi level can affect the electrical conductivity in two ways: through the reduction of the number of current-carrying states as a gap forms, and secondly, if the current carriers are scattered by electronic excitations, through the reduction in the density of such excitations. The standard formula for the current $\boldsymbol{J}$ in the presence of an electric field $\boldsymbol{E}$ (Ashcroft and Mermin 1996):

$$\boldsymbol{J} = \boldsymbol{\sigma} \cdot \boldsymbol{E} = \frac{e^2}{4\pi^3} \int \frac{\tau_k \boldsymbol{v}_k \boldsymbol{v}_k}{1 - \mathrm{i}\tau_k \omega} \frac{\mathrm{d}S_F}{v_k} \cdot \boldsymbol{E}_0 \tag{4}$$

where $\boldsymbol{\sigma}$ is the conductivity tensor, $\boldsymbol{E}_0$ the applied field, τ_k the lifetime of state $\boldsymbol{k}$ and $\boldsymbol{v}_k$ the velocity of state $\boldsymbol{k}$. The integration is carried out over the Fermi surface. The conductivity is proportional to the component of the velocity in the direction of the applied field $\boldsymbol{E}$ averaged over the Fermi surface and it is also proportional to the factor τ_k which can vary over the Fermi surface independently.

If one further assumes that τ is a constant one gets the classical Drude formula for the conductivity:

$$\sigma(\omega) = \frac{1}{4\pi} \frac{\omega_p^2}{1/\tau - \mathrm{i}\omega} \tag{5}$$

which yields a Lorentzian peak centred at zero frequency with an oscillator strength $\omega_p^2/8$, where $\omega_p^2 = e^2/(3\pi^2\hbar) \int \boldsymbol{v} \cdot \mathrm{d}\boldsymbol{S}_F$ and $\boldsymbol{v}$ is the electron velocity and $\boldsymbol{S}_F$ is an element of Fermi surface. For a spherical Fermi surface $\omega_p^2 = 4\pi n e^2/m_e$, where n is the free-carrier density and m_e is the electronic band mass. The imaginary part of $\sigma(\omega)$ is just the real part multiplied by $\omega\tau$.

The simple Drude formula is widely used to describe the optical conductivity of metals but it is only valid for impurity scattering where τ is a frequency-independent constant. If the processes that limit the lifetime τ are inelastic τ becomes frequency dependent, and to preserve the causal nature of $\sigma(\omega, T)$, it is necessary to generalize the Drude formula. This is usually done through the extended Drude model or memory function technique (Mori 1965, Götze and Wölfle 1972, Allen and Mikkelsen 1976, Puchkov *et al* 1996a). The extended Drude formula is written as:

$$\sigma(\omega, T) = \frac{1}{4\pi} \frac{\omega_p^2}{1/\tau(\omega, T) - \mathrm{i}\omega[1 + \lambda(\omega, T)]} \tag{6}$$

where $1/\tau(\omega, T)$ describes the frequency-dependent scattering rate and $\lambda(\omega, T)$ can be viewed as a mass enhancement of the electronic excitations due to the interactions.

One can solve for $1/\tau(\omega)$ and $1 + \lambda(\omega)$ in terms of the experimentally determined optical conductivity to find

$$1/\tau(\omega) = \frac{\omega_p^2}{4\pi} \mathrm{Re}\left(\frac{1}{\sigma(\omega)}\right). \tag{7}$$

The dc resistivity is the zero-frequency limit $\rho_{dc}(T) = 1/\sigma_{dc}(T) = m_e/(\tau(T)ne^2)$ since $\sigma(\omega, T)$ is real in the zero-frequency limit.

The mass enhancement factor, $\lambda(\omega)$, is given as the imaginary part of $1/\sigma(\omega)$:

$$1 + \lambda(\omega) = -\frac{\omega_p^2}{4\pi} \frac{1}{\omega} \mathrm{Im}\left(\frac{1}{\sigma(\omega)}\right). \tag{8}$$

The total plasma frequency, ω_p^2, can be can be found from the sum rule $\int_0^\infty \sigma_1(\omega)\,\mathrm{d}\omega = \omega_p^2/8$.

Memory-function analysis has been widely used to describe electron–phonon scattering (Allen 1971). Shulga *et al* (1991) give the following expression for $1/\tau(\omega, T)$:

$$\frac{1}{\tau}(\omega, T) = \frac{\pi}{\omega}\int_0^\infty \mathrm{d}\Omega\, \alpha^2_{tr}(\Omega)F(\Omega)\left[2\omega \coth\left(\frac{\Omega}{2T}\right) - (\omega+\Omega)\coth\left(\frac{\omega+\Omega}{2T}\right) + (\omega-\Omega)\coth\left(\frac{\omega-\Omega}{2T}\right)\right] + \frac{1}{\tau_{\mathrm{imp}}}. \tag{9}$$

Here $\alpha^2_{tr}(\Omega)F(\Omega)$ is a weighted phonon density of states and T is the temperature measured in frequency units. The last term in equation (9) represents impurity scattering.

The quantity $\alpha^2_{tr}(\Omega)F(\Omega)$ is closely related to $\alpha^2(\Omega)F(\Omega)$ obtained from the inversion of tunnelling spectra in BCS superconductors (Allen 1971) and can be found by inverting the optical conductivity spectra at $T = 0$ (Allen 1971, Farnworth and Timusk 1974, Marsiglio *et al* 1998) to yield:

$$\alpha^2(\Omega)F(\Omega) = \frac{1}{2\pi\omega}\frac{\partial}{\partial\omega}\left[\omega^2\frac{\partial}{\partial\omega}\frac{1}{\tau(\omega)}\right]. \tag{10}$$

The presence of the second derivatives in the expression places severe demands on the signal to noise ratio of the $1/\tau(\omega)$ experimental spectrum. The method has been applied with considerable success for BCS superconductors to extract $\alpha^2(\Omega)F(\Omega)$ and most recently to K_3C_{60} (Marsiglio *et al* 1998). It has not been explored to date for the high-T_c cuprates.

We will first discuss the coherent ab-plane conductivity. The conductivity normal to the copper–oxygen planes, the c-axis conductivity, will be discussed separately below.

5.1. dc resistivity

One of the striking properties of the high-temperature superconductors is the remarkable temperature dependence of the normal-state resistivity. Seen most clearly in optimally doped materials, the variation is linear with temperature, extending from 10–1000 K and extrapolating to zero resistance at zero degrees. This singular behaviour (Gurvich and Fiory 1987, Martin *et al* 1990) is to be contrasted with the behaviour in conventional, good metals: where the resistivity is linear only over a limited range of temperatures, has an intercept on the temperature axis at some fraction of the Debye temperature and saturates at high temperature. The saturation occurs when the inelastic mean-free path approaches the lattice spacing, the Ioffe–Rigel criterion, which in two-dimensions reads $\rho = \rho_M/k_F l$ where $\rho_M = (h/e^2)d$, where d is the interplane distance and l must be larger than the CuO bond length $a_0/2$. For a Fermi surface with $k_F \approx \pi/a$ this yields a resistivity that saturates at $\approx$1 mΩ cm. It is clearly illustrated in figure 24, from the work of Takagi *et al* (1992), that the resistivity of optimally doped $La_{2-x}Sr_xCuO_4$ shows no sign of saturation at this value and in the underdoped materials appears to be much higher than what is allowed by the Ioffe–Rigel limit.

In underdoped materials, the presence of the pseudogap leads to striking deviations from this simple linear behaviour. Bucher *et al* (1993) observe a reduced resistivity in $YBa_2Cu_4O_8$ below T^*, near the temperature where the pseudogap, as seen by NMR, opened. The double chain YBCO 124 is an almost ideal system for the study of the pseudogap phenomenon. It is simultaneously underdoped, stoichiometric with a fixed doping level and naturally untwinned (Bucher *et al* 1993). By measuring the resistivity with currents normal to the chains it is, to a large extent, possible to suppress the chain response. As figure 25 shows, the resistivity of $YBa_2Cu_4O_8$ is linear at high temperature with a slight positive intercept but has a clear break in slope below 200 K. The authors point out that the temperature where this happens is correlated with the NMR pseudogap. The Knight shift has its lower crossover temperature

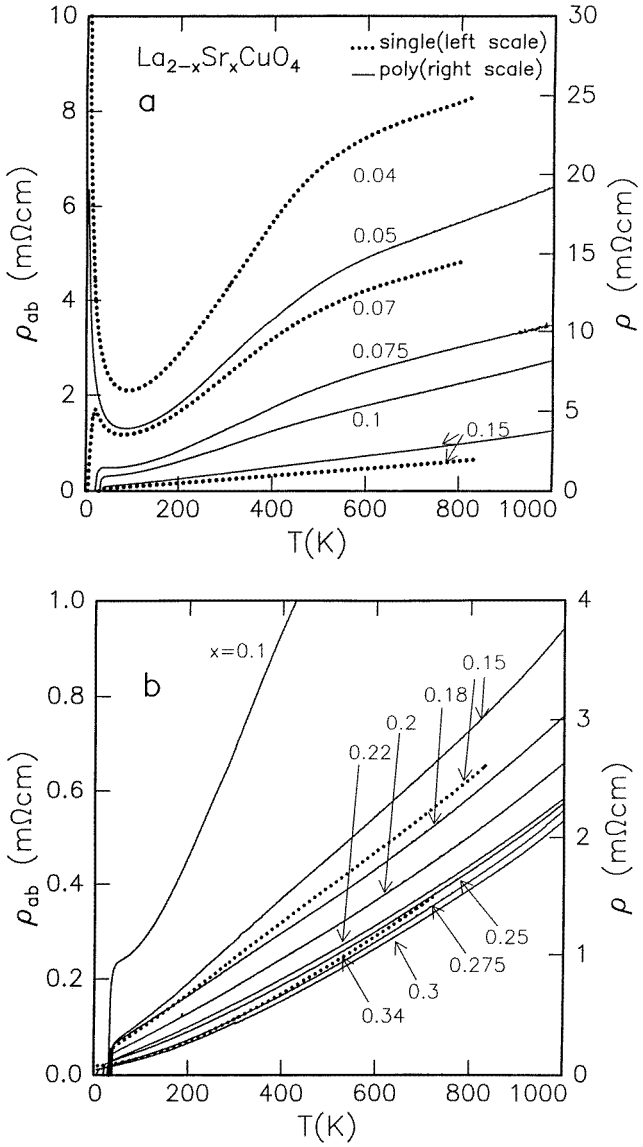

Figure 24. Temperature dependence of the resistivity of $La_{2-x}Sr_xCuO_4$ at various doping levels: underdoped (top panel), and optimal and overdoped (lower panel). Both single crystals and polycrystalline films are shown. There is a drop in resistivity at a temperature T^* due to reduced scattering as the result of the formation of the pseudogap.

below ≈250 K and the spin-lattice relaxation time $1/T_1T$ below ≈200 K. Thus the resistivity anomaly coincides roughly with these two temperatures and Bucher *et al* suggest that the decrease in resistivity below 180 K is caused by the reduced scattering by spin fluctuations resulting from the opening of the gap in the spin-excitation spectrum.

A complete study of the doping dependence of the characteristic temperature T^* was done for $La_{2-x}Sr_xCuO_4$ (Takagi *et al* 1992, Batlogg *et al* 1994). Figure 24 (upper panel) shows the resistivity data for a series of Sr compositions. At the lowest temperatures $\rho_{ab}(T)$

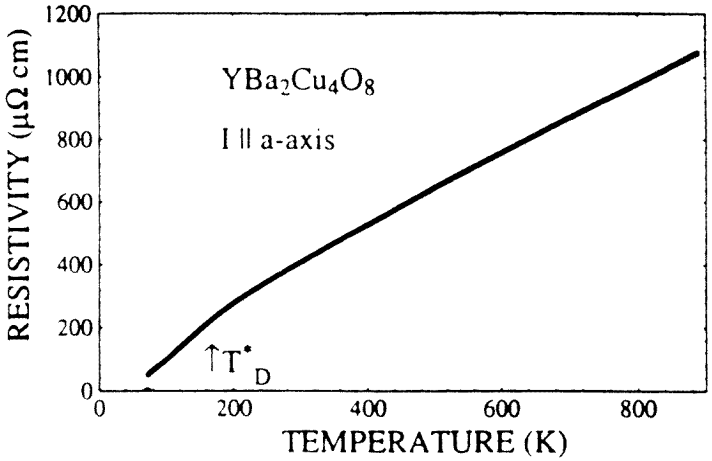

Figure 25. Formation of the pseudogap state in the resistivity of $YBa_2Cu_4O_8$. This naturally underdoped material shows the presence of a pseudogap below 200 K. Here the dc resistivity drops below the linear dependence set at higher temperatures.

shows 'semiconducting' behaviour with the resistivity decreasing with temperature, a signature of localization. At intermediate temperatures, the resistivity increases superlinearly up to a temperature T^* where there is a clear break in slope and the temperature dependence becomes approximately linear. Batlogg *et al* use the variation of T^* with x to define a boundary of the low-temperature 'pseudogap' phase. This phase diagram is shown in figure 26 from Batlogg *et al* (1994) with $1/\tau$ data from Startseva *et al* (1998a, b).

Deviations from T-linear resistivity in $YBa_2Cu_3O_{6+x}$ have been investigated by Ito *et al* (1993), Carrington *et al* (1993) and Takenaka *et al* (1994). A systematic depression of $\rho(T)$ is found below the linear trend set at high temperature. The crossover temperature T^* decreases as the doping level rises much in the same way as it does in the $La_{2-x}Sr_xCuO_4$ system. Figure 27 from Ito *et al* (1993) shows a plot of $(\rho_{ab}(T) - \rho_{ab}(0))/\alpha T$ where $\rho_{ab}(0))/\alpha T$ is the $T = 0$ intercept of the extrapolated T-linear high-temperature curve and α the slope of the linear part of the resistivity. It is clear from the figure that a temperature T^* can be defined from the deviations from the linear variation as the curves fall below unity. Ito *et al* suggest that the reduced scattering below T^* is the result of the development of the pseudogap as seen in the NMR Knight shift and spin-relaxation rate as discussed in section 4.

The inset in figure 27 shows that both the inverse slope and the Drude weight vary linearly with the doping level (Orenstein *et al* 1990). The authors suggest that since $\rho_{ab} = (4\pi/\omega_{pD}^2)\tau^{-1}$, where ω_{pD}^2 is the Drude weight and τ^{-1} the scattering rate, the scattering rate is independent of doping level in the underdoped region and all the variation of the in-plane resistivity arises from the changing Drude weight. This suggestion is in approximate agreement with the optical results reviewed by Puchkov *et al* (1996a) where the 300 K scattering rate for a large variety of systems with different doping levels was found to be $\approx 1050 \pm 200$ cm^{-1} (130 ± 25 meV).

The measurements of Ito *et al* (1996) were done mainly on untwinned single crystals of $YBa_2Cu_3O_{6+x}$ with some checks on detwinned samples to show that there was relatively little ab contribution from the chains. This is a little surprising since it has been shown by Basov *et al* (1995) that in very pure materials where the copper oxygen chains are intact, the chain contribution is very large. This suggests that the crystals of Ito *et al* contained a substantial

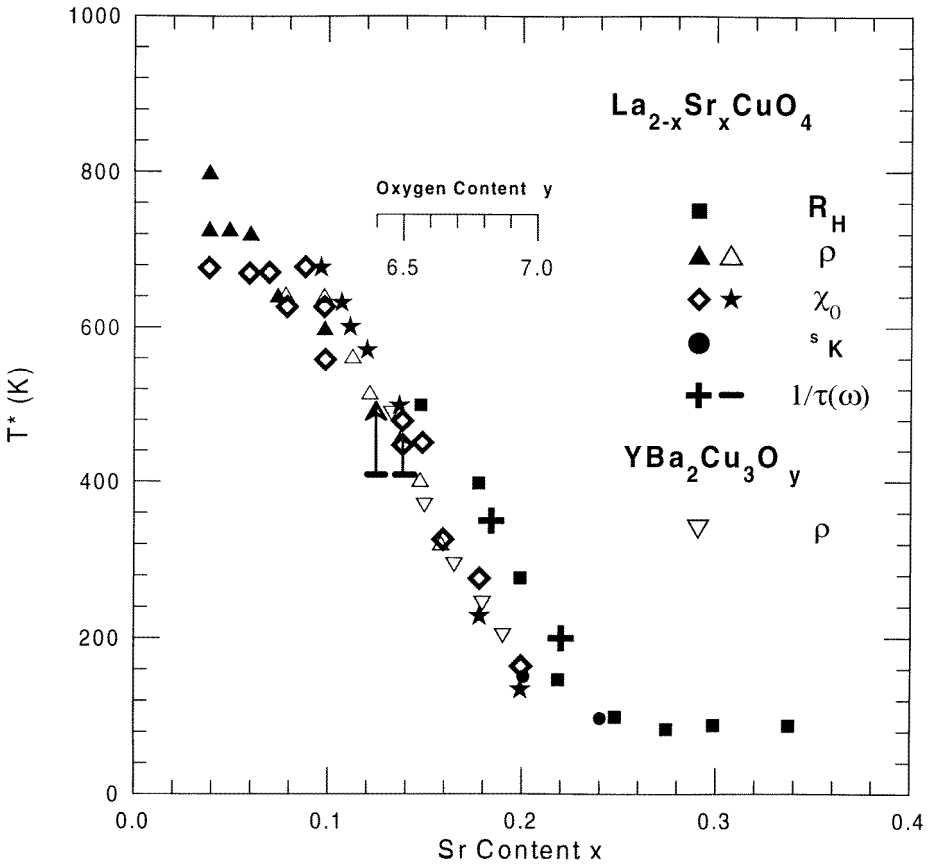

Figure 26. Variation of T^* with doping for $La_{2-x}Sr_xCuO_4$ as measured by various probes. The full squares denote the temperature below which the Hall coefficient has a rapid temperature dependence. The open circles refer to maxima in the static susceptibility $\chi(T)$ and the full circles the temperature where the Knight shift starts to decrease. The triangles refer to the temperature where there is a slope change in the dc resistivity, the crosses infrared measurements of $1/\tau$ supression and the horizonatal lines to lower limits of infrared data.

concentration of chain-breaking defects which acts to localize the chain conductivity at low frequencies. However, from a comparison with YBCO 124 untwinned measurements of Bucher *et al* and the infrared work of Basov *et al*, there is good reason to conclude that the data of Ito *et al* do indeed represent the properties of the copper–oxygen plane.

Underdoped Hg 1223 (Fukuoka *et al* 1997) shows very similar deviations from the T-linear law. The optimally doped sample, the one with the maximum T_c, has a deviation from the linear relationship at $T^* \approx 200$ K. For the most underdoped sample $T^* = 280$ K.

Another remarkable property of the normal state in high-temperature superconductors is the temperature-dependent Hall coefficient. In a normal metal the Hall coefficient $R_H = E_y/J_xB = -1/ne$ is a constant since it only depends on the carrier concentration, which in a metal is temperature independent. Hwang *et al* (1994) studied the in-plane Hall coefficent as a function of doping in $La_{2-x}Sr_xCuO_4$and found that this anomalous temperature dependence is confined to the low-temperature, low-doping region of the phase diagram where the NMR spin gap exists. Figure 26 shows (full squares) the temperatures T^* below which the Hall coefficient is temperature dependent. Above T^* the Hall coefficient R_H approaches a

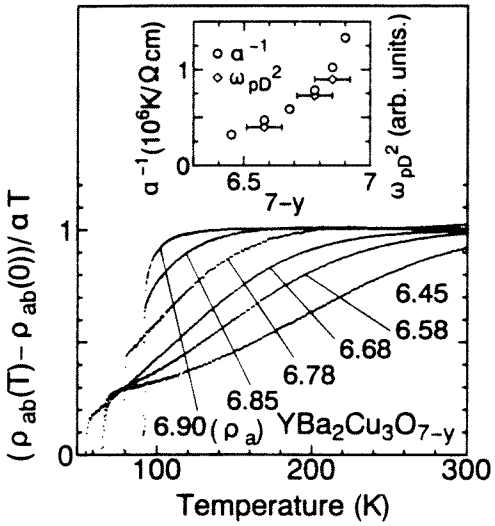

Figure 27. dc resistivity of $YBa_2Cu_3O_{6+x}$ at various doping levels plotted to show the deviation from the high-temperature linear variation, unity on this plot. A pseudogap onset temperature can be defined from this plot. The inset shows the variation of the Drude plasma frequency with doping along with the slope of the resistivity.

temperature-independent constant value. Similar effects in the Hall angle at T^* were seen in YBCO 124 by Bucher *et al* (1993).

5.2. The ab-plane optical conductivity

We now turn to the evidence for the pseudogap from an analysis of the optical conductivity. Much of this work has been reviewed by Puchkov *et al* (1996a) and Basov and Timusk (1998). Here we will briefly summarize this work and update it with recent results.

The optical conductivity $\sigma(\omega, T)$ offers several advantages over the dc resistivity which is the zero-frequency limit of $1/\sigma(\omega, T)$. By extending the measurements to finite frequencies one can separate the factors Ω_p^2 and τ in the Drude formula and investigate their frequency dependence. Experimental problems with electrical contacts are eliminated and accurate absolute values are easily obtained without the need for precision measurements of the geometries of submillimetre size samples. However, when the crystals lack natural shiny growth faces they have to be polished which introduces the possibility of damage.

It was clear from the earliest work on the optical properties of cuprates that their infrared reflectance spectra did not resemble those of simple metals which are basically flat from dc to the plasma frequency. Instead, there was a knee-like onset of strong absorption in the 500 cm^{-1} region which was present in the normal-state spectra in all the cuprates. Some of this work is reviewed by Puchkov *et al* (1996a) and by Basov and Timusk (1998). When the NMR measurements began to be interpreted in terms of a spin gap it was also conjectured that this feature was associated with the spin gap (Orenstein *et al* 1990, Rotter *et al* 1991) This suggestion was based on the observation that the 500 cm^{-1} structure was seen in the temperature and doping range that matched T^*, the crossover temperature where the spin gap appeared.

Most of the early analysis of the optical properties was focused on a study of the optical conductivity $\sigma(\omega, T)$ with an aim to find a conductivity gap such as the one seen in dirty limit

BCS superconductors (Mattis and Bardeen 1958). However, in a coherent system dominated by inelastic scattering, one does not expect to see a gap in the conductivity if there is a pseudogap in the density of states. In this clean limit scenario the Drude peak narrows and there will be a shift of spectral weight from the Drude peak to an incoherent sideband at the frequency of the excitations. These processes result in changes to the simple Drude line shape and are best described by the extended Drude model, first used to discuss single crystal high-T_c spectra by Thomas *et al* (1988).

Basov *et al* (1996) pointed out that the scattering rate $1/\tau$, as determined from the extended Drude analysis of reflectance spectra, provided clear evidence of the pseudogap in the transport properties of underdoped YBCO 6.6 and the naturally underdoped double chain material YBCO 124 (Basov *et al* 1996). Figure 28 shows the scattering rate in YBCO 124 as a function of frequency at three temperatures. At 300 K, well above T^*, the scattering rate has a characteristic linear frequency dependence with a rather large zero-frequency intercept. At 85 K, still in the normal state, a gap-like depression in the scattering is seen below 750 cm^{-1}. At 10 K, in the superconducting state, there is a further sharpening of the gap-like spectrum. The effective mass, shown in the lower panel of figure 28, develops a resonance in the superconducting state at 550 cm^{-1}.

These observations of a pseudogap in the scattering rate of YBCO 124 in the normal state at 85 K are in agreement with other evidence for a pseudogap in this material. Bucher *et al* (1993) find a break in the dc resistivity at 160 K and Zimmermann *et al* (1989, 1990) find a spin gap by NMR opening at $\approx$160 K in polycrystalline c-axis oriented YBCO 124.

The pseudogap in Bi 2212 has received the most attention through the extensive angle-resolved photoemission work discussed in detail in section 2. Puchkov *et al* (1996c) reported on $\sigma(\omega, T)$ in crystals from the same source as those used in the some of the photoemission work. They found strong evidence for a pseudogap in several underdoped samples of this material as well as in some of the slightly overdoped ones. Figure 29 shows the frequency-dependent scattering rate at a series of temperatures. At high frequencies, $\omega > 700$ cm^{-1}, the frequency dependence is approximately linear but there is no temperature dependence. At low frequencies, for $\omega < 700$ cm^{-1}, there is a pronounced temperature dependence in the form of a gap-like depression that starts below 150 K, well above the superconducting transition temperature of 67 K.

Recently, Startseva *et al* (1998a, b) have shown that a pseudogap can also be seen below a temperature T^* which is well above room temperature in several underdoped and slightly overdoped samples of LSCO. The gap is defined as a region of depressed scattering below the high-frequency linear behaviour. As in the case of the two plane materials, $1/\tau(\omega)$ is temperature independent in the pseudogap temperature region, i.e. $T < T^*$. Startseva *et al* find that above T^* a temperature dependence *does* appear at all frequencies and the linear curves move parallel to one another as the temperature is raised. This is illustrated in figure 30.

The scattering rates of the optimally doped YBCO and Tl 2201 do not show any evidence of a pseudogap in the normal state. However, below the superconducting transition temperature a gap-like depression appears which is very similar to that seen in the normal state in the underdoped materials. There are some differences, however, between the spectra at optimal doping below T_c and the spectra of underdoped samples below T^*. First, there is an overshoot in the $1/\tau$ spectra as shown in figure 31. Secondly, there is a slight reduction of slope as the temperature is raised above T_c.

One should note that the YBCO 123 and Tl 2201 spectra in figure 31 are very similar. Yet they refer to HTSC materials that are very different in many ways. YBCO 123 is a two-plane material with a copper–oxygen chain layer, while Tl 2201 is a single-plane material with thallium oxide layers. The almost identical scattering-rate spectra suggest that the properties

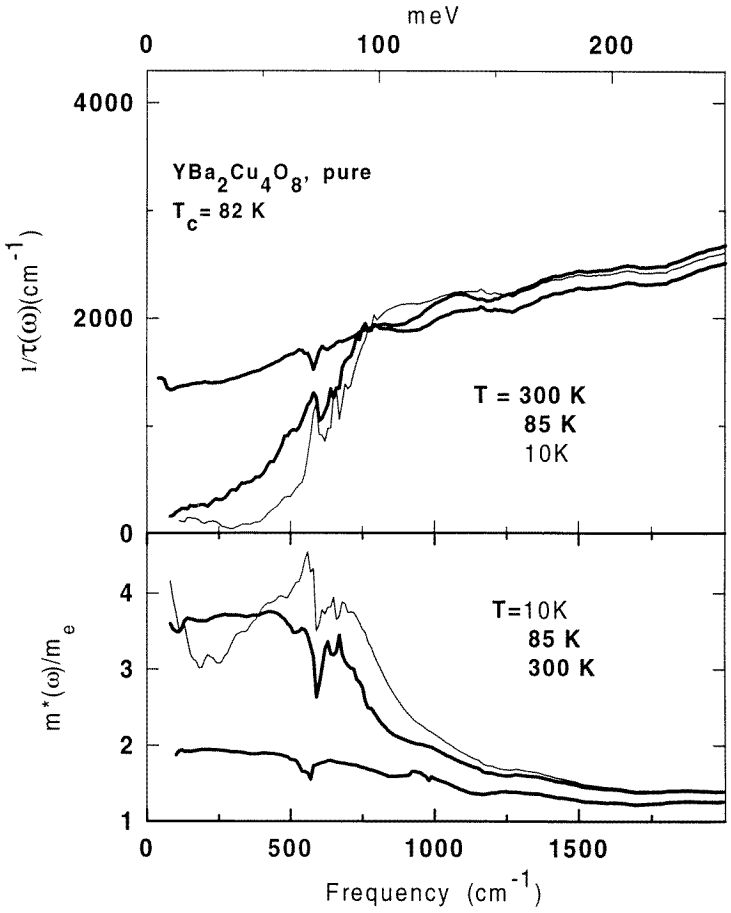

Figure 28. The frequency-dependent scattering rate and the effective mass of $YBa_2Cu_4O_8$. The scattering rate varies linearly at room temperature but develops a gap like depression in the normal state. At the same time the effective mass of the carriers develops a resonance peak at $\approx$600 cm^{-1} (75 meV).

displayed here are those of the copper–oxygen plane without significant contamination from interplane interactions or other constituents in the unit cell such as the charge transfer layers. However, there is an overall change in the magnitude of the scattering rates: in the one-plane material the scattering is a factor of two weaker at all temperatures and frequencies. In contrast, the Bi 2212 system shows vestiges of the pseudogap at optimal doping in the form of a clear break in the scattering at 90 K in the normal state.

Finally, we address the question of the relationship between the pseudogap seen in the underdoped materials in the normal state well above T_c and the superconducting gap that seems to appear at T_c in the optimally doped samples. Figure 32 shows the scattering-rate spectrum of an underdoped YBCO 6.6 crystal and for comparison an optimally doped crystal of the same material YBCO 6.95. It is clear that the general shape of the scattering-rate suppression is similar in the pseudogap state and in the superconducting state of the optimally doped crystal. There are, however, important differences. There is an overshoot of the scattering rate in the optimally doped material whereas in the underdoped sample there is a monotonic increase in scattering with frequency. It is not possible to get such a steep decrease of $1/\tau(\omega)$ from any

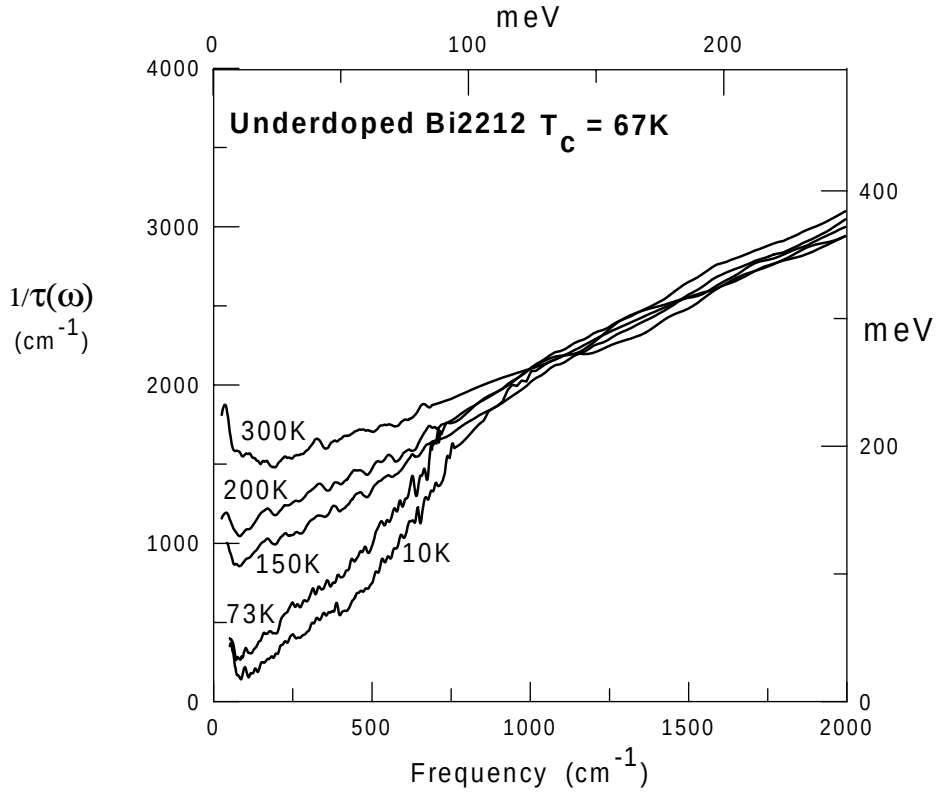

Figure 29. The frequency-dependent scattering rate and the effective mass of underdoped Bi 2212. The linear scattering rate develops a gap below 150 K. The frequency scale of this gap is only slightly enhanced in the superconducting state. There is no temperature dependence of the scattering at high frequency.

spectrum of $\alpha^2 F(\Omega)$ using equation (9) and one must conclude that the simplified analysis derived from equation (7) is not appropriate in the presence of a superconducting gap. The second feature, seen in the optimally doped samples but not in the underdoped samples, is a slight temperature dependence in the slope of the scattering rate in the normal state.

We will summarize the salient features of the scattering-rate spectra as they relate to the issue of the pseudogap, neglecting for the moment the small differences that are seen between the different materials. First, there is in *all materials* a suppression of scattering below the linear trend seen at high temperatures or high frequencies at all temperatures. Second, there is the similarity in the spectra in the underdoped state to those in the optimally doped materials in the superconducting state. This leads us to the notion that the pseudogap in the normal state and the superconducting gap are closely related. One should add, however, that in the superconducting state there is a slight increase in the overall frequency scale of the gap of the order of 125 cm^{-1} (16 meV).

Table 2 shows the approximate width of the pseudogap in $1/\tau(\omega)$ in various samples that have been studied (Puchkov *et al* 1996a). It seems from the table that the pseudogap is relatively constant at $\approx$700 cm^{-1} with perhaps a small tendency to increase slightly with doping.

Model calculations of the pseudogap in the ab-plane scattering rate have been done by

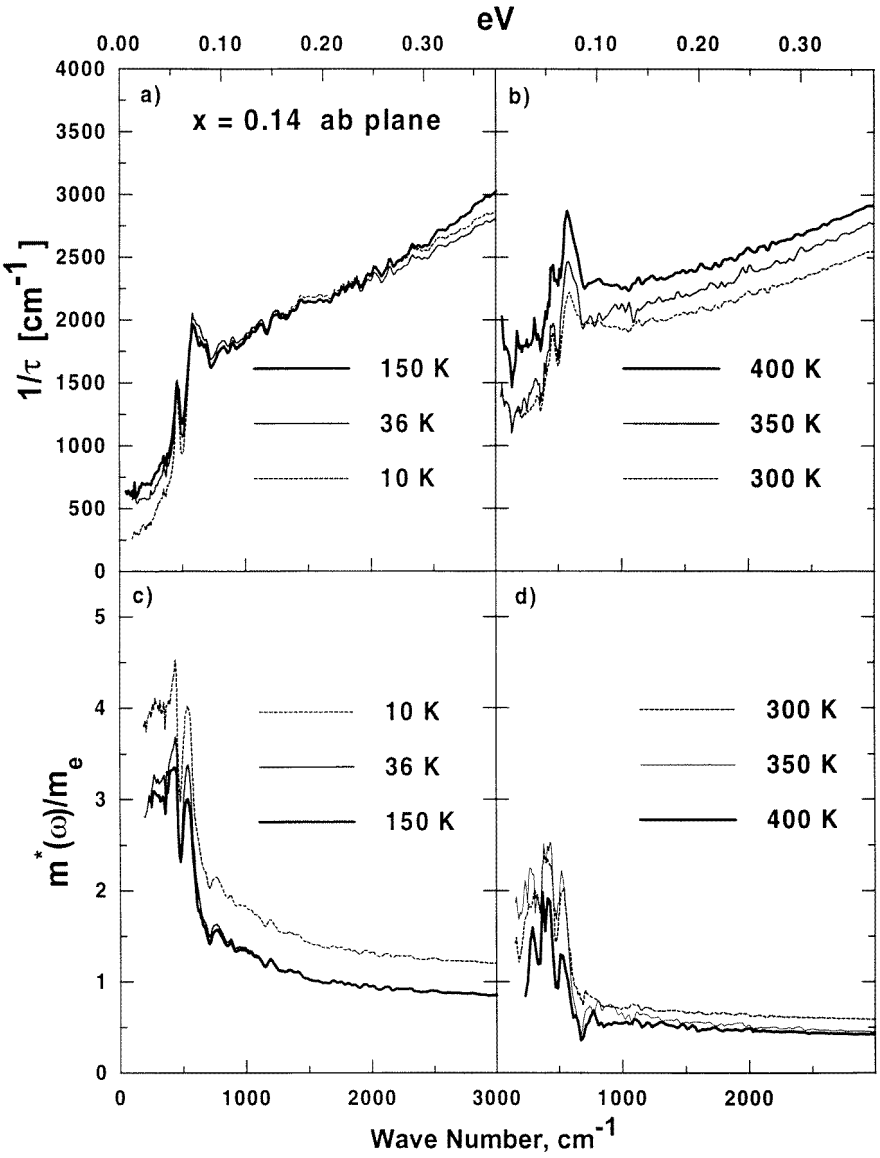

Figure 30. Frequency-dependent scattering rate in underdoped $La_{2-x}Sr_xCuO_4$ (*a*), (*b*) and effective mass (*c*), (*d*). There is a marked depression of scattering below a frequency scale 700 cm^{-1} (85 meV) in the normal state and temperature-independent scattering at higher frequencies. The high-frequency scattering becomes temperature dependent at $T > 300$ K and the pseudogap vanishes at ≈450 K.

Stojković and Pines (1997) and by Branch (1996). Based on the nearly antiferromagnetic Fermi liquid model of spin-fluctuation scattering these authors use formulae similar to equation (4) to calculate an accurately weighted conductivity as a function of frequency and then use equation (7) to calculate an 'effective' scattering rate in the same way the experiments are analysed. An example of such a calculation is shown in figure 33 from the work of Branch (1996). A calculation of $1/\tau$ for the t–J model by Plakida (1997) gives similar results. While

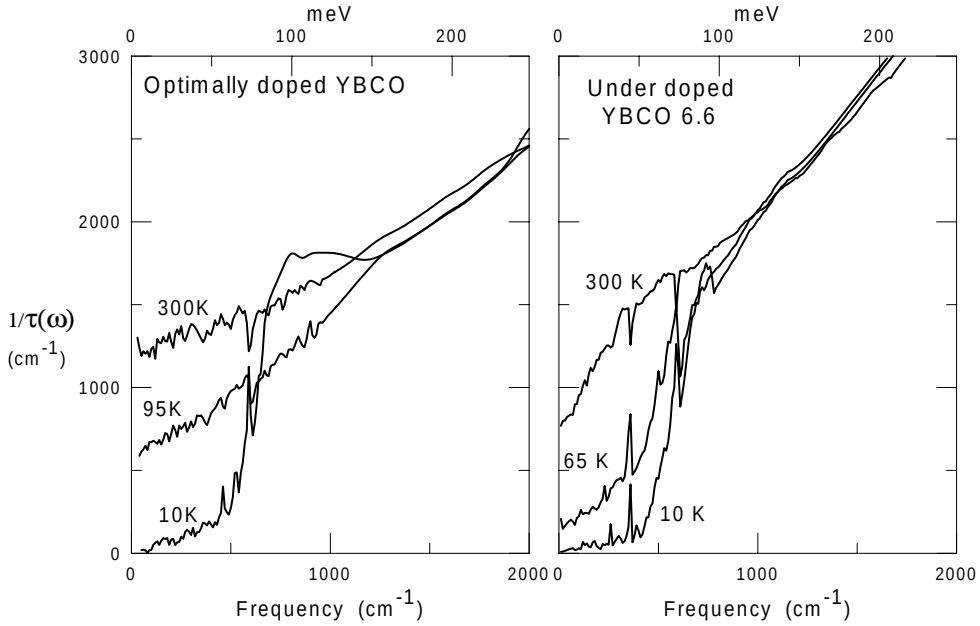

Figure 31. Scatttering rate in optimally doped YBCO (*a*) and underdoped YBCO (*b*). The scattering-rate spectrum is similar in the superconducting state of the optimally doped and the pseudogap state of the underdoped sample (at 65 K).

Table 2. Maximum pseudogap 2Δ from the ab-plane.

Material	T_c(K)	2Δ (cm^{-1})
YBCO 6.6	58	660
YBCO 124	82	770
Bi 2212	67	660
Bi 2212	82	660
Bi 2212	90	740
Bi 2212	82 (OD)	810
LSCO $x = 0.13$	32	$\approx$700

the general trend and magnitude of the scattering-rate variation is reproduced well by these models, there is no sharp break in the scattering as seen in the experiments in the 700 cm^{-1} region. Also these calculations fail to reproduce the temperature-independent scattering seen above 700 cm^{-1}.

5.3. The c-axis pseudogap

The earliest spectroscopic measurement of the pseudogap in charge fluctuations was the observation by Homes *et al* (1993) of a region of depressed conductivity in the c-axis optical conductivity of underdoped YBCO 6.6. Since most cuprate single crystals grow in the form of thin plates, measurements with $\boldsymbol{E} \parallel c$ are difficult because of the small areas of their ac faces. The earliest data on σ_c showed a very low conductivity in that direction, much lower than the Ioffe–Rigel limit. Consistent with this low absolute value, the frequency dependence is flat and there is no temperature dependence. Thus the c-axis transport can be described as

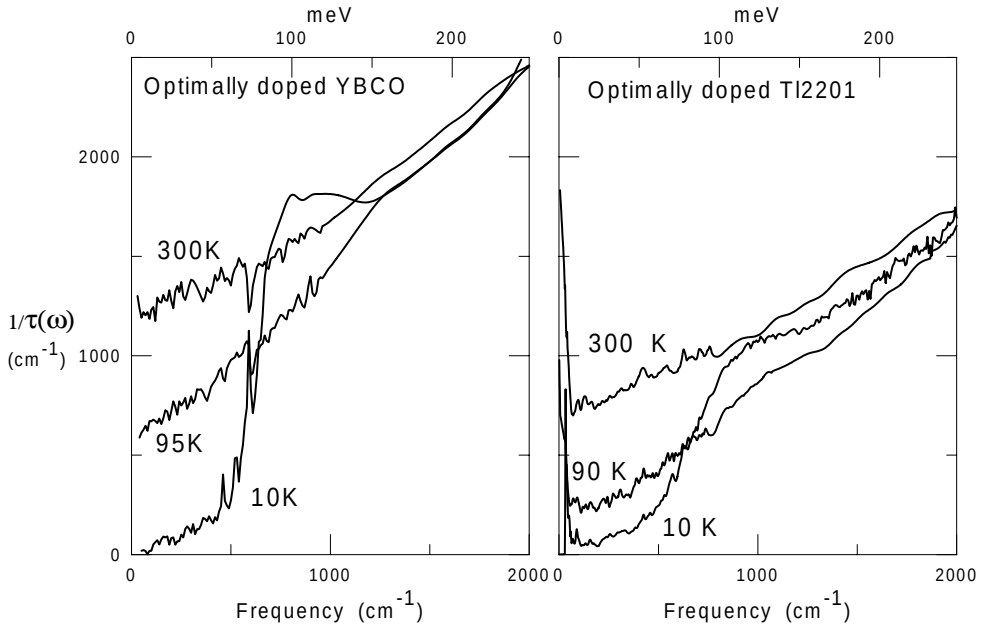

Figure 32. Comparison of the pseudogap in the ab-plane scattering rate in optimally doped YBCO (*a*) and underdoped YBCO (*b*). As in the two-chain material the pseudogap and the superconducting gap have very similar frequency dependences. The middle curve in each panel is taken at a temperature just above the superconducting transition.

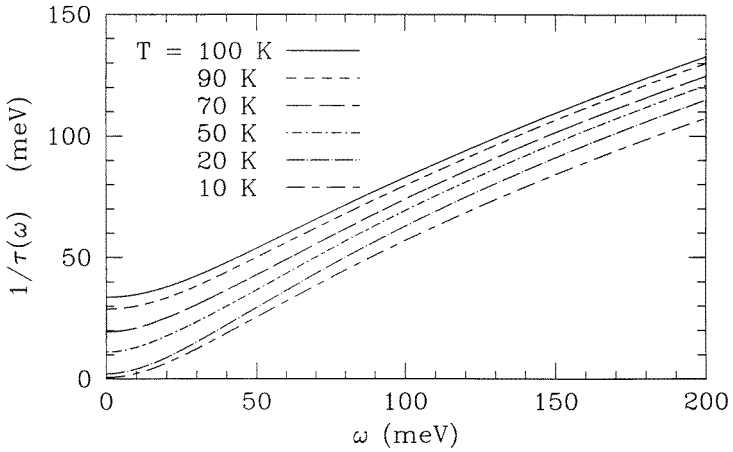

Figure 33. Calculated scattering rate based on the nearly antiferromagnetic Fermi liquid model.

incoherent hopping (Cooper 1993a, b, Leggett 1994, Timusk 1996).

Figure 34 shows the c-axis conductivity of YCBO 6.6 at a series of temperatures obtained from a Kramers–Kronig analysis of the reflectance (Homes *et al* 1993). The top panel shows the raw conductivity which is dominated by several strong optic phonons. In the lower panel the phonons have been subtracted and the electronic background is shown more clearly. At room temperature the background is flat and frequency independent. As the temperature is lowered below T^*, which in this material from NMR data is of the order of 250 K, a pseudogap

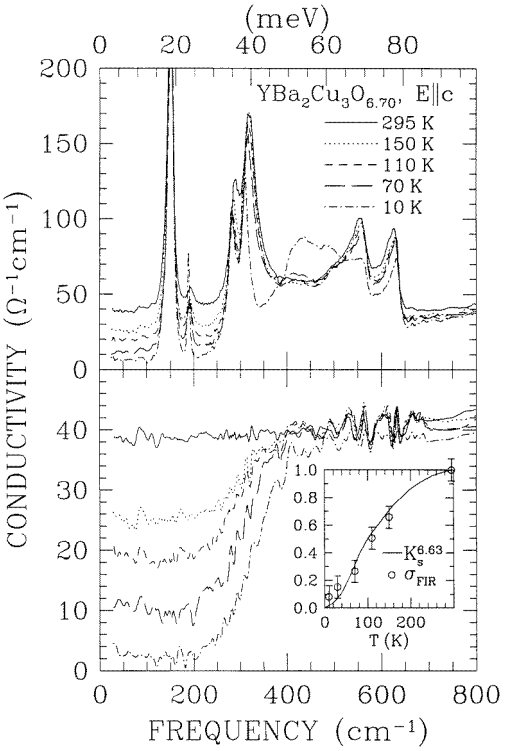

Figure 34. Optical conductivity measured along the c-axis, normal to the planes for underdoped $YBa_2Cu_3O_{6+x}$ (top panel). There is marked depression of conductivity at low frequency. There are considerable changes in the phonon spectra between 250 and 650 cm^{-1} including the appearance of a broad peak at 420 cm^{-1}. These features have been subtracted in the lower panel which displays a pseudogap in the normal state. The actual magnitude of the gap frequency depends on assumptions made when the phonons are subtracted. The inset in the bottom panel compares the low-frequency conductivity (open circles) with the Knight shift.

develops in the conductivity. The inset in the lower panel compares the Knight shift with the conductivity in the low-frequency, pseudogap region.

The striking feature of the pseudogap as seen in the c-axis conductivity is its unusual temperature dependence. The gap frequency appears to be temperature independent and the gap fills in as the temperature increases. This behaviour of the pseudogap is consistent with what has been seen with other spectroscopic probes such as ARPES, vacuum tunnelling spectroscopy and the ab-plane scattering rate. It should also be noted that at the lowest temperatures there is still a residual conductivity at low frequency and no true gap exists in the optical conductivity. One should also note that the conductivity in the c-axis pseudogap region is flat and frequency independent in contrast to what is seen in tunnelling where the tunnelling conductance rises uniformly in the gap region (Mandrus *et al* 1993, Renner *et al* 1998).

The magnitude of the c-axis conductivity, when extrapolated to zero frequency, agrees with the dc value quite well (Homes *et al* 1995a). This suggests that there is no low-lying coherent peak in the conductivity below the lowest frequency of the infrared measurements. Recent microwave measurements of $\sigma(\omega, T)$ (Hosseini *et al* 1998) have confirmed this up to a frequency of 25 GHz. In accord with these observations Takenaka *et al* (1994) noted that the temperature region where the ab-plane dc resitivity showed its characteristic deviation from the high-temperature linear behaviour coincided with the temperature and doping region where the c-axis resitivity became 'semiconducting', i.e. acquires a positive temperature coefficient of resistivity.

When the YBCO materials become superconducting a further reduction in the c-axis conductivity takes place but over a wider spectral region than the normal-state pseudogap scale. The total spectral weight transferred to the delta function is shown as the hatched box at low frequency in figure 34. This effect is even clearer in the YBCO 124 case, shown in

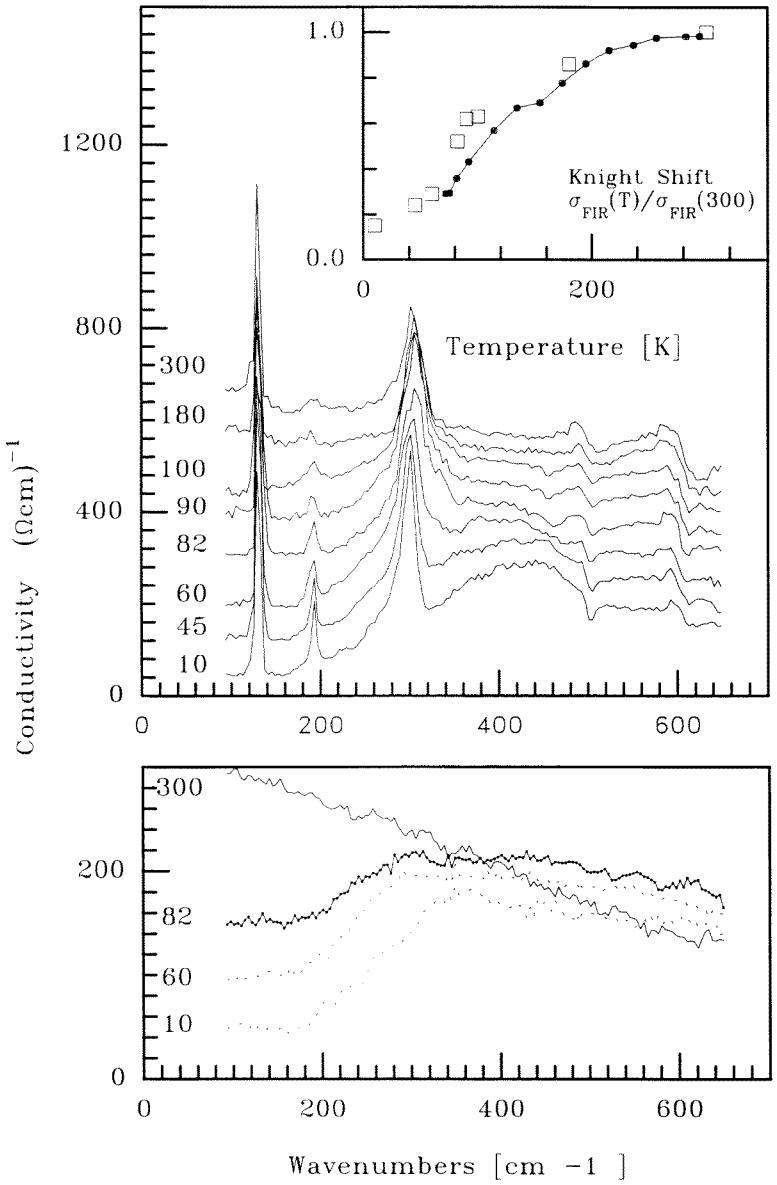

Figure 35. Pseudogap in the c-axis conductivity of $YBa_2Cu_4O_8$. There is a marked depression of conductivity below 300 cm^{-1} in the normal state and a further depression at T_c extending to higher frequencies. The inset compares the low-frequency conductivity with the Knight shift. The bottom panel shows the conductivity without the phonon lines.

figure 35, where there is a uniform depression in conductivity up to as high as 80 meV (Basov *et al* 1994a) in the superconducting state. It appears that, at least in these two compounds, the c-axis pseudogap scale is lower than the characteristic energies where the spectral weight of the superconducting condensate originates, but it should be recognized that because of uncertainties in the phonon subtraction process having to do with assumed baselines, there is great uncertainty in the energy scale of the c-axis pseudogap. A pseudogap in the c-axis

conductivity has also been seen by Tajima *et al* (1995) in YBCO and Reedyk *et al* (1997) in underdoped $Pb_2Sr_2(Y/Ca)Cu_3O_8$.

The overall evidence of the presence of the pseudogap in the single-layer $La_{2-x}Sr_xCuO_4$ is controversial, particularly since the NMR Knight-shift reduction is weak and no sign of a gap is seen in the spin-lattice relaxation rate. In the same way, the c-axis conductivity depression does not show the strong gap signature seen in the YBCO systems. Basov *et al* (1995b) found depressed conductivity from 10 to 5 Ω cm^{-1} in the normal state for a slightly underdoped crystal with $x = 0.15$ over a very large frequency range of 1000 cm^{-1} at the expense of increased conductivity in the 2000–4000 cm^{-1} range. More recently, Uchida *et al* (1996) and Startseva *et al* (1998) have found reduced normal-state conductivity in the frequency below $\approx$500–600 cm^{-1} (60–75 meV) in underdoped LSCO: $x = 0.12$ and $x = 0.13$, respectively.

Any discussion of the pseudogap phenomenon in the c-axis conductivity must address the anomalous broad peak at 400 cm^{-1} shown in figure 34 which appears below 150 K in YBCO. It grows in intensity as the temperature is lowered with no discontinuity at the superconducting transition. We will call it the c-axis resonance in analogy with the 41 meV resonance seen in neutron scattering, with which it has many similarities.

Like the neutron resonance, the c-axis resonance frequency Ω_0 increases with doping with $\Omega_0 \propto T_c$ in the underdoped range and it is not seen in the $La_{2-x}Sr_xCuO_4$ material. The temperature dependence of the resonance intensity is similar as well in the underdoped case. A similar mode is seen in the c-axis spectrum of YBCO 124 (Basov *et al* 1994a) shown in figure 35 as well as in $Pb_2Sr_2RCu_3O_8$ where R is a rare earth (Reedyk *et al* 1997). It is not seen in the c-axis spectra of $La_{2-x}Sr_xCuO_4$ (Basov *et al* 1995b) or in Bi 2212 (Tajima *et al* 1993). In the former case the peak in the (π, π) scattering occurs at 25 meV which coincides with an anomalously strong phonon at this frequency and may well hide the infrared resonance.

Homes *et al* (1993) originally included the resonance as a part of the electronic conductivity but in a later publication (Homes *et al* 1995b) they noted that the spectral weight in the 200–700 cm^{-1} region was constant in the temperature range where the peak grew, suggesting that the new peak was growing at the expense of the phonons, particularly the plane-buckling mode at 319 cm^{-1}. This suggested that the resonance had a strong phonon component. However, in view of many similarities between the c-axis resonance and the magnetic mode seen in neutron scattering, it is clear that the mode is coupled to the electronic degrees of freedom. More work is needed to establish the exact nature of these resonances.

6. Specific heat

The electronic specific heat is a fundamental property that provides thermodynamic evidence for a gap in the normal state of high-temperature superconductors (Loram *et al* 1994a). The measurements are difficult since, at high temperatures where the normal-state gap can be seen, the specific heat of a typical high-temperature superconductor is dominated by phonons (Junod 1989). Typically, the phonon contribution is a hundred times stronger than that of the charge carriers. Nevertheless, using a sensitive differential technique, Loram *et al* have succeeded in accurately measuring the electronic specific heat of several high-temperature superconductors in the pseudogap temperature range.

In the differential technique a reference sample is compared with an undoped standard sample, both in the form of fine powders containing exactly the same number of moles of material (Loram *et al* 1993). The undoped reference is assumed to have zero electronic specific heat. If the same quantity of heat $\mathrm{d}Q$ is injected into the two samples, then according to $\mathrm{d}Q = C\,\mathrm{d}T$ where C is the specific heat and $\mathrm{d}T$ the temperature change, the specific heat difference is $\delta C = C_0\delta T/\mathrm{d}T_r$, where $\mathrm{d}T_r$ is the temperature rise of the reference and δT is

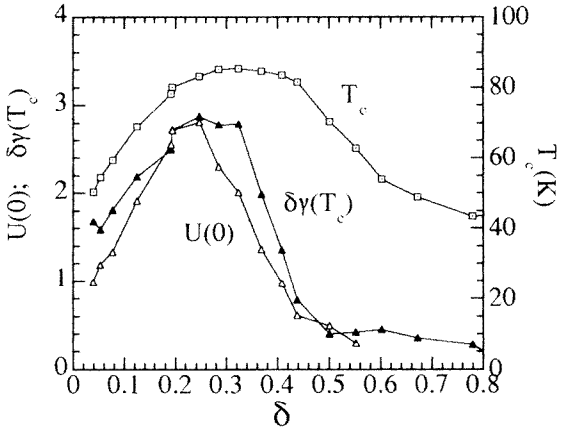

Figure 36. T_c, $\delta\gamma(T_c)$ the specific heat jump (mJ/g-at.K^2) at T_c and the condensation energy $U(0)$ (J/g-at.K) versus doping level δ in $Y_{0.8}Ca_{0.2}Ba_2Cu_3O_{7-\delta}$. Both the condensation energy and the specific heat jump drop on the underdoped side (right-hand side of the diagram).

the temperature difference between the reference and the sample due to the extra electronic specific heat.

A number of corrections have to be made, the largest being the change in the phonon spectrum due to doping which alters the phonon contribution of the specific heat (Loram *et al* 1993). For example, in $YBa_2Cu_3O_{6+x}$ the additional oxygens that enter the chains not only give rise to new modes involving the chain oxygens, but also shift the frequency of the bridging oxygen from its twofold coordinated copper position at 615 cm^{-1} to the 560 cm^{-1} of the fourfold coordinated site as the chain is built up (Homes *et al* 1995b). The corresponding changes to the phonon specific heat are, at their maximum at $T = 40$ K, an order of magnitude larger than the electronic term. Loram *et al* use a Zn doped sample as a reference to estimate these changes by noting that 7% Zn destroys superconductivity but leaves a constant, temperature-independent metallic γ term. An independent estimate of doping induced changes to the phonon density of states comes from inelastic neutron scattering. Loram *et al* find that for an estimated uncertainty of 1–2% in the residual change in the phonon contribution an error of 10% is propagated to the electronic specific heat.

In a recent paper Loram *et al* (1997) investigate the electronic specific heat of $Y_{0.8}Ca_{0.2}Ba_2Cu_3O_{7-\delta}$ as a function of oxygen doping. The replacement of some of the yttrium by calcium shifts the maximum T_c from $O_{6.92}$ for 0% Ca to $O_{6.68}$ for 20% Ca. By varying the oxygen level from $O_{6.20}$ to $O_{6.96}$ the same sample can be studied from the underdoped region with $T_c = 44$ K to the substantially overdoped region with $T_c = 53$ K, as shown in figure 36 from Loram *et al* (1997). The specific heat coefficient γ, where $\gamma = C/T$, of both the overdoped ($\delta < 0.32$) and underdoped ($\delta > 0.32$) samples is shown in figure 37. There are three regions of interest: the underdoped region where a pseudogap is seen, the plateau where T_c remains roughly constant and finally the overdoped region where T_c decreases as oxygen is added. We will first examine the overdoped region.

In the overdoped samples, figure 37(*a*), the normal-state γ is temperature independent. Since γ is proportional to the density of states at the Fermi surface this shows that the overdoped material resembles a normal metal. Surprisingly, γ is also doping independent. However, a doping-independent infrared spectral weight was also seen in all overdoped high-temperature superconductors examined by Puchkov *et al* (1996b). The overdoped samples show a specific

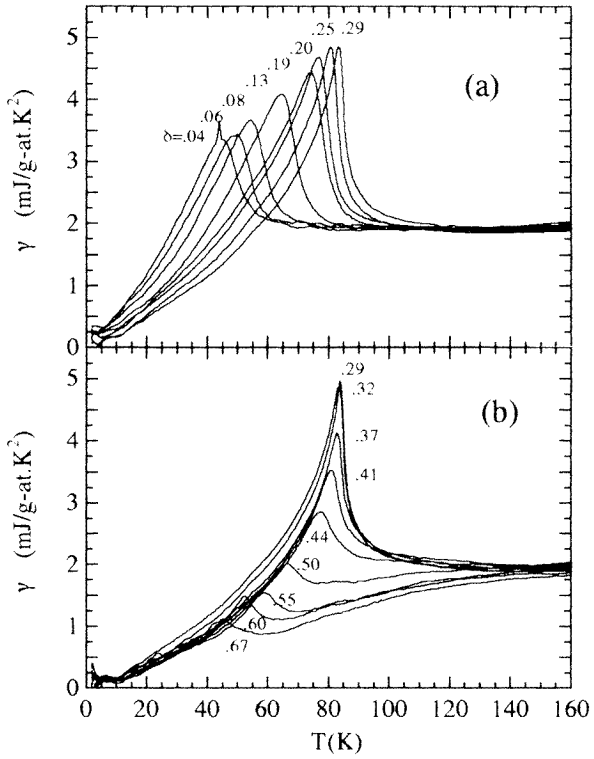

Figure 37. Specific heat coefficient γ for (*a*) overdoped and (*b*) underdoped $Y_{0.8}Ca_{0.2}Ba_2Cu_3O_{7-\delta}$. In the overdoped material a gap, signalled by a depression in γ, opens up below T_c. In the underdoped samples a gap starts to form in the normal state below 140 K.

heat jump at T_c, larger than the $\Delta\gamma/\gamma = 1.43$ expected for the weak-coupling BCS model, suggesting possible strong-coupling superconductivity. Evidence of nodes in the density of states in the overdoped state is shown by the approximately linear temperature dependence of γ in the superconducting state at low temperatures, where $\gamma = \alpha T$. The authors use the slope of this linear term to estimate the d-wave superconducting gap. This yields $\alpha = 3.29\gamma_n k_B/\Delta_0$ where γ_n is the normal-state specific heat coefficient and Δ_0 the zero-temperature maximum gap. Figure 38 shows the superconducting gap found this way as a function of doping.

As we move towards the underdoped region by reducing the oxygen content below the maximum T_c value, there is a plateau where T_c does not vary but the condensation energy collapses rapidly, an effect first seen by Junod *et al* (1989) in specific heat and by Däumling *et al* (1991) from reversible magnetization measurements. This effect can be seen clearly in the sudden decrease in the height of the specific heat jump $\delta\gamma$ at T_c (the condensation energy is $\propto \delta\gamma(T_c)T_c^2$). Figure 36 shows that between $\delta = 0.34$ and $\delta = 0.50$ the condensation energy drops rapidly while T_c only drops slowly.

In the underdoped samples Loram *et al* find a pseudogap. Where the overdoped samples show a temperature-independent γ above T_c, both the 20% calcium series (Loram *et al* 1997) and the calcium-free material (Loram *et al* 1994a) have a depression of the specific heat coefficient γ in the normal state below a temperature T^*, as shown in figures 37 and 39. As oxygen is removed the depression starts at higher temperatures.

In $La_{2-x}Sr_xCuO_4$ Loram *et al* (1996) also found evidence for a pseudogap in the normal

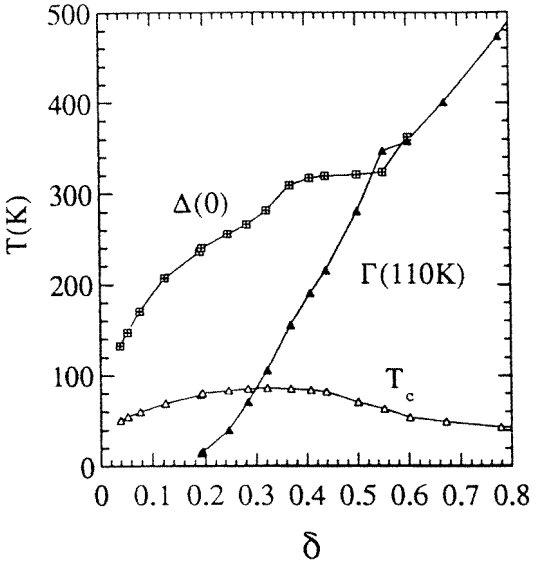

Figure 38. Magnitude of the superconducting gap $\Delta(0)$ and the normal-state gap $\Gamma(110\ \mathrm{K})$ as a function of doping δ. At optimal doping the normal-state gap goes to zero whereas the superconducting gap has a magnitude of ≈300 K (25 meV).

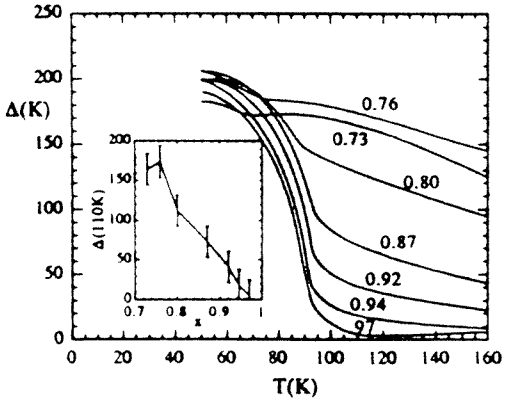

Figure 39. The energy gap Δ for $YBa_2Cu_3O_{7-\delta}$ as a function of temperature T. In the underdoped state, with $\delta = 0.76$, the gap appears well above 160 K and its magnitude does not change substantially on entry into the superconducting state.

state. As figure 40 shows, there is loss of condensation energy below $x = 0.15$ and $x = 0.135$ but, in contrast with the $YBa_2Cu_3O_{6+x}$ system, the pseudogap appears already in the overdoped state. The specific heat coefficient is depressed below values seen in the overdoped state already at $x = 0.20$ below ≈100 K. This is in accord with measurements with other techniques: the pseudogap temperature scale is much higher in $La_{2-x}Sr_xCuO_4$ than in $YBa_2Cu_3O_{6+x}$ and the pseudogap state extends well into the overdoped region. In the superconducting state the specific heat coefficient has a linear dependence on T, $\gamma = \gamma(0) + \alpha T$, first observed by Momono *et al* (1994).

In both systems Loram *et al* also measure the bulk magnetic susceptibility χ of their specific heat samples. They find that in the normal state, there is striking agreement between the entropy S, as determined from an integration of γ ($S(T) = \int^T \gamma(T')\,\mathrm{d}T'$) and χT. This is expected for a Fermi liquid where the Wilson ratio $a_0 = S/\chi T$ is a constant, $a_0 = (\pi k_B/\mu_B)^2/3$. This shows that the spin and charge densities of states have similar energy dependences and are equally weighted. In spin–charge separation models the Wilson ratio is found to deviate from unity. In the one-dimensional Hubbard model simulations Schultz (1991) finds that for non-interacting fermions $v_\sigma = v_\rho = v_F$ where v_σ, v_ρ and v_F

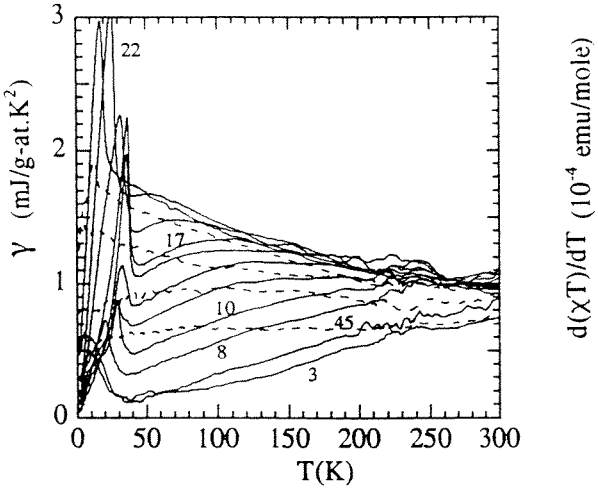

Figure 40. Specific heat coefficient γ of $La_{2-x}Sr_xCuO_4$ for $x = 0.08$ to $x = 0.30$. There is a suppression of γ in the normal state for $x < 0.22$ signalling the presence of a pseudogap.

are the spin and charge and fermion velocities respectively. In the limit of complete spin and charge separation the Wilson ratio $a = a_0/2$. For disordered local moments the Wilson ratio is $a = a_0/4.75$. Orbital angular momentum affects the Wilson ratio, which for $g = 2.1$ yields about a 10% reduction. The electron–phonon interaction enhances the Wilson ratio by $(1+\lambda)$.

Within the Fermi liquid model, inelastic interactions enhance the mass of the electrons through the mass enhancement factor λ given by $m^* = m(1+\lambda)$, where m^* is the effective mass and m the band mass. Loram *et al* find a weak coupling value of $\lambda \approx 0.5$ for both pure and zinc doped YBCO (Loram *et al* 1994b). This observation is in contradiction with the masses deduced from the frequency-dependent scattering-rate analysis of the optical conductivity where it is found that $\lambda \approx 4$. However, this is a high-frequency result. At low frequencies, at energies that are relevant to the specific heat measurements, a smaller λ can be inferred; for example, from the resistivity slope in the context of a two component model $\lambda = 0.3$ is obtained. For a review of this issue see Tanner and Timusk (1992).

7. Electronic Raman scattering

In metals, the Raman effect is difficult to observe. First, the Raman process is an intrinsically weak second-order process, much weaker than the dipole absorption responsible for the optical conductivity. Second, in conductors, electromagnetic radiation only penetrates a few thousand Å, making the effective interaction volume small. Finally, for free carriers, momentum conservation dictates that only carriers up to an energy of qv_F can be excited, $\approx$50 cm^{-1} for the cuprates. Here v_F is the Fermi velocity and q the reciprocal skin depth. In addition to this low-frequency band, free carriers are also expected to show Raman activity at the plasma frequency. Such a band has been observed in doped semiconductors (Mooradian *et al* 1960).

In the cuprates the normal-state Raman spectrum is dominated by phonons which are superimposed on a broad frequency-independent continuum extending up to 2 eV. The origin of this continuum has been a mystery, but it is now clear that it arises from the same incoherent processes that are responsible for the strong scattering seen in other probes of the electronic

excitations (Varma *et al* 1989, Shastry and Schraimann 1990, Kostur and Eliashberg 1991, Branch 1996).

In conventional superconductors excitations across the energy gap are Raman-active. Predicted by Abrikosov and Fal'kovskii (1961), these transitions which break Cooper pairs into pairs of quasiparticles at $\boldsymbol{k}$ and $-\boldsymbol{k}$, thus conserving momentum, result in a threshold in scattering at 2Δ. They were first observed by Sooryakumar and Klein in (1980) in 2H–$NbSe_2$ and in V_3Si by Klein and Dierker (1984) and Hackl *et al* (1983). The Raman response of superconductors should be contrasted to the infrared response. For the infrared conductivity, type II coherence factors cancel out the pairbreaking excitations, and there is no absorption at 2Δ in a clean superconductor. For the Raman response (being proportional to $\boldsymbol{A}\dot{\boldsymbol{A}}$ rather than $\boldsymbol{p}\dot{\boldsymbol{A}}$ of the infrared) type I coherence factors apply and even in a clean s-wave superconductor there is a distinct feature at 2Δ.

It was found early on that in the cuprates there was no clear onset of the expected scattering at 2Δ. Instead, in the superconducting state, there is a redistribution of spectral weight where the broad continuum scattering is depressed at low frequencies and the spectral weight lost is transferred to higher frequencies, forming a broad peak whose position depends on scattering geometry. This peak, often referred to as the pairbreaking peak in the high-T_c Raman literature, is not present in all experiments. Furthermore, there is no sharp 2Δ threshold. Instead, there is scattering intensity to the lowest frequencies. As in the case of the optical conductivity, some of these deviations from the expected BCS behaviour can be understood in terms of a d-wave order parameter and inelastic scattering that increases as a function of frequency (Branch 1996).

Unlike the optical conductivity which, for a tetragonal system, yields a single constant for the ab-plane conductivity, Raman scattering can be used to give two spectra, B_{1g} and B_{2g}, each representing a different average over the Fermi surface. The A_{1g} spectrum cannot be obtained independently. The different geometries are illustrated in figure 41 from Branch (1996). It can be shown (Chen *et al* 1994) that the B_{1g} spectra emphasize processes that involve states in the $(\pi, 0)$ direction of the maximum gap, whereas the B_{2g} spectra involve states near the nodes of the $d_{x^2-y^2}$ function at (π, π).

Recent measurements by Hackl *et al* (1996) for the Raman intensity in the superconducting state for various symmetries in optimally doped Bi 2212 are shown in figure 42 from Einzel and Hackl (1996). As this figure illustrates, the Raman spectra of B_{1g} and B_{2g} symmetry are quite different. The full curves are theoretical predictions that assume d-wave ($d_{x^2-y^2}$) symmetry of the gap function and a maximum gap of $\Delta_0 = 280$ cm^{-1} (34.7 meV). Kendziora *et al* (1996), using similar analysis find that $\Delta_0 = 264$ cm^{-1} (32.7 meV).

The earliest evidence for a pseudogap in the Raman spectra came from the observations of Slakey *et al* (1990) in underdoped YBCO 123 with $T_c = 60$ K. They noted that a peak at 500 cm^{-1}, seen at low temperature in B_{1g} spectra, and associated with superconductivity, could be seen well into the normal state. They also noted that the frequency of the feature did not depend on the carrier concentration, in clear contradiction to the expectation from BCS theory that the $2\Delta/k_BT_c$ ratio would remain constant or even decrease as one moved into the underdoped state. The authors suggest that if the 500 cm^{-1} energy is a pairing energy then their experiments could be understood in terms of models of preformed pairs advanced by Randeria *et al* (1989) and by Friedberg and Lee (1989). They also pointed out that this pairing energy did not show any significant temperature dependence below T_c.

These early observations have been confirmed by recent work. A loss in spectral weight below 700 cm^{-1} in underdoped Bi 2212 and YBCO 123 has been reported by Nemetschek *et al* (1997) in the B_{2g} spectrum but not in the B_{1g}. The overall low-frequency spectral weight is reduced by some 10% starting at 200 K in both materials.

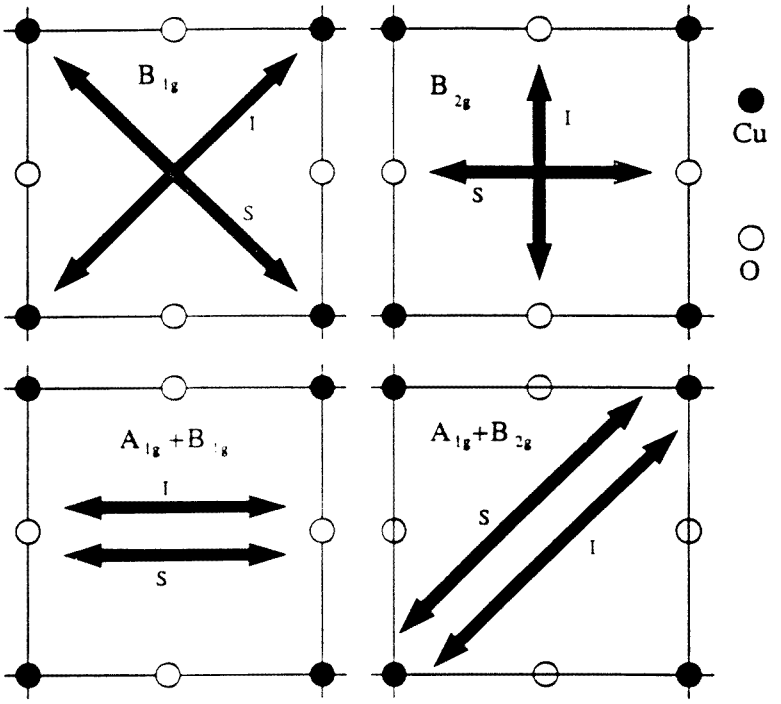

Figure 41. Relation between Raman symmetries and photon polarization. Incident (I) and scattered (S) polarizations are shown. With crossed polarizers B_{2g} is measured along the CuO bond axes whereas B_{1g} is measured when the polarizers are rotated by 45° to the bond directions.

The power-law behaviour of the Raman continuum below the gap frequency has been the subject of much recent discussion. It is generally found that in the normal state the Raman continuum, after corrections for Bose occupation factors, varies linearly with frequency. This can be understood in terms of the collision limited or 'Drude' model of Raman response for a conducting system (Zawadowski and Cardona 1990, Hackl *et al* 1996) where the Raman cross section σ_s for a channel s ($s = A_{1g}, B_{1g}, B_{2g}$) is given by:

$$\frac{\partial^2\sigma_s}{\partial\omega\partial\Omega} = (1 + n_\omega)\frac{\omega\Gamma_s B_s}{\omega^2 + \Gamma_s^2} \tag{11}$$

where $n_\omega = [\exp(\hbar\omega/k_B T) - 1]^{-1}$ is the Bose–Einstein factor and Γ_s the electronic scattering rate. The quantity B_s is a Raman response, proportional to the reciprocal of the band mass, averaged over the Fermi surface with a weight that depends on symmetry s (Deveraux and Einzel 1995). The scattering rate Γ_s is also a weighted symmetry-dependent average over the Fermi surface.

In the normal state this collision limited model predicts a slope of the Raman spectrum that is a direct measure of the magnitude of Γ_s the scattering rate for the symmetry s. Thus if a pseudogap develops at $(\pi, 0)$, the slope of the Raman response at low frequencies will be proportional to $1/\Gamma_{B_{1g}}$. Experimental results in optimally doped materials show that the scattering rate determined this way has a linear temperature dependence with a zero intercept very similar to that observed in the optical conductivity (Hackl *et al* 1996, Naeini *et al* 1998). The absolute magnitude of the renormalized Raman scattering rate for optimally doped Bi 2212 at 300 K is 450 cm^{-1} (Hackl *et al* 1996), in reasonable agreement with the infrared

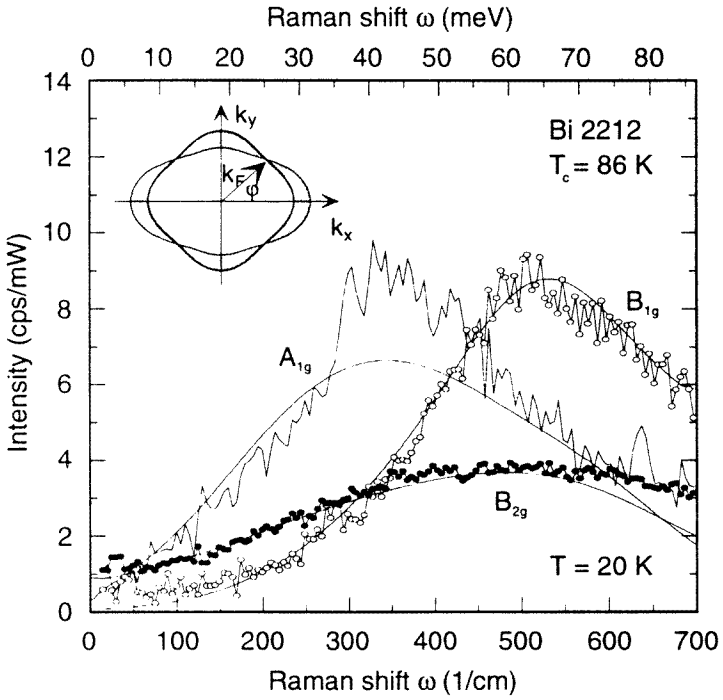

Figure 42. Raman spectra of Bi 2212. B_{1g} emphasizes processes in the $(\pi, 0)$ direction whereas B_{2g} is sensitive to the (π, π) direction. The full curves are the result of a d-wave model for the Raman tensor shown in the inset.

conductivity value of 600 cm^{-1} (Puchkov *et al* 1996a). One does not expect the infrared and Raman scattering rates to be identical in the presence of anisotropy since they result from different averages around the Fermi surface. The comparison between Raman and conductivity scattering rates is discussed in detail by Branch (1996).

Raman scattering data at various doping levels of $Bi_2Sr_2CaCu_2O_8$ is presented by Blumberg *et al* (1998). The authors argue that the B_{1g} Raman continuum is a measure of both the gapped density of states and the low-frequency dependent scattering rate. Figure 43 shows the Raman continuum for a series of doping levels for $Bi_2Sr_2CaCu_2O_8$ samples. There is a prominent peak in the B_{1g} Raman spectra, at 600 cm^{-1} in the overdoped state. Blumberg *et al* argue that this narrow peak is evidence of a bound state between the carriers, such as preformed pairs.

8. Magnetic neutron scattering

Magnetic neutron scattering is a powerful spectroscopic tool that provides information on both the energy and momentum dependence of excitations that involve the change of the spin of an electron. In insulators, elastic magnetic scattering has been used to map out the static spin structure and inelastic scattering to excite spin waves. In metals, inelastic scattering is similar to Raman and optical spectroscopy in that the final result of the scattering process is a hole below the Fermi level and an excited electron above it. But unlike optical spectroscopies, where the momentum transfer to the electron–hole system is nearly zero, a neutron scattering experiment can be set up to transfer any momentum $\boldsymbol{Q}$ to the electron–hole pair. Since the

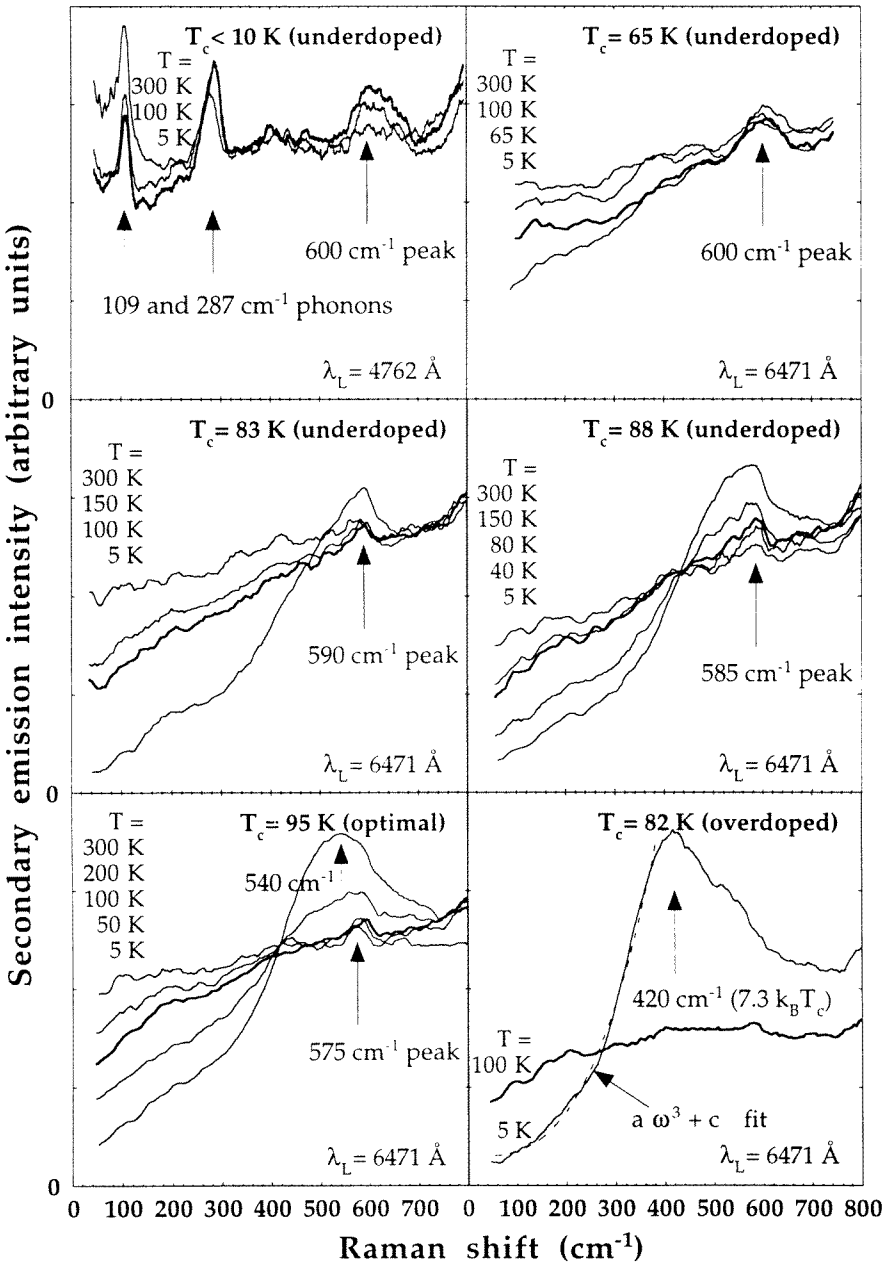

Figure 43. Raman intensity for B_{1g} symmetry in Bi 2212 at different doping levels. There is a suppression of spectral weight below a frequency of $\approx$600 cm^{-1} and a sharp resonance at this frequency. The suppression of scattering has been attributed to the formation of a pseudogap in the normal state.

neutron interacts with the magnetic moment of the electron, the electron spin can be flipped in the course of the scattering.

The drawback of this technique is that due to the weak interaction between the neutron and

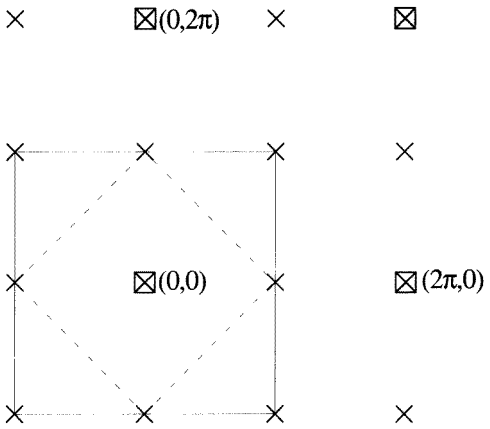

Figure 44. Magnetic Brillouin zone shown as broken lines. The squares denote the reciprocal lattice points of the atomic unit cell. With the onset of antiferromagnetic order the unit cell is doubled in both directions and the new reciprocal lattice, shown as crosses, is formed.

the electron spin, very large centimetre-size crystals must be used. Because of this limitation only two high-T_c systems have been investigated in detail by magnetic neutron scattering: $La_{2-x}Sr_xCuO_4$ and $YBa_2Cu_3O_{6+x}$.

The Bragg diffraction pattern of an antiferromagnetic insulator with a square lattice and a lattice spacing a is illustrated in figure 44. Nuclear scattering occurs at momentum transfers of $2\pi/a(h, k, l)$ where h, k, l are integers. Because the alternating spins double the unit cell, in a three-dimensional antiferromagnet scattering takes place at $2\pi/a(h/2, k/2, l/2)$. (In the neutron scattering literature momentum transfer is measured in reciprocal lattice units with $(Q_x, Q_y, Q_z) = (2\pi/ah, 2\pi/bk, 2\pi/cl)$, with $a \approx b = 1.63$ Å^{-1} and $2\pi/c \approx 0.53$ Å^{-1} for $YBa_2Cu_3O_{6+x}$.) Since the doped cuprates are two-dimensional antiferromagnetic insulators, with no coherence between the two-dimensional layers, their Bragg pattern will consist of 'rods' of magnetic scattering located at $(h/2, k/2, l)$ where h and k are integers but l is a continuous variable and the scattering intensity is independent of l. In the limit of zero doping three-dimensional magnetic order is established and the rods turn into Bragg spots at $l/2$.

In doped $YBa_2Cu_3O_{6+x}$ there is a coupling between the spin systems of the two CuO_2 layers in the unit cell. As a result the rods acquire a sinusoidal modulation with a spatial frequency corresponding to the interlayer spacing of 3.227 Å and not the c-axis spacing $c = 11.83$ Å. The first maximum of intensity occurs at $\boldsymbol{Q} = (\frac{1}{2}, \frac{1}{2}, 1.83)$. Spectra at $l = 1.83$ are called odd or acoustic since at this l value spins in the two bilayers rotate out of phase. Even or 'optic' spectra can be observed at $(\frac{1}{2}, \frac{1}{2}, 0)$. Most of the work to date has been done on the odd spectra since the even scattering is absent in the normal thermal neutron range. Recent experiments show, that in the metallic regime, even scattering has a sharp threshold at 50 meV (Bourges *et al* 1997, Hayden *et al* 1997) as shown in figures 45 and 49. In the insulating regime there is an optic gap at ≈70 meV (Reznik *et al* 1996).

The early work on magnetic neutron scattering in $YBa_2Cu_3O_{6+x}$ has been reviewed by Rossat-Mignod (1993). The undoped material is a two-dimensional antiferromagnet with the copper spins pointing along the CuO_2 planes. The Néel temperature is 415 K and the in-plane exchange constant $J = 0.170$ eV. With doping, T_N decreases and drops to zero sharply at $x = 0.4$ and long-range order can no longer be seen at $x = 0.42$. At the same time the three-dimensional ordered magnetic moment decreases to reach zero abruptly at $x = 0.4 \pm 0.02$. The inelastic magnetic scattering is mainly confined to the vicinity of the antiferromagnetic

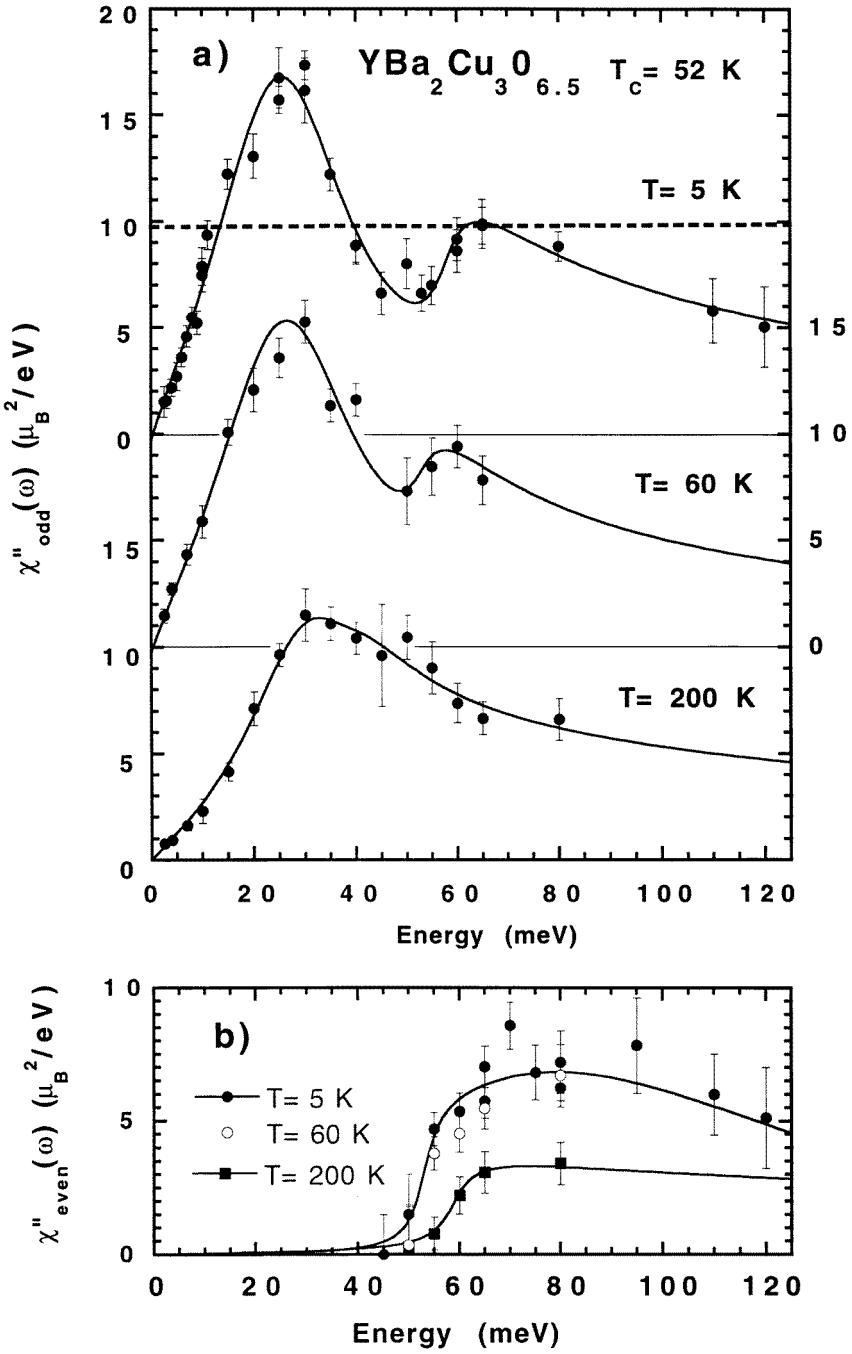

Figure 45. Magnetic neutron scattering in underdoped YBCO. (*a*) The susceptibility in the odd channel where the spins rotate out of phase in the bilayers is plotted. The scattering is dominated by a peak at ≈30 meV. (*b*) Even channel magnetic scattering. The even channel is dominated by a gap at ≈50 meV.

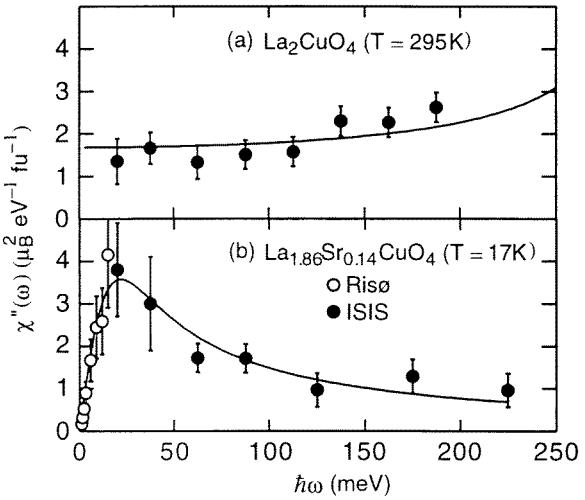

Figure 46. Magnetic neutron scattering in $La_{2-x}Sr_xCuO_4$. (*a*) The scattering by spin waves in the antiferromagnetic parent compound. (*b*) In an underdoped sample where the scattering is peaked at ≈25 meV.

point $(\frac{1}{2}, \frac{1}{2})$ but there is a tendency for the scattering to spread away from $(\frac{1}{2}, \frac{1}{2})$ and recently Dai *et al* (1998) reported the presence of four incommensurate peaks centred on $(\frac{1}{2}, \frac{1}{2})$.

The spin wave spectrum in the undoped materials, as measured around the antiferromagnetic Q, forms a continuum from zero frequency up to the maximum of the spin wave spectrum $\approx 2J \approx 250$ meV in both $YBa_2Cu_3O_{6+x}$ and $La_{2-x}Sr_xCuO_4$ (Hayden *et al* 1997, Bourges *et al* 1997). Hole doping has several effects on this spectrum. The magnetic Bragg spots disappear, showing the destruction of long range coherence but *inelastic* magnetic scattering in the $(\frac{1}{2}, \frac{1}{2}, l)$ region remains at all doping levels including in the superconducting state. The inelastic spectrum is broadened in Q and the spectral weight is redistributed towards a broad peak at lower frequency. This is illustrated in figure 46 for $La_{2-x}Sr_xCuO_4$ and in figures 45 and 49 for $YBa_2Cu_3O_{6+x}$.

In fully oxygenated $YBa_2Cu_3O_{6+x}$ Rossat-Mignod *et al* (1991) reported a narrow resonance in $\chi(\boldsymbol{q}, \omega)$ in the superconducting state at 41 meV in the odd spectrum at $\boldsymbol{Q} = (\frac{1}{2}, \frac{1}{2}, 1.7)$. This was subsequently verified by Mook *et al* (1993) with polarized neutrons.

The resonance peak can also be seen in underdoped $YBa_2Cu_3O_{6+x}$. The frequency position of the peak varies with doping, decreasing as T_c is reduced in proportion to T_c with a linear dependence (Bourges *et al* 1995, Dai *et al* 1996, Fong *et al* 1997). Figure 47 shows the doping dependence of the resonance energy from the work of Fong *et al* (1997). Figure 48 (top right panel) shows the peak in underdoped YBCO 6.6 from the work of Dai *et al* (1996). The bottom right panel shows intensity of the resonance as a function of L, the reciprocal lattice vector normal to the layers. It is clear that the resonance is only seen in the odd spectrum since it has zero intensity at $L = 0$ where the even channel is expected to peak. The left panels show the resonance at higher temperatures.

We now turn to the temperature dependence of the resonance and the question of its possible presence in the normal state.

To start, we note that the odd channel susceptibility of underdoped YBCO in the normal state is dominated by a broad peak in the 25–40 meV region. This peak develops from the spin wave spectrum of the undoped cuprates through a shift of spectral weight from higher (and

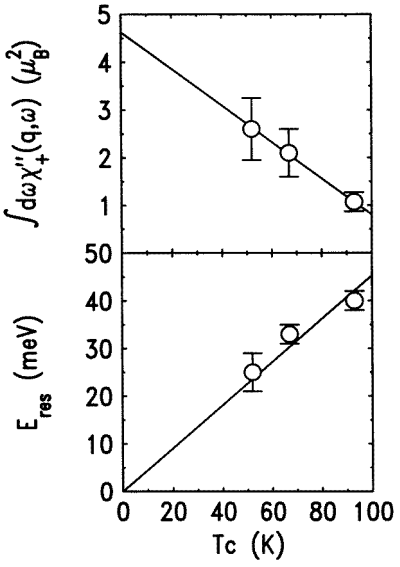

Figure 47. The position and frequency of the magnetic scattering peak as a function of doping. Unlike the pseudogap frequency which is doping independent, the magnetic scattering peak, or resonance frequency, varies linearly with T_c.

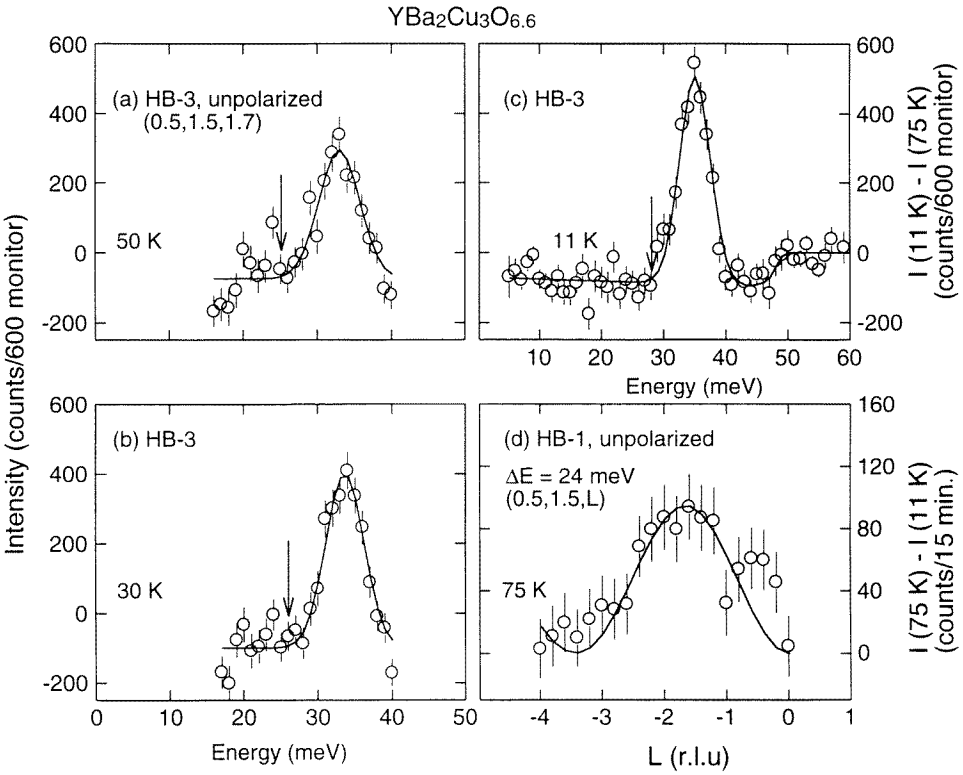

Figure 48. The resonance peak in underdoped YBCO 6.6. Magnetic neutron scattering is concentrated in the (π, π) region of reciprocal space forming a sharp peak at 35 meV in the odd channel: (*a*)–(*c*). Panel (*d*) shows that the variation of scattering with $\boldsymbol{q}$ normal to the planes is sinusoidally modulated with a spatial frequency corresponding to the spacing between the bilayers.

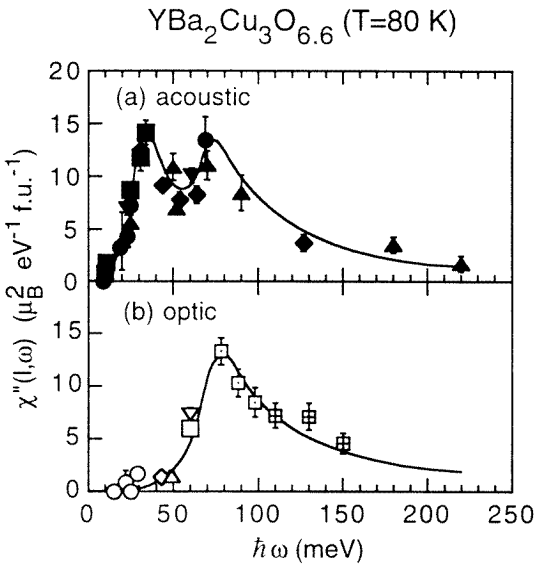

Figure 49. (*a*) Acoustic (odd) and (*b*) optic (even) spectra in underdoped YBCO 6.6.

lower) frequencies to the peak.

As the temperature is lowered the low-frequency tail of this peak develops a gap-like depression which has been termed a pseudogap (Rossat-Mignod *et al* 1991, Tranquada *et al* 1992, Sternlieb *et al* 1994). This depression is seen in the normal state but as the peak sharpens in the superconducting state a true gap develops below the peak (Bourges *et al* 1996, Dai *et al* 1996).

Bourges *et al* (1996) study the magnetic scattering of overdoped YBCO 6.97. In the overdoped region, the magnetic contribution in the normal state has almost completely vanished. Bourges *et al* find that the magnetic response is restricted to the 33–46 meV region with a very narrow (in $\boldsymbol{q}$) resonant contribution at 39 meV. Since there is no scattering below 33 meV they assign this figure to the spin gap and note that it is higher than what is seen in underdoped samples. Very similar results are reported by Dai *et al* (1996) who use polarized neutrons, and find in underdoped samples of YBCO 6.6 the resonance at 35 meV and the gap at 28 meV, figure 49.

The (π, π) resonance and the associated gap are only seen in the odd spectra with $l = 1.83$. The even spectra recorded with $l = 0$ show no scattering at low energy but above a threshold of 50–60 meV strong scattering sets in (Bourges *et al* 1997, Hayden *et al* 1997), as shown in figures 45 and 49. Another way of interpreting the odd–even channel difference is to say that above 50 meV the interlayer coherence is destroyed since the sinusoidal modulation in the l direction is replaced by uniform rods.

The magnetic scattering in $La_{2-x}Sr_xCuO_4$ has many parallels with that in $YBa_2Cu_3O_{6+x}$ (Hayden *et al* 1997). The main difference is the appearance of four incommensurate peaks symmetrically placed around (π, π). Their location can be understood in terms of Fermi surface nesting. In a Fermi liquid the excitations correspond to spin-flip transitions across the Fermi surface that are enhanced for (π, π) scattering because this vector, at least for the simple tight binding Fermi surface, nests regions of the Fermi surface with high density of states. In good agreement with this picture in $La_{2-x}Sr_xCuO_4$ there are four incommensurate peaks shifted away from the commensurate (π, π) position by an amount δ that matches the

shrinking Fermi surface as hole doping proceeds (Cheong *et al* 1991, Mason *et al* 1993, 1996, Hayden *et al* 1996).

Mason *et al* (1993) looked for a gap in the magnetic excitations associated with the four incommensurate peaks and found a suppression of excitations below $3.5k_BT_c$ but no clear gap. They find no evidence of the node structure associated with clean d-wave superconductivity. Instead there is isotropic residual scattering at the lowest frequencies. The authors suggest this may be due to localized magnetic impurities.

Yamada *et al* (1995) report the observation of a low-lying gap in the optimally doped $La_{2-x}Sr_xCuO_4$ with a $T_c = 37.3$ K in the form of a clear depression of low-frequency scattering below the transition temperature, below a frequency of 3.5 meV which they call a magnetic superconducting gap. It should be noted that within the Fermi liquid picture of a d-wave superconductor, the gap measured in a magnetic neutron scattering experiment is not the maximum gap. In terms of detailed calculations within d-wave models (Tanamoto *et al* 1991, Bulut and Scalapino 1994, Zha *et al* 1993) these measurement are consistent with $d_{x^2-y^2}$ models with a maximum gap of $2\Delta_0 = 19.3$ meV (155 cm^{-1}).

9. Theories of the pseudogap

Just as the experimental evidence of the pseudogap does not yet provide a single consistent view, neither do the available theoretical models. A few selected models are described below.

Several of the models described below involve preformed pairs. Early references to these ideas include the work of Uemura *et al* (1989) and Randeria *et al* (1989). One scenario which has received considerable attention involves spin–charge separation. This idea was first proposed by P W Anderson (1987) as the resonating valence bond, RVB, model with a mean-field treatment developed by Baskaran *et al* (1997). The possibility of separate transition temperatures for the RVB state and the BEC state was discussed by Kotliar and Lin (1988). Nagaosa and Lee (1992) produced a Ginzburg–Landau theory of the spin–charge separated system calculating various transport properties in the pseudogap state. Tanamoto *et al* (1991) have calculated NMR properties using the Nagaosa and Lee model.

Spin–charge separation creates holons with zero spin and spinons which are zero-charge, spin-$\frac{1}{2}$ fermions. In the mean-field description the spinons pair to form a gap in the spin excitations, identified as the pseudogap. The holons Bose-condense at T_c to form the superconducting state. At present it is believed that even though it is the holons which Bose-condense, gauge-field fluctuations lead to a strong coupling between the spinons and holons. A gauge theory of the normal state, including the pseudogap, has been developed by Lee and Nagaosa (1992) and Lee and Wen (1997).

Emery *et al* (1997) have developed a preformed pair model of the pseudogap based on microstripes. Phase separation takes place on a microscopic scale generating dynamical charged stripes separated by insulating antiferromagnetic stripes. These microstripes form at the upper crossover temperature T°. Above this temperature the charge is uniformly distributed. Below T° charge is confined to the metallic stripes forming a one-dimensional electron gas (1DEG). Spin and charge are separated as spin resides in the AF stripes. As the temperature is lowered, AF correlations build up. At the lower crossover temperature T^*, pairing behaviour emerges.

Pairing is a result of a spin gap in the AF stripes. This is manifested in the 1DEG via pair hopping between the 1DEG and AF stripes. Emery and Kivelson describe this as a magnetic proximity effect. At this point there are only one-dimensional superconducting correlations. The pseudogap is associated with this spin gap. At T_c Josephson coupling between the metallic stripes becomes large enough to yield global phase coherence. Note that the pairing correlations

below T^* are not giving rise to real space pairing; the pairing correlations are dynamical.

A natural consequence of this model is that the symmetry of the order parameter as measured by local probes will hold in the pseudogap state, as will other superconducting properties.

For underdoped systems the transition into the superconducting state is determined by the stiffness against classical phase fluctuations (Emery and Kivelson 1995), proportional to $n_s(T)$. In this context the observation by Uemura *et al* (1989) of a universal relation between T_c and $\lambda^{-2}(0) \propto n_s$ can be thought of as an upper bound on T_c given by the ordering temperature for classical phase fluctuations.

Pines and co-workers have developed the nearly antiferromagnetic Fermi liquid (NAFL) model to describe the physics of the cuprate superconductors, reviewed in Pines (1997a, b). As described in the original MMP paper (Millis *et al* 1990), the dominant interaction between quasiparticles arises from spin fluctuations, as characterized in the dynamical spin susceptibility $\chi(\boldsymbol{q}, \omega)$. The strong AF correlations cause $\chi(\boldsymbol{q}, \omega)$ to peak at $\boldsymbol{Q} = (\pi, \pi)$. This has led the authors to distinguish two classes of quasiparticles: *hot* quasiparticles which are located near $(0, \pi)$, connected to each other by $\boldsymbol{Q}$, and *cold* quasiparticles which are not strongly connected by AF fluctuations. The cold quasiparticles behave like a strongly coupled Landau–Fermi liquid whereas the hot quasiparticles are anomalous and non-Landau–Fermi liquid-like.

Chubukov *et al* (1996) have developed a scenario to describe the crossover temperatures and pseudogap. At high temperatures, mean-field behaviour is observed with weak AF correlations. As the temperature is lowered, in the underdoped region, a crossover occurs at T° where the correlation length $\xi \approx 2a$. Below this temperature non-universal pseudoscaling is observed where, for example, ${}^{63}T_1T$, ${}^{63}T_{2G}$ and the Knight shift are linear in T. This behaviour is a result of the hot quasiparticle spectrum being modified by the strengthening AF correlations with decreasing temperature; i.e. $1/\xi \approx a + bT$.

Upon reaching T^* a gap opens in the hot quasiparticle spectrum, thus establishing the pseudogap. Below T^* the spin-relaxation rates and Knight shift decrease more quickly than above T^*. Superconductivity occurs when the cold quasiparticles become gapped, independent of the hot quasiparticles which are already gapped at T_c. Thus the magnitude of the pseudogap and T^* are unrelated to T_c. As it is only the cold quasiparticles which participate in the superconducting transition, the superfluid density n_s will be considerably less than the total number of quasiparticles.

Millis and Monien (1993) proposed that the pseudogap in bilayer compounds was due to interlayer exchange coupling. Further work by Altshuler *et al* (1996) produced a model with interlayer pairing of holons producing a spin pseudogap. The authors claim that the pseudogap crossover temperature T^* for single-layer materials, namely $La_{2-x}Sr_xCuO_4$, is just slightly above T_c. Interlayer coupling enhances T^* to temperatures well above T_c. Recent data on other single-layer compounds throw this scenario into doubt. The single-layer mercury compound shows a crossover temperature well above T_c (Bobroff *et al* 1997).

Maly *et al* (1998) introduce a description of the pseudogap state in terms of resonant pairs, somewhere between the preformed pairs that Bose condense at T_c and free fermions. Their paper offers a nice review of the currently competing models.

Castellani *et al* (1997) find a quantum critical point at optimal doping associated with a charge density wave instability related to the observations of Boebinger (1996) in high pulsed magnetic fields of an apparent metal–insulator transition at $T = 0$ below optimal doping. They find an order parameter that has d-wave symmetry and a superconducting T_c that strongly depends on doping in the overdoped region but is flat at optimal doping in agreement with experiments.

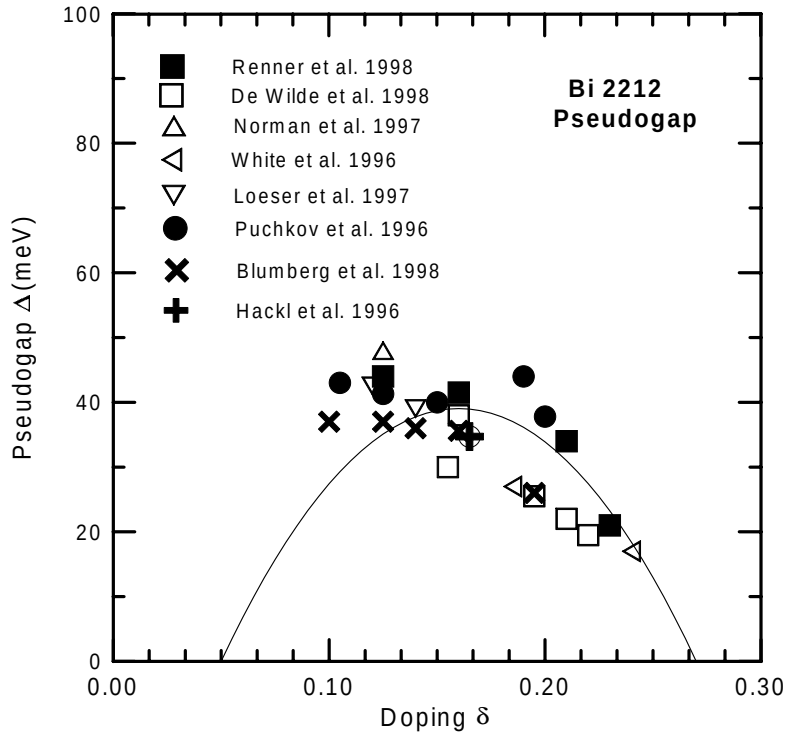

Figure 50. The width Δ of the pseudogap in Bi 2212 measured with various experimental techniques as function of doping δ. The curve is an empirical formula for T_c assuming $2\Delta = 9.5k_BT_c$. The triangles are photoemission data; the squares, tunnelling; the full circles, ab-plane optical conductivity; and the open circles, Raman scattering.

10. Summary and conclusions

The experiments reviewed here have given evidence of the presence of a pseudogap in the normal state of all the cuprates. The pseudogap seems to be related to the superconducting gap in the sense that it evolves smoothly into the superconducting gap and has the same d-wave symmetry. Unlike a conventional superconducting gap though, the pseudogap magnitude is temperature independent. Tunnelling, ARPES and optical data indicate that the magnitude of the gap does not change significantly on going through T_c. Thus, in the case of the cuprates, in contrast to a conventional superconducting gap, the gap starts as the pseudogap in the normal state and evolves into the superconducting gap below T_c (i.e. $\Delta(T)$ does not go to zero at T_c).

The pseudogap appears in the underdoped side of the phase diagram and weakens as optimal doping is approached. A weak pseudogap is still present at optimal doping but disappears not too far into the overdoped region. This is illustrated in the phase diagram where T^* approaces T_c just into the overdoped region. T^* is strongly temperature dependent in the underdoped region in contrast to the magnitude of the pseudogap which weakly decreases as the doping level is increased. Thus T^* is not a direct measure of the pseudogap energy scale. Well into the overdoped region, the pseudogap merges with the superconducting gap, i.e. T^* has merged into T_c and there are no remaining signatures of the pseudogap in the normal state.

As an example, figure 50 shows a summary of pseudogap energy scale from various laboratories on Bi 2212 as a function of doping (according to an empirical law $T_c/T_{c,\max} =$

$1 - 82.6(\delta - 0.16)^2$ (Presland *et al* 1991, Groen *et al* 1990). The general trend for any given technique is a rough tracking of T_c in the overdoped ranges keeping $2\Delta/k_B T_c$ roughly constant at 9.5 (shown as the curve) and an approximately constant, or even slightly increasing gap value, as oxygen is removed, in the underdoped region. This graph should be treated with some caution. First, all techniques measure slightly different properties of the gap and in the absence of a microscopic theory such comparisons are very approximate. Secondly, there are built-in sample-to-sample variations and there is some uncertainty in the case of Bi 2212 whether a given sample is overdoped or underdoped.

The above discussion largely is concerned with frequency-dependent information. ARPES, INS, NMR and Raman spectroscopy provide $\boldsymbol{q}$-dependent information. INS, in principle, probes all of reciprocal space but due to background subtraction is predominantly probing the region near (π, π). The Knight shift is proportional to $\chi(q = 0)$ and the spin-lattice relaxation rate $1/^{63}T_1$ is dominated by fluctuations near (π, π). ARPES more or less uniformly covers the whole zone. NMR measurements reveal that the crossover temperature T^* is somewhat $\boldsymbol{q}$ dependent. The temperature evolution of the pseudogap provided by ARPES is also $\boldsymbol{q}$ dependent. Hence it is insufficient to describe the pseudogap evolution with only a temperature dependent suppression factor.

The pseudogap in the excitation spectrum opens up in the region near $(\pi, 0)$, largely influenced by the susceptibility at (π, π). Excitations on the Fermi surface near the diagonal remain ungapped. The susceptibility near $q = 0$ averages over both of these regions. Given the nature of the ARPES results it is not surprising that NMR yields somewhat different results for $q = 0$ and $\boldsymbol{q} = (\pi, \pi)$.

Measurements taken with a wide variety of techniques demonstrate that the pseudogap is present in both the spin and charge channel. For example, ARPES measures the charge channel and magnetic susceptibility the spin channel. Loram's work has shown quantitatively, through Wilson's ratio, that the number of excitations in both channels is approximately the same. Thus retention of the term pseudogap seems justified as this is not just a spin gap as some would suggest. Near-equal occupation of excitations in both channels also serves to rule out extreme models which have all the excitations in one channel only. For example, a charge separation model in which the holons condense out with no consequence to the spinon excitations is inconsistent with this observation.

Many measurements of the pseudogap depict a smooth evolution of a physical observable as a function of temperature. Typical examples are the electronic specific heat and magnetic susceptibility of underdoped $YBa_2Cu_3O_{6+x}$. On the other hand, some techniques reveal a distinct crossover temperature, namely resistivity and NMR. Magnetic resonance is unique in that it reveals two crossover temperatures in several compounds. Comparison with other techniques suggests that the lower crossover temperature T^* is associated with the pseudogap and that the origin of the upper crossover T° may be unrelated to the pseudogap. Indeed, the linear temperature evolution between T^* and T° of the Knight shift, $^{63}T_1T$ and $^{63}T_{2G}$ is more indicative of an physical evolution than a gap. In particular, if the curves are extrapolated to zero temperature they have positive intercepts, whereas below T^*, the curves extrapolate to zero at a positive temperature—consistent with a gap.

Crossovers observed in some compounds and not others raise the question as to whether a crossover at T^* is intrinsic to the pseudogap. At this point it is unclear as to whether the crossover is unique to some compounds and not others. One possibility is that the crossover is smeared out by inhomogeneities in only some compounds.

Special mention must be made of the $La_{2-x}Sr_xCuO_4$ compound. Although many measurements are indicative of a pseudogap, even in the strongly overdoped region, there are several contradictory observations. Susceptibility and resistivity data in the 'pseudogap' region

extrapolate to a positive intercept rather than intersecting zero at a positive temperature as is the case with other compounds. A pseudogap is completely absent in the spin-lattice relaxation rate in the underdoped region. One possible cause of these differences is the presence of paramagnetic centres. These moments have been observed in specific heat measurements of Mason *et al* (1993) and are intrinsic to $La_{2-x}Sr_xCuO_4$, a random alloy. As in the case of Zn doped YBCO 124, local moments may be responsible for the absence of the pseudogap in the spin-lattice relaxation rate. In any case, it seems that $La_{2-x}Sr_xCuO_4$ must be treated as a special case; it is not consistent with the general properties of the pseudogap observed in the other cuprate families. Finally, last but not least, $La_{2-x}Sr_xCuO_4$ is unique in having a maximum T_c of only 40 K in contrast to the other compounds, both single layer and double layer, with maximum T_c of 90 K and above.

Theoretical views of the pseudogap are just as diverse as the views on the mechanism of high-T_c superconductivity. One point of view which stands out in the context of experimental evidence is the idea of preformed pairs. Several relevant observations are as follows.

(1) The pseudogap evolves into the superconducting gap. There is no evidence that the magnitude of the superconducting gap goes to zero at T_c.
(2) Both the pseudogap and superconducting gap have d-wave symmetry.
(3) The crossover temperature T^* merges with T_c in the overdoped region of the phase diagram.

These factors are consistent with the existence of preformed pairs, of some description. They need not be real space pairs and could just be dynamic correlations. Although the evidence so far is consistent with preformed pairs, it does not prove their existence.

Acknowledgments

We would like to acknowledge the support of this work by the Natural Science and Engineering Research Council of Canada (NSERC) and the Canadian Institute of Advanced Research (CIAR). We have also gained valuable insight from discussions with the following people: P W Anderson, D N Basov, A J Berlinski, D A Bonn, G Blumberg, J P Carbotte, J C Cooper, V J Emery, W N Hardy, C C Homes, J C Irwin, B Keimer, C Kallin, P A Lee, J W Loram, F Marsiglio, T E Mason, H A Mook, A J Millis, M Norman, J Preston, A V Puchkov, D Pines, M Reedyk, C Renner, T Rõõm, Z-X Shen, T Startseva, R Stern, D B Tanner, S Tajima, D van der Marel, Y Uemura, M B Walker and J F Zasadzinski.

References

Abrikosov A A and Fal'kovskii L A 1961 *Sov. Phys.–JETP* **13** 179
Allen J W and Mikkelsen J C 1976 *Phys. Rev.* B **15** 2953
Allen P B 1971 *Phys. Rev.* B **3** 305
Alloul H, Mendels P, Casalta H, Marucco J F and Arabski J 1991 *Phys. Rev. Lett.* **67** 3140
Alloul H, Ohno T and Mendels D 1989 *Phys. Rev. Lett.* **63** 1700
Altshuler B L, Ioffe L B and Millis A J 1996 *Phys. Rev.* B **53** 415
Anderson P W 1987 *Science* **235** 1196
Anderson R O *et al* 1993 *Phys. Rev. Lett.* **70** 3163
Arnold G B, Mueller F M and Swihart J C 1991 *Phys. Rev.* B **78** 1771
Ashcroft N W and Mermin N D 1996 *Solid State Physics* (New York: Holt, Rinehart and Winston) p 252
Bankay M, Mali M, Roos J and Brinkmann D 1994 *Phys. Rev.* B **50** 6416
Barzykin V and Pines D 1995 *Phys. Rev.* B **52** 13 585
Baskaran G, Zou Z and Anderson P W 1987 *Solid State Commun.* **63** 973
Basov D N, Liang R, Bonn D A, Hardy W N, Dabrowski B, Quijada M, Tanner D B, Rice J P, Ginsberg D M and Timusk T 1995a *Phys. Rev. Lett.* **74** 595

Basov D N, Liang R, Dabrowski B, Bonn D A, Hardy W N and Timusk T 1996 *Phys. Rev. Lett.* **77** 4090
Basov D N, Mook H A, Dabrowski B and Timusk T 1995b *Phys. Rev.* B **52** R13 141
Basov D N and Timusk T 1998 Infrared properties of high-T_c superconductors: an experimental overview *Handbook on the Physics and Chemistry of Rare Earths* ed K A Dschneidner, LeRoy Eyring and M B Maple (Amsterdam: North-Holland)
Basov D N, Timusk T, Dabrowski B and Jorgensen J D 1994a *Phys. Rev.* B **50** 3511
Batlogg B, Hwang H Y, Takagi H, Cava R J, Kao H L and Kwo J 1994 *Physica* C **235–240** 130
Bednorz J G and Müller K A 1986 *Z. Phys.* **64** 189
Blumberg G, Klein M V, Kadowaki K, Kendziora C, Guptasarma P and Hinks D 1998 *Preprint* cond-mat/9711073
Bobroff J, Alloul H, Mendels P, Viallet V, Marucco H F and Colson D 1997 *Phys. Rev. Lett.* **78** 3757
Boebinger G S 1996 *Phys. Rev. Lett.* **77** 5417
Bonn D A, Dosanjh P, Liang R and Hardy W N 1992 *Phys. Rev. Lett.* **68** 2390
Bourges P, Fong H F, Regnault L P, Bossy J, Vettier C, Milius D L, Aksay I A and Keimer B 1997 *Phys. Rev.* B **56** R11 439
Bourges P, Regnault L P, Henry J Y, Vettier C, Sidis Y and Burlet P 1995 *Physica* B **215** 30
Bourges P, Regnault L P, Sidis Y and Vettier C 1996 *Phys. Rev.* B **53** 876
Branch D 1996 Optical properties of strongly-coupled d-wave superconductors with an anisotropic momentum dependent interaction *PhD Thesis* McMaster University
Bucher B, Steiner P, Karpinski J, Kaldis E and Wachter P 1993 *Phys. Rev. Lett.* **70** 2012
Campuzano J C *et al* 1990 *Phys. Rev. Lett.* **64** 2308
Carbotte J P 1990 *Rev. Mod. Phys.* **62** 1027
Carrington A, Walker D J C, Mackenzie A P and Cooper J R 1993 *Phys. Rev.* B **48** 130 351
Castellani C, Di Castro C and Grilli M 1997 *Z. Phys.* **130** 137
Chakravarty S, Halperin B I and Nelson D R 1989 *Phys. Rev.* B **39** 2344
Chen X K, Naeni J G, Hewitt K C, Irwin J C, Linag R and Hardy W N 1994 *Phys. Rev. Lett.* **73** 3290
Cheong S W, Aeppli G, Mason T E, Mook H, Hayden S M, Canfield P C, Fisk Z, Clausen K N and Martinez J L 1991 *Phys. Rev. Lett.* **67** 1791
Chubukov A V, Pines D and Stojković B P 1996 *J. Phys.: Condens. Matter* **8** 10 017
Coffey L and Coffey D 1993 *Phys. Rev.* B **48** 4184
Cooper S L, Nyhus P, Reznik D, Klein M V, Lee W C, Ginsberg D M, Veal B W, Paulikas A P and Dabrowski B 1993a *Phys. Rev. Lett.* **70** 1533
Cooper S L *et al* 1993b *Phys. Rev.* B **47** 8233
Corey R L, Curro N J, O'Hara K, Imai T, Slichter C P, Yoshimura K, Katoh M and Kosuge K 1996 *Phys. Rev.* B **53** 5907
Dai P, Mook H A and Doĝan F 1998 *Phys. Rev. Lett.* **80** 1738
Dai P, Yethiraj M, Mook H A, Lindmer T B and Doĝan F 1996 *Phys. Rev. Lett.* **77** 5425
Däumling M 1991 *Physica (Amsterdam)* **183c** 293
Dessau D S *et al* 1993 *Phys. Rev. Lett.* **71** 2781
Dessau D S, Wells B O, Shen Z-X, Spicer W E, List R S, Arko A J, Mitzi D B and Kapitulnik A 1991 *Phys. Rev. Lett.* **66** 2160
Deveraux T P and Einzel D 1995 *Phys. Rev.* B **51** 16 336
DeWilde Y *et al* 1998 *Phys. Rev. Lett.* **80** 153
Ding H, Norman M R, Yokaya T, Takeuchi T, Randeria M, Campuzano J C, Takahashi T, Mochiku T and Kadowaki K 1997 *Phys. Rev. Lett.* **78** 2628
Ding H, Yokaya T, Campuzano J C, Takahashi T, Randeria M, Norman M R, Mochiku T, Kadowaki K and Giapinzakis J 1996 *Nature* **382** 51
Einzel D and Hackl R 1996 *J. Raman Spectrosc.* **27** 307
Emery V J and Kivelson S A 1995 *Nature* **374** 4347
Emery V J, Kivelson S A and Zachar O 1997 *Phys. Rev.* B **56** 6120
Farnworth B and Timusk T 1974 *Phys. Rev.* B **10** 2799
Fong H F, Keimer B, Milius D L and Aksay I A 1997 *Phys. Rev. Lett.* **78** 713
Fong H F, Keimer B, Reznik D, Milius D L and Aksay I A 1997 *Phys. Rev.* B **54** 6708
Friedberg R and Lee T D 1989 *Phys. Rev.* B **40** 6745
Fujimori A, Ino A, Mizokawa T, Kim C and Shen Z-X 1998 *J. Phys. Chem. Solids (Proc. SNS'97 J. Phys. Chem. Solids)* to be published
Fukuoka A, Tokiwa-Yamamoto A, Itoh M, Usami R, Adachi S and Tanabe K 1997 *Phys. Rev.* B **55** 6612
Giaver I 1960 *Phys. Rev. Lett.* **5** 147
Groen W A, de Leeuw D M and Feiner L F 1990 *Physica* C **165** 55

Gurvich M, and Fiory A T 1987 *Phys. Rev. Lett.* **59** 1337
Götze W and Wölfe P 1972 *Phys. Rev.* B **6** 1226
Hackl R, Kaiser R and Schicktanz 1983 *J. Phys. C: Solid State Phys.* **16** 1729
Hackl R, Krug G, Nemetshcek R, Opel M, and Stadlober B 1996 *Spectroscopic Studies of Supercondcutors (Proc. SPIE 2696)* vol V, ed I Bozovic and D van der Marel, p 194
Harris J M, Loeser A G, Marshall D S, Schabel M C and Shen Z-X 1996 *Phys. Rev.* B **54** R15 665
Harris J M *et al* 1997 *Phys. Rev. Lett.* **79** 143
Hayden S M, Aeppli G, Dai P, Mook H A, Perring T G, Cheong S-W, Fisk Z, Doĝan F and Mason T E 1998 *Physica* B **241–243** 765
Homes C C, Timusk T, Bonn D A, Liang R and Hardy W N 1995a *Physica* C **265–280** 265
——1995b *Can. J. Phys.* **73** 663
Homes C C, Timusk T, Liang R, Bonn D A and Hardy W N 1993 *Phys. Rev. Lett.* **71** 1645
Horvatic M, Auler T, Berthier Y, Butaud P, Clark W G, Gillet J A and Segransan P 1993 *Phys. Rev.* B **47** 3461
Hosseini A, Kamal S, Bonn D A, Liang Ruxiang and Hardy W N 1998 *Phys. Rev. Lett.* **81** 1298
Hsueh Ya-Wei, Statt B W, Reedyk M, Xue J S, Greedan J E 1997 *Phys. Rev.* B **56** 8511
Hwang H Y, Batlogg B, Takagi H, Kao H L, Kwo J, Cava R J, Krajewski J J and Peck W F Jr 1994 *Phys. Rev. Lett.* **72** 2636
Hwu Y *et al* 1991 *Phys. Rev. Lett.* **67** 2573
Imai T, Yasuoka H, Shimizu T, Ueda Y, Yoshimura K and Kosuge K 1989 *Physica* C **162–164** 169
Imer J-M, Patthey F, Dardel B, Schneider W-D, Baer Y, Petroff Y and Zettl A 1989 *Phys. Rev. Lett.* **62** 336
Ino A, Kim C, Mizokawa T, Shen Z-X, Fujimori A, Takaba M, Tamasaku K, Eisaki H, and Uchida S 1997 *Preprint* cond-mat/9809311
Ito T, Takenaka K and Uchida S 1993 *Phys. Rev. Lett.* **70** 3995
Itoh Y, Machi T, Fukuoka A, Tanabe K and Yasuoka H 1996 *J. Phys. Soc. Japan* **65** 3751
Julien M-H, Carretta P, Horvatić M, Berthier C, Berthier Y, Ségransan P, Carington A and Colson D 1996 *Phys. Rev. Lett.* **76** 4238
Junod A 1989 *Physical Properties of High Temperature Superconductors* vol 2, ed D M Ginsberg (Singapore: Scientific)
Kendziora C A, Kelley R J and Onellion M 1996a *Spectroscopic Studies of Superconductors (Proc. SPIE 2696)* vol V, ed I Bozovic and D van der Marel p 223
——1996b *Phys. Rev. Lett.* **77** 727
King D M *et al* 1993 *Phys. Rev. Lett.* **70** 3159
Klein M V and Dierker S B 1983 *Phys. Rev.* B **32** 4976
Kostur V N and Eliashberg G M 1991 *JETP Lett.* **53** 391
Kotliar G and Liu J 1988 *Phys. Rev.* B **38** 5142
Lee P A and Nagaosa N 1992 *Phys. Rev.* B **46** 5621
Lee P A and Wen X-G 1997 *Phys. Rev. Lett.* **78** 4111
Leggett A J 1994 *Braz. J. Phys.* B **50** 496
Liu R, Veal B W, Paulikas A P, Downey J W, Shi H, Olson C G, Gu C, Arko A J and Joyce R R 1991 *Phys. Rev.* **45** 5614
Loeser A G, Shen Z-X, Dessau D S, Marshall D S, Park C H, Fournier P and Kapitulnik A 1996 *Science* **273** 325
Loeser A G, Shen Z-X, Schabel M C, Kim C, Zhang M, Kapitulnik A and Fournier P 1997 *Phys. Rev.* B **56** 14 185
Loram J W, Mirza K A, Cooper J R, Athanassopoulou N and Liang W Y 1996 *Proc. 10th HTS Anniversary Workshop on Physics, Materials and Applications* ed B Batlogg *et al* (Singapore: World Scientific) p 341
Loram J W, Mirza K A, Cooper J R and Liang W Y 1993 *Phys. Rev. Lett.* **71** 1740
Loram J W, Mirza K A, Cooper J R, Liang W Y and Wade J M 1994a *J. Supercond.* **7** 243
Loram J W, Mirza K A, Cooper J R and Tallon J L 1997 *Physica* C **282-287** 1405
Loram J W, Mirza K A, Wade J M, Cooper J R and Liang W Y 1994b *Physica* C **235** 134
Mahajan A V, Alloul H, Collin G and Marucco J F 1994 *Phys. Rev. Lett.* **72** 3100
Maly J, Boldizar J and Levin K 1998 *Preprint* cond-mat/9805018
Mandrus D, Forro L, Koller D, and Mihaly L 1991 *Nature* **351** 460
Mandrus D, Hartge J, Kendziora C, Mihaly L and Forro L 1993 *Europhys. Lett.* **22** 199
Manzke R, Buslaps T, Claessen R, and Fink J 1989 *Europhys. Lett.* **9** 477
Marshall D S *et al* 1996 *Phys. Rev. Lett.* **76** 4841
Marsiglio F, Startseva T and Carbotte J C 1998 *Phys. Lett.* A **245** 172
Martin S, Fiory A T, Fleming R M, Schneemeyer L F and Waszczak J V 1990 *Phys. Rev. Lett.* **41** 846
Martindale J A and Hammel P C 1996 *Phil. Mag.* B **74** 573
Mason T E, Aeppli G, Hayden S M, Ramirez A P and Mook H 1993 *Phys. Rev. Lett.* **71** 919

Mason T E, Schröder A, Aeppli G, Mook H and Hayden S M 1996 *Phys. Rev. Lett.* **77** 1604
Mattis D C and Bardeen J 1958 *Phys. Rev.* **111** 412
Millis A J and Monien H 1993 *Phys. Rev. Lett.* **70** 2810
Millis A J, Monien H and Pines D, 1990 *Phys. Rev.* B **42** 167
Miyatake T, Yamauchi K, Takata T, Koshizuka N and Tanaka S 1991 *Phys. Rev.* B **44** 10 139
Momono M, Ido M, Najano T, Oda M, Okajima and Yamaya K 1994 *Physica* C **233** 395
Monien H, Monthoux P and Pines D 1991 *Phys. Rev.* B **43** 275
Mook H A, Yethiraj M, Aeppli G, Mason T E and Armstrong T 1993 *Phys. Rev. Lett.* **70** 109
Mori H 1965 *Prog. Theor. Phys.* **34** 399
Morr D K and Pines D 1998 *Phys. Rev. Lett.* **81** 1086
Naeini J G, Chen X K, Hewitt K C, Irwin J C, Devereaux T P, Okuya M, Kimura T and Kishio K 1998 *Phys. Rev.* B **57** R11 077
Nagaosa N and Lee P A 1992 *Phys. Rev.* B **45** 966
Nemetschek R, Opel M, Hoffman C, Müller P F, Hackl R, Berger H, Forró L, Erb A and Walker E 1997 *Phys. Rev. Lett.* **78** 4837
Norman M R *et al* 1997a *Preprint* cond-mat/9710163
Norman M R, Ding H, Campuzano J C, Takeuchi T, Randeria M, Yokaya T, Takahashi T, Mochiku T and Kadowaki K 1997b *Phys. Rev. Lett.* **79** 3506
Ohsugi S, Kitaika Y, Ishida K and Asayama K 1991 *J. Phys. Soc. Japan* **60** 2351
Olson C G, Liu R, Yang A-B, Lynch D W, Arko A J, List R S, Veal B W, Chang Y C, Jiang P Z and Paulikas A P 1989 *Science* **245** 731
Pines D 1997b *Z. Phys.* B **103** 129
——1997a *Physica* C **282-287** 273
Plakida N M 1997 *Z. Phys.* **103** 383
Presand M R, Tallon J L, Buckley R G, Liu L S and Flower N F 1991 *Physica* C **176** 95
Puchkov A V, Basov D N and Timusk T 1996a *J. Phys.: Condens. Matter* **8** 10 049
Puchkov A V, Fournier P, Basov D N, Timusk T, Kapitulnik A and Kolesnikov N N 1996c *Phys. Rev. Lett.* **77** 3212
Puchkov A V, Fournier P, Timusk T and Kolesnikov N N 1996b *Phys. Rev. Lett.* **77** 1853
Randeria M and Campuzano J-C 1997 *Preprint* cond-mat/9709107
Randeria M, Duan J-M and Shieh L-Y 1989 *Phys. Rev. Lett.* **62** 981
Reedyk M, Timusk T, Xue J S and Greedan J E 1997 *Phys. Rev.* B **56** 9134
Regnault L P, Bourges P, Burlet P, Henry J Y, Rossat-Mignod J, Sidis Y and Vettier C 1994 *Physica* C **235–240** 59
Renner C, Revaz B, Genoud J-Y and Fischer O 1996 *J. Low Temp. Phys.* **105** 1083
Renner Ch, Revaz B, Genoud J-Y, Kadowaki K and Fischer O 1998 *Phys. Rev. Lett.* **80** 149
Reyes A P, MacLaughlin D E, Takigawa M, Hammel P C, Heffner R H, Thompson J D and Crow J E 1991 *Phys. Rev.* B **43** 2989
Reznik D, Bourges P, Regnault L P, Bossy J, Vettier C, Milius D L, Aksay I A, and Keimer B 1996 *Phys. Rev.* B **53** R14 741
Rossat-Mignod J, Regnault L P, Bourges P, Burlet P, Vettier C and Henry J Y 1993 *Selected Topics Superconductivity (Frontiers in Solid State Physics 1)* ed L C Gupta and M S Multani (Singapore: World Scientific)
Rossat-Mignod J, Regnault L P, Vettier C, Bourges P, Burlet P, Bossy J, Henry J Y and Lapertot G 1991 *Physica* C **185–189** 86
Rotter L D *et al* 1991 *Phys. Rev. Lett.* **67** 2741
Rozenberg M I, Kotliar G, Kajueter H, Thomas G A, Rapkine D H, Honig J M and Metcalf P 1995 *Phys. Rev. Lett.* **75** 105
Scalapino D J 1969 *Superconductivity* vol 1, ed R D Parks (New York: Marcel Dekker) p 449
Schulz H J 1991 *Prog. High Temp. Supercond.* **29** 57
Shastry B S and Shraiman B I 1990 *Phys. Rev. Lett.* **65** 1068
Shen Z-X *et al* 1993 *Phys. Rev. Lett.* **70** 3999
Shen Z-X and Dessau D S 1995 *Phys. Rep.* **253** 1
Shen Z-X and Schrieffer J R 1997 *Phys. Rev. Lett.* **78** 1771
Shulga S V, Dolgov O V and Maksimov E G 1991 *Physica* C **178** 266
Slakey F, Klein M V, Rice J P and Ginsberg D 1990 *Phys. Rev.* B **42** 2643
Sooryakumar R and Klein M V 1980 *Phys. Rev. Lett.* **54** 660
Startseva T, Timusk T, Okuya M, Kimura T and Kishio K 1998a unpublished
Startseva T, Timusk T, Puchkov A, Basov D, Okuya M, Kimura T and Kishio K 1998b unpublished
Statt B W and Griffin A 1992 *Phys. Rev.* B **46** 3199
——1993 *Phys. Rev.* B **48** 619

Stern R, Mali M, Mangelschots I, Roos J, Brinkmann D, Genoud J-Y, Graf T and Muller J 1994 *Phys. Rev.* B **50** 426
Stern R, Mali R, Roos J and Brinkmann D 1995 *Phys. Rev.* B **51** 15 478
Sternlieb B J, Tranquada J M, Shirane G, Sato M and Shamato S 1994 *Phys. Rev.* B **50** 12 915
Stojković B P and Pines D 1997 *Phys. Rev.* B **56** 11 931
Tajima S, Gu G D, Miyamoto S, Odagawa A and Koshizuka N 1993 *Phys. Rev.* B **48** 16 164
Tajima S, Schützmann J and Miyamoto S 1995 *Solid State Commun.* **95** 759
Takagi H, Batlogg B, Kao H L, Kwo J, Cava R J, Krajewski J J and Peck W F Jr 1992 *Phys. Rev. Lett.* **69** 2975
Takenaka K, Fukuzumi Y, Mitzuhasi K, Uchida S, Asaoka H and Takei H 1997 *Phys. Rev.* B **56** 5654
Takenaka K, Mizuhashi K, Takagi H and Uchida S 1994 *Phys. Rev.* B **50** 6534
Takigawa M, Reyes A P, Hammel P C, Thompson J D, Heffner R H, Fisk Z and Ott K C 1991 *Phys. Rev.* B **43** 247
Tanamoto T, Kuboki K and Fukuyama H 1991 *J. Phys. Soc. Japan* **60** 3072
Tanner D B and Timusk T 1992 *The Physical Properties Of High Temperature Superconductors* ed D M Ginsberg (Singapore: World Scientific) p 363
Tao H J, Lu F and Wolf E J 1997 *Physica* C **282–287** 1507
Thomas G A, Orenstein J, Rapkine D H, Capizzi M, Millis A J, Bhatt R N, Schneemeyer L F and Waszczak J V 1988 *Phys. Rev. Lett.* **61** 1313
Timusk T, Cao N, Basov D N and Homes C C 1996 *Spectroscopic Studies of Superconductors (Proc. SPIE 2696)* ed I Bozovic and D van der Marel p 2
Tinkham M 1975 *Introduction to Superconductivity* (Malabar, FL: Krieger)
Tranquada J M, Gehring P M, Shirane G, Shamato S and Sato M 1992 *Phys. Rev.* B **46** 5561
Uemura Y J *et al* 1989 *Phys. Rev. Lett.* **62** 2317
Uchida S, Tamasaki K and Tajima S 1996 *Phys. Rev.* B **53** 14 558
Varma C M, Littlewood P B, Schmitt-Rink S, Abrahams E and Ruckenstein A E 1989 *Phys. Rev. Lett.* **63** 1996
Walstedt R E, Bell R F and Mitzi D B 1991 *Phys. Rev.* B **44** 7760
Walstedt R E, Warren W W Jr, Bell R F, Cava R J, Espinosa G P, Schneemeyer L F and Waszczak J V 1990 *Phys. Rev.* B **41** 9574
Warren W W Jr, Walstedt R E, Brennert J F, Cava R J, Tycko R, Bell R F and Dabbagh G 1989 *Phys. Rev. Lett.* **62** 1193
Wells B O, Shen Z-X, Dessau D S, Spicer W E, Mitzi D B, Lombardo L, Kapitulnik A and Arko A J 1992 *Phys. Rev.* B **46** 11 830
White P J, Shen Z-X, Kim C, Harris J M, Loeser A G, Fournier P and Kapitulnik A 1996 *Phys. Rev.* B **54** R15 669
Williams J V M, Tallon J L, Haines E M, Michalak R and Dupree R 1997 *Phys. Rev. Lett.* **78** 721
Winzek N *et al* 1993 *Physica* C **205** 45
Zawadowski A and Cardona M 1990 *Phys. Rev.* B **42** 10 732
Zheng G-q, Odaguchi T, Kitaoka Y, Asayama K, Kodama Y, Mizuhashi K and Uchida S 1996 *Physica* C **263** 367
Zheng G-q, Odaguchi T, Mito T, Kitaoka Y, Asayama K and Kodama Y 1993 *J. Phys. Soc. Japan* **62** 2591
Zimmermann H, Mali M, Brinkmann D, Karpinski J, Kaldis E and Rusiecki 1989 *Physica* C **190** 681
Zimmermann H, Mali M, Mangelshots I, Roos J, Pauli L, Brinkmann D, Karpinski J, Kaldis E and Rusiecki 1990 *J. Less Common Met.* **164–165** 138